Identification of platinum ores via trace element signatures

by

Maisson Mohamed Zeinelabieden Hassan

A thesis submitted in partial fulfillment for the
degree of Master of Science

in the

Department of Physics

Faculty of Science

UNIVERSITY OF CAPE TOWN

May 2011

Declaration of Authorship

I, Maisson M. Z. Hassan, declare that this thesis titled, 'Identification of platinum ore via trace element signature' and the work presented in it are my own. I confirm that:

- This work was done wholly or mainly while in candidature for a research degree at this University.
- Where any part of this thesis has previously been submitted for a degree or any other qualification at this University or any other institution, this has been clearly stated.
- Where I have consulted the published work of others, this is always clearly attributed.
- I have acknowledged all main sources of help.
- Where the thesis is based on work done by myself jointly with others, I have made clear exactly what was done by others and what I have contributed myself.

Signed: _____

Date: _____

"If we knew what it was we were doing, it would not be called research, would it?."

– Albert Einstein (1879-1955)

UNIVERSITY OF CAPE TOWN

Abstract

Faculty of Science
Department of Physics

Master of Science in Physics

by Maisson Mohamed Zeinelabieden Hassan

Within the minerals industry, accurate knowledge of the elemental composition of unprocessed and processed ore is often required for purposes of quality control and improving efficiencies. In particular, neutron activation analysis is one of the standard techniques used for the determination of elements such as platinum, palladium, gold and iridium in geological materials. For example, the current state-of-the-art allows sub-ppm amounts of Au, Cu, Ir, K, La, Mn, Pd and Zn to be determined in milligram samples of pure platinum metal.

There is significant interest from the platinum industry in South Africa to explore whether processed ore or concentrate from different mines may be identified via characteristic trace element signatures. This project studies the natural variation in the elemental composition of processed platinum ore from different extraction locations in South Africa in order to assess whether this provides sufficient information for the "elemental fingerprinting" of the material.

The experimental work has been undertaken in South Africa via two approaches. One approach was constructing a source of thermal neutrons by moderating the fast neutrons emitted from an ^{241}AmBe radioisotopic source at iThemba LABS. A more traditional approach was using the thermal neutron flux from the SAFARI-I reactor at NECSA (Pelindaba). This project relied on cooperation from members of the Centre for Minerals Research (CMR) at the university of Cape Town (UCT) to provide ore samples of known origin and chemical composition. The study was carried out on the concentrations of constituent (major, minor and trace) elements present in ore and concentrates samples collected from Lonmin mines in the Bushveld Complex in South Africa.

Acknowledgements

Words would not be enough to express my thanks to Andy Buffler for teaching me all about research. This thesis would never have taken this shape without his inspired problem solving, limitless help, continuous guidance and support on every possible level throughout the development of the thesis. I am honoured that he gave me the opportunity to be one of his students. I cannot thank him enough.

Particular thanks and gratitude go to Aubery Mainza, my co-supervisor who gave me the honour to work in the Centre of Mineral Research (CMR) at the Chemical Engineering Department. Thanks also for making this project possible by providing the sufficient financial funding and the mine samples. I would like to express my thanks for arranging the necessary training in the CMR froth flotation laboratories where I was trained to prepare the concentrates samples. I highly appreciate the opportunity to present the results of my work at various conferences. Thanks for everything.

I would like to extend thanks to everyone who contributed with their expertise and work to the realisation of this research. Arnaud Faanhof and Deon Kotze from NECSA deserve special mention for their professional and resolute support in conducting the experimental work at the SAFARI-1 reactor. I would also like to express my humble gratitude to the members of the CMR technicians for their uninterrupted support during the samples preparation process.

My final words go to my family and friends. I want to thank my parents, without whom I would never have been able to achieve so much. I cordially thank my sisters Maisa and Anne for their support throughout my studies in South Africa. I must thank my husband Yousif and my beautiful daughters Jood and Reel for their endless love, patience, and understanding. I am also very grateful to all my friends at UCT for being just wonderful.

Great thanks to all of you!.

Contents

List of Figures

List of Tables

Abbreviations

BIC	**B**ushveld **I**geneous **C**omplex
cps	**c**ounts **p**er **s**econd
eV	**e**lectron **v**olt
FWHM	**F**ull **W**idth at **H**igh **M**aximum
g	**g**ram
HPGE	**H**igh **P**urity **G**ermanium
MRY	**M**erensky **R**eef
n	**n**eutron
NAA	**N**eutron **A**ctivation **A**nalysis
NECSA	**S**outh **A**frican **N**uclear **E**nergy **C**orporation
PGE	**P**latinum **G**roup **E**lement
PGM	**P**latinum **G**roup **M**ineral (or **M**etal)
ppb	**p**art **p**er **b**illion
PPL	**P**latreef
ppm	**p**art **p**er **m**illion
SIBX	**S**odium - **i**sobutyl- **x**anthate
UG2	**U**pper **G**roup Chromitite Layer 2

To my beloved daughters, Jood and Reel...

Chapter 1

Introduction

Within the minerals industry, accurate knowledge of the elemental composition of unprocessed and processed materials is required for purposes of quality control and improving efficiencies. In particular, the platinum industry has a key interest in accurate knowledge of the platinum group elements (PGEs, Section 2.1) in geological samples. Development of reliable methods for the determination of the abundances of individual platinum-group elements, as well as gold, silver, nickel and copper in ores, are required in many aspects of the industry. Furthermore, methods for the profiling of platinum materials (concentrate, converter matte, etc.) are necessary for the unambiguous identification of the material after recovery from theft. Such methods remain largely undeveloped. The theft of platinum group metals (PGM) occurs mostly above ground during one of the extraction processes, since platinum can only be removed from its natural state through complicated processes of refining and extraction, in contrast to gold where the valuable metals (such as PGEs, gold and silver)can be easily extracted. Nearly half of the PGM materials stolen are from inside the secure areas of the platinum mines [1]. Furthermore, the precious metals mining industries are not capable of determining exactly how much product is lost during processing phases, leaving a window of opportunity for theft and corruption. The possibility of establishing methods and techniques that could be used to unambiguously identify the recovered products in term of localities and ownership is clearly required. It is noted here that"unambiguous identification" requires careful definition, and for the present purpose is taken to mean that the measurement technique provides data with uncertainties small enough for the inferences derived from the measurement to bear a 95% confidence interval.

There are two broad approaches that can be taken to identify PGM materials: either using naturally-occurring variation in one or more characteristics of the material (trace element

composition, mineralogy, etc.), or artificially adding some feature to the material. Analysis techniques may be classified as "chemical" or "radiation" based, the former likely to require destruction of a sample. Radiation-based techniques probe the material with radiation (X-rays, gamma-rays, neutrons or charged particles), and measure some form of exiting radiation which bears characteristic features. Recent years have shown a considerable development of the analytical techniques used for the analysis of geological materials. Common analytical techniques used are X-ray fluorescence (XRF), proton-induced X-ray emission (PIXE), and neutron activation analysis (NAA). Various instrumental techniques are also being used, such as flame atomic absorption spectrometry (FAAS), graphite furnace atomic absorption spectrometry (GFAAS), inductively coupled plasma atomic emission spectrometry (ICP-AES) and inductively coupled plasma mass spectroscopy (ICP-MS).

1.1 Activation analysis

Activation analysis has been recognised as an analytical technique for over 70 years. In this technique, a sample of an unknown material is irradiated in a field of particles or electromagnetic radiation, such as neutrons, protons or high-energy photons. The incident particle interacts with a target nucleus either by scattering or by absorption. The interaction of the nuclear particles with the nuclei of the unknown sample will produce excited nuclei that will decay by emitting radiation. The measurement and analysis of this radiation give information about the elemental constituents of the sample [2, 3]. Thus the major steps of activation analysis are: preparation of the sample, irradiation of the sample, measurement of the spectra of exiting radiation, and analysis of the measured spectra (see Fig 1.1). The technique can be reliable, since each induced radionuclide has its own particular decay constant and type(s) of radiation, neither of which is exactly duplicated in any other radionuclide. Activation methods can be categorised as being either destructive or nondestructive. In destructive methods, the irradiated sample is dissolved, and the element of interest is counted after it has been isolated by suitable chemical or physical means; possible interferences from other elements made radioactive by the irradiation are thus eliminated. In the nondestructive procedure, the activated sample is counted without pre-treatment [4, 5].

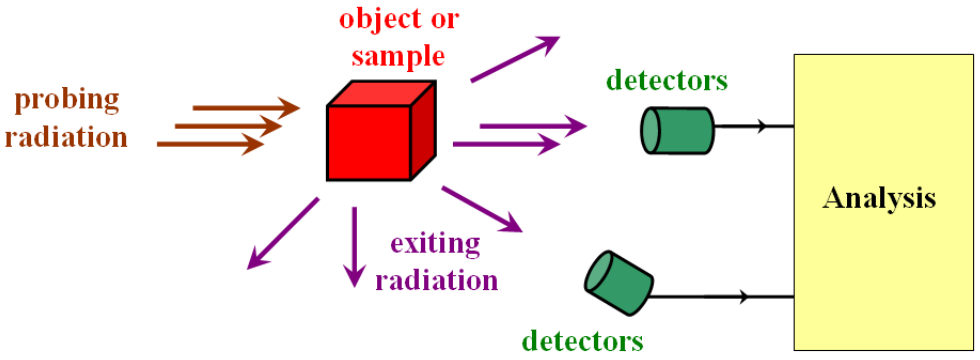

FIGURE 1.1: Analysing an unknown sample with radiation.

1.2 Neutron activation analysis

In 1932 Chadwick [6], following observations by other researchers, discovered the neutron and described it as a particle of unit mass and zero charge. The neutron is a highly effective bombarding particle, being unaffected by the electrostatic charge barrier surrounding a target nucleus in contrast to charged particles, which require high kinetic energies to surmount such barriers.

Neutron activation analysis involves exposing the sample of interest to a neutron flux from a suitable neutron source. The nuclides of the target sample will capture the neutrons and be left in a high excited state forming unstable nuclides (radionuclides). These radionuclides will decay to their stable form by the emission of beta particles and/or gamma radiation. The gamma-ray energies are characteristic of the product radionuclides. When detected, they provide positive identification of the targeted elements present in the sample, while quantification is achieved by measuring the intensity of the emitted gamma-rays that are directly proportional to the amount of the respective elements in the sample [7].

The method was applied for the first time in 1936 by G. von Hevesy and H. Levi, when they exposed rare-earth salts to a naturally emitting Ra(Be) neutron source, and succeeded to determine the amount of dysprosium in an yttrium sample [8]. From this discovery, the potential of identifying elements present in the samples through measurement of different radiations has been recognised. The capabilities of NAA increased dramatically after the mid-forties, when nuclear reactors became available as intense neutron sources for activation [9]. The technique was fully developed in the early 1960s as a result of the introduction of the scintillation detector, soon followed by the multi-channel pulse-height analyser. With the advent of high-resolution semiconductor gamma-ray spectrometers, it became possible to analyse materials producing complex spectra, such as geological materials, without restoring

to chemical separations [10]. Sensitivity and accuracy resulting from these developments were sufficient for NAA to maintain a strong position among other techniques for trace element analysis and became universally accepted. It has been estimated that more than 100000 samples undergo analysis via NAA each year [11, 12].

Isotopes may be activated by thermal, epithermal or fast neutrons. Thermal neutrons are generally more reactive than high-energy neutrons. There are several different types of neutron reactions. The most common modes of reactions are neutron capture, transmutation, fission and inelastic scattering. Neutron capture is the most important nuclear reaction for thermal neutron activation analysis. However, the occurrence of a particular neutron reaction will depend on the cross-section of the target nucleus.

In spite of the competition from the various analytical methods available for the determination of the average abundance of elements in geological materials, neutron activation analysis still retains a distinguished place because of its potential for blank-free, matrix-independent, and multi-element determinations, which makes it an excellent reference technique [13, 14]. It has the advantage over other analytical techniques whenever it is necessary to determine not only the major elements within the sample but also the elements in trace and ultra-trace levels [15]. NAA is readily capable of simultaneous determination of many elements at parts per million (ppm) and some at parts per billion (ppb) levels, often without destruction of the sample [16]. The accuracy and the limit of detection depend, however, strongly on the type and the elemental content of material analysed [17, 18]. Neutron activation analysis is a valuable tool for many applications. It has great advantages for the certification of reference materials, and has, for example, been used at the National Institute of Standards and Technology (NIST) for this purpose for the last four decades [19]. It has been used extensively and successfully in almost all conceivable fields of science. Its fields of applications include semiconductors [20], criminology [21], explosives detection [22], petroleum industry [23], environmental applications [24, 25], pollutants [26, 27], biological [28, 29], nutritional and epidemiological, archaeological [30], geological sciences [31–33], rocks [34], minerals [35], clays [36], water [4, 9], and applications involved monitoring the platinum in environmental related samples as well as in biological materials [37, 38]. Analysis of rocks by neutron activation analysis assists geochemists in research on the processes involved in the formation of different rocks through the analysis of the rare earth elements (REEs) and other trace elements. Advances leading to the increasing application of NAA to geoscience problems have come from radiochemists, physicists and geochemists [39].

1.3 The present work

There is significant interest from the platinum industry in South Africa to explore whether processed ore, concentrates and converter mattes from different mines may be identified via characteristic trace element signatures. This project aims at measuring, via NAA, natural variations in particular isotopes present in platinum ores and concentrates from different extraction locations in South Africa, in order to assess whether this provides sufficient information for the "elemental fingerprinting" of the material. Three major platinum group mineral bearing ore bodies have been used in the study: the Merensky reef, Upper Group chromite (UG2), and Platreef.

The research questions for the present work were:

- Does fast neutron activation analysis (FNAA) offer a reliable means of profiling platinum materials, in particular ores and concentrates?
- Which naturally-occurring isotopes can be used to provide unambiguous signatures to the ore and concentrate materials, measured via NAA?

NAA measurements were made at the SAFARI-1 reactor facility at NECSA, Pelindaba, and using an AmBe isotopic neutron source at iThemba LABS. The project relied on cooperation from members of the Centre for Minerals Research at UCT to provide ore samples of known origin.

Chapter 2

Geological and Geochemical Review

2.1 The platinum-group elements

The platinum-group elements (PGEs) consist of six elements that have similar extraordinary physical and chemical characteristics. The six elements are platinum (Pt), palladium (Pd), iridium (Ir), osmium (Os), rhodium (Rh), and ruthenium (Ru). They fall in the Periodic Table (Fig 2.1) into two horizontal rows: three heavier metals (Ru, Rh and Pd) and three lighter metals (Os, Ir and Pt) [40, 41]. Platinum-group elements, together with gold and silver, are referred to as the "precious metals" due to their rare existence in the earth's crust, while because of their high resistance to oxidation and corrosion are also called the "noble metals" [41]. Furthermore, due to their resistance to corrosion and oxidation, high melting points, electrical conductivity, and catalytic activity, these elements are of high economical, social, and industrial value. They have wide applications in chemical, medical, electrical, electronic, glass, and most recently automotive industries [42, 43].

2.2 The platinum-group minerals

The members of platinum-group elements occur in nature as various mineral species chiefly as antimonides, arsenides, bismuthides, sulfides, tellurides and native state [44]. The mode of occurrence of platinum-group minerals (PGM) ranges from being predominantly associated with base-metal sulphides (BMS), nickel and copper, to being predominantly associated with gangue minerals [45].

There are around 109 PGM species recognised by the International Mineralogical Association (IMA). The known PGM species are listed with their ideal formula, ranging from anduoite ($RuAs_2$) to zvyagintsevite (Pd_3Pb) in Table 2.1, although compositions may vary locally.

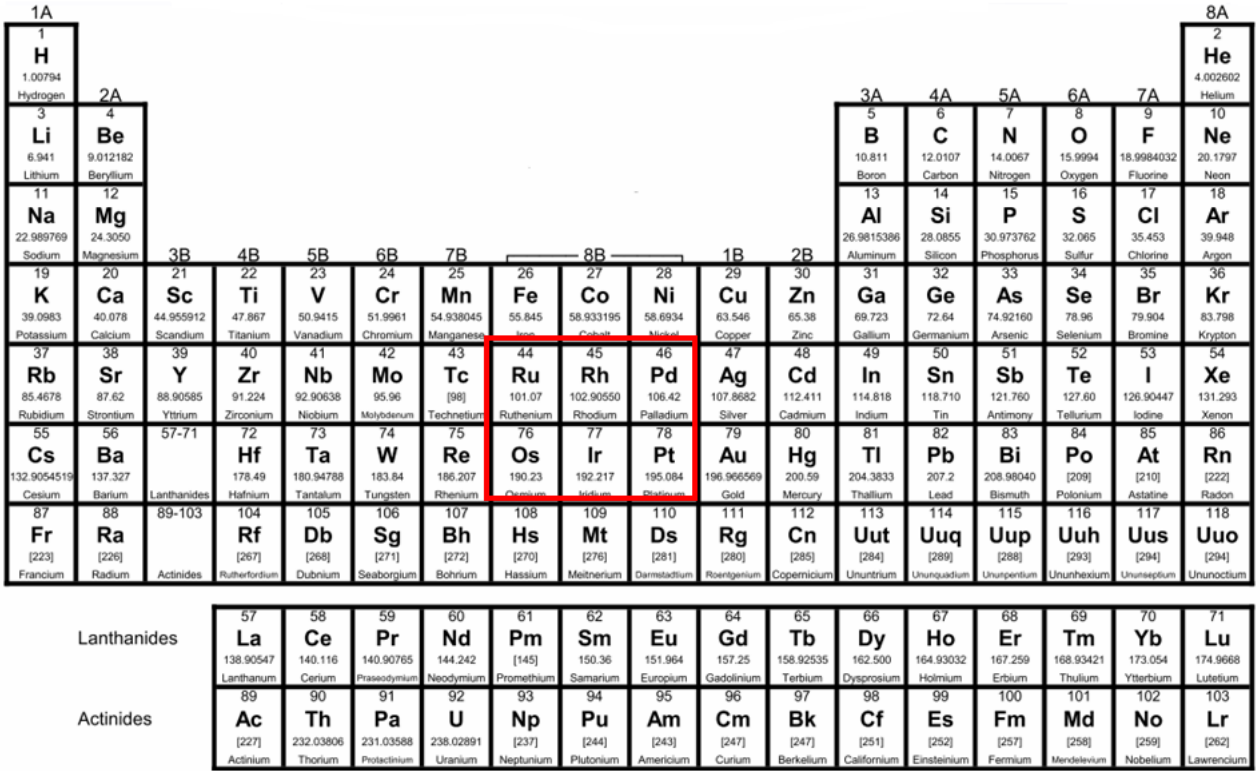

FIGURE 2.1: The location of the PGEs, enclosed in the bold square, in the Periodic Table. The Periodic Table, adopted from [40].

No.	Name	Ideal Formula	No.	Name	Ideal Formula
1.	Andouite	$RuAs_2$	56.	Oosterboschite	$(Cu,Pd)_7Se_5$
2.	Arsenopalladinite	$Pd_8As_{2.5}Sb_{0.5}$	57.	Osarsite	OsAsS
3.	Atheneite	$(Pd,Hg)_3As$	58.	Osmium	Os
4.	Atokite	Pd_3Sn	59.	Oulankaite	$Pd_5Cu_4SnTe_2S_2$
5.	Borovskite	Pd_3SbTe_4	60.	Padmaite	PdBiSe
6.	Bowieite	Rh_2S_3	61.	Palarstanide	$Pd_5(Sn,As)_2$
7.	Braggite	(Pt,Pd)S	62.	Palladium	Pd
8.	Cabriite	Pd_2SnCu	63.	Palladoarsenide	Pd_2As
9.	Changchengite	IrBiS	64.	Palladobismutharsenide	$Pd_2As_{0.8}Bi_{0.2}$
10.	Chengdeite	Ir_3Fe	65.	Palladodymite	$(Pd,Rh)_2As$
11.	Cherepanovite	RhAs	66.	Palladseite	$Pd_{17}Se_{15}$
12.	Chrisstanleyite	$Ag_2Pd_3Se_4$	67.	Paolovite	Pd_2Sn
13.	Cooperite	PtS	68.	Platarsite	PtAsS
14.	Crerarite	$(Pt,Pd)Bi_3S_{4-X}$	69.	Platinum	Pt
15.	Cuproiridsite	$CuIr_2S_4$	70.	Plumbopalladinite	Pd_3Pb_2
16.	Cuprorhodsite	$CuRh_2S_4$	71.	Polarite	PdBi
17.	Damiaoite	$PtIn_2$	72.	Polkanovite	$Rh_{12}As_7$
18.	Daomanite	$PtCuAsS_2$	73.	Potarite	PdHg
19.	Erlichmanite	OsS_2	74.	Prassoite	$Rh_{17}S_{15}$
20.	Ferronickelplatinum	$PtFe_{0.5}Ni_{0.5}$	75.	Rhodarsenide	$(Rh, Pd)_2As$
21.	Ferrohodsite	$FeRh_2S_4$	76.	Rhodium	Rh
22.	Froodite	$PdBi_2$	77.	Rhodplumsite	$Rh_3Pb_2S_2$
23.	Gaotaiite	Ir_3Te_8	78.	Ruarsite	RuAsS
24.	Genkinite	$(Pt,Pd)_4Sb_3$	79.	Rustenburgite	Pt_3Sn
25.	Geversite	$PtSb_2$	80.	Ruthenarsenite	RuAs
26.	Hexaferrum	(Fe,Ru,Os,Ir)	81.	Rutheniridosmine	(Ir,Os,Ru)
27.	Hollingworthite	RhAsS	82.	Ruthenium	Ru
28.	Hongshiite	PtCu	83.	Shuangfengite	$IrTe_2$
29.	Inaglyite	$Cu_3PbIr_8S_{16}$	84.	Sobolevskite	PdBi
30.	Insizwaite	$PtBi_2$	85.	Sopcheite	$Ag_4Pd_3Te_4$
31.	Irarsite	IrAsS	86.	Sperrylite	$PtAs_2$
32.	Iridarsenite	$IrAs_2$	87.	Stannopalladinite	Pd_5Sn_2Cu
33.	Iridium	Ir	88.	Stibiopalladinite	$Pd_{5+X}Sb_{2-X}$
34.	Isoferroplatinum	Pt_3Fe	89.	Stillwaterite	Pd_8As_3
35.	Isomertieite	$Pd_{11}Sb_2As_2$	90.	Stumpflite	PtSb
36.	Kashinite	Ir_2S_3	91.	Sudburyite	PdSb
37.	Keithconnite	$Pd_{3-X}Te$	92.	Sudovikovite	$PtSe_2$
38.	Kharaelkhite	$(Cu,Fe)_4(Pt,Pb)_4NiS_8$	93.	Taimyrite	$(Pd,Cu)_3Sn$
39.	Konderite	$Cu_3PbRh_8S_{16}$	94.	Tatyanaite	$Pt_9Cu_3Sn_4$
40.	Kotulskite	PdTe	95.	Telargpalite	$(Pd,Ag)_{3+X}Te$
41.	Laflammeite	$Pd_3Pb_2S_2$	96.	Telluropalladinite	Pd_9Te_4
42.	Laurite	RuS_2	97.	Temagamite	Pd_3HgTe_3
43.	Luberoite	Pt_5Se_4	98.	Testibiopalladite	PdSbTe
44.	Majakite	PdNiAs	99.	Tetraferroplatinum	PtFe
45.	Malanite	$CuPt_2S_4$	100.	Tischendorfite	$Pd_8Hg_3Se_9$
46.	Maslovite	PtBiTe	101.	Tolovkite	IrSbS
47.	Mayingite	IrBiTe	102.	Tulameenite	$PtFe_{0.5}Cu_{0.5}$
48.	Menshikovite	$Pd_2Ni_2As_3$	103.	Urvantsevite	$Pd(Bi,Pb)_2$
49.	Merenskyite	$PdTe_2$	104.	Vasilite	$Pd_{16}S_7$
50.	Mertieite I	$Pd_{11}(Sb,As)_4$	105.	Verbeekite	$PdSe_2$
51.	Mertieite II	$Pd_8(Sb,As)_3$	106.	Vincentite	$(Pd,Pt)_3(As,Sb,Te)$
52.	Michenerite	PdBiTe	107.	Vystoskite	PdS
53.	Moncheite	$PtTe_2$	108.	Yixunite	Pt_3In
54.	Niggliite	PtSn	109.	Zvyagintsevite	Pd_3Pb
55.	Omeiite	$OsAs_2$			

TABLE 2.1: Platinum-group minerals (ideal formulas, when known) recognised by the Commission on New Minerals and Mineral Names (CNMMN), International Mineralogical Association (IMA) [42, 46].

2.3 PGEs deposits in the Bushveld Complex

The deposits of platinum-group elements are rare, and occur mainly in mafic and ultramafic igneous rocks in which they were concentrated by mainly high-temperature magmatic processes [42]. There are two types of mafic igneous intrusions, those where the PGEs are the major product, such as the Bushveld Complex (South Africa), the Stillwater intrusion (USA), and the Great Dyke (Zimbabwe), and others where the PGEs are by-product of copper and nickel mining, as at Noril'sk-Talnakh Complexes (Russia), Sudbury (Canada), and Jinchuang (China) [47].

2.3.1 The Bushveld Igneous Complex

The Bushveld Igneous Complex (BIC) in South Africa (Fig. 2.2) is the largest (65000 km^2 and up to 10 km thick), and most important resource of the platinum group elements in the world [47, 48]. The Bushveld Complex is a layered intrusion that has developed two thousand millions years ago as a result of the occurrence of a major magmatic event. It consists of igneous rocks that have been formed after the slow cooling of the molten magma. The slow drop of the temperature of the magma caused the formation of different layers with mineral compositions that vary from *mafic*, which are magnesium- and iron-rich minerals, to *silicic*, which are calcium-, aluminum- and sodium-rich silicate minerals [49]. These minerals accumulated into sub-horizontal layers building up from the base of the chamber. The re-occurring of the magma causes the repetition of the minerals layering and hence controls the distribution of the ore deposits [50].

As shown in Fig 2.2, the Bushveld Complex consists of five major geological limbs (i.e., eastern, western, far-western, northern, and Bethal limb). Stratigraphically, the Complex consists of three suites: the Rustenburg Layered Suite, the Rashoop Granophyre Suite and the Lebowa Granite Suite. The Rustenburg Layered Suite (RLS) is the oldest and contains the economically mineable platinum group ore deposits. From the base of the chamber to the top, the RLS is generally subdivided into five zones: the basal Marginal Zone (MZ), the Lower Zone, the Critical Zone (CZ), Main Zone and Upper Zone (Fig 2.3). These make up the succession of mafic and ultramafic rocks of the Rustenburg Layered Suite [52]. All the economic PGE deposits occur in the Critical Zone [47].

The platinum-bearing deposits of the Bushveld Complex are represented by three very different ore bodies: the Merensky Reef, the Upper Group Chromitite 2 (UG2), and the Platreef

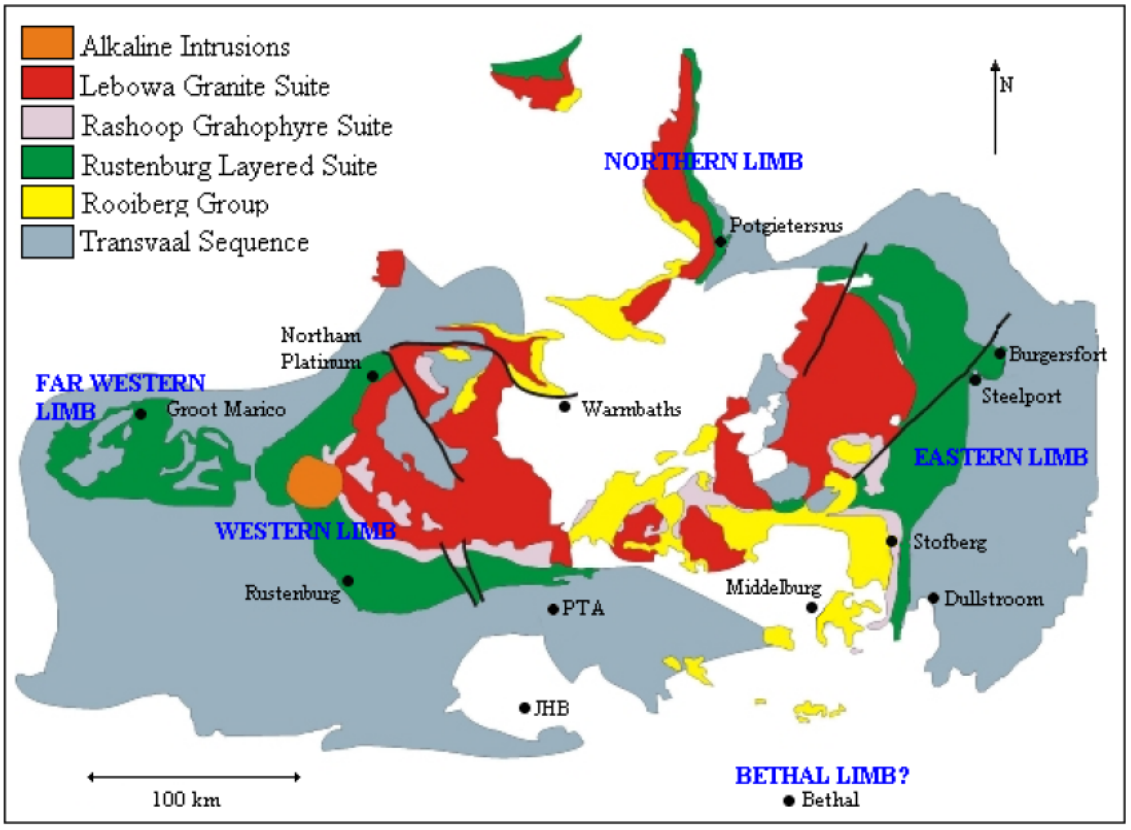

FIGURE 2.2: A geological map of the Bushveld Complex, showing the four exposed limbs of the Complex, the location of Northam Platinum and the possible positioning of the buried Bethal Limb [51].

[41, 50]. The Merensky Reef and UG2 reefs occurred within the top of the Critical Zone (Upper Critical Zone) of the Bushveld Complex, the Zone also hosts the Platreef mineralization of the northern limb of the Bushveld Complex. The stratigraphic column shown in Fig 2.3 illustrates the relative positioning of the UG2 in relation to the Merensky Reef, and the position of the Platreef [49].

2.3.1.1 Merensky Reef

The Merensky Reef is the source of over 80 per cent of platinum mined in South Africa. This has been successfully exploited since the late 1920s [54]. The term 'reef' is a mining term inherited from the gold mines on the Witwatersrand and refers to a layer within the Merensky Unit that is enriched in platinum-group elements [55]. Although the Merensky Reef is generally regarded as a uniform reef type, large variations occur in reef thickness, reef composition, as well as the position of the mineralisation [55]. Regardless of these variations, it is evident that the entire thickness of the Merensky pyroxenite contains virtually the same total amount of PGE all around the main Bushveld Complex [41].

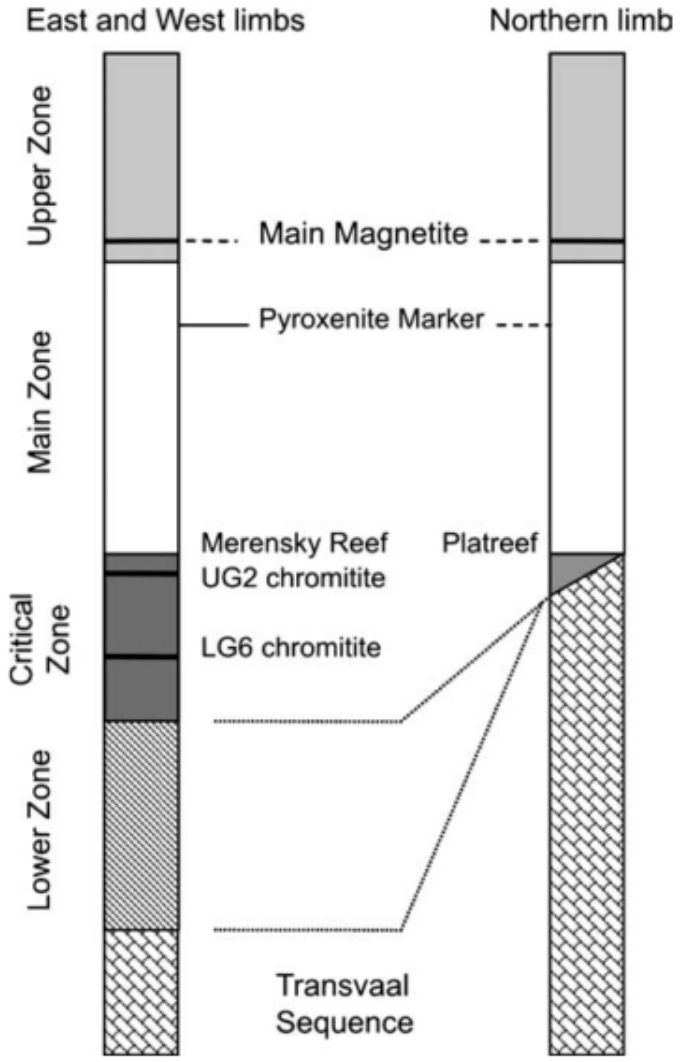

FIGURE 2.3: Currently accepted stratigraphic relationships between the eastern and western limb of the Bushveld Complex [53].

The rock-forming minerals of the Merensky Reef comprise approximately equal amounts of dark iron-magnesium silicate minerals and lighter calcium-aluminium-sodium minerals (feldspathic pyroxenite) [56]. The platinum group elements (PGE) in the Merensky Reef in the Bushveld Complex are strongly associated with the base metal sulphide (BMS) minerals present in the Reef, either as discrete platinum group minerals (PGM) included or attached to the sulphides, or in solid solution with these sulphides [54, 57]. In some cases, the PGEs are also associated with chromites [42].

Three principal base-metal sulphides occur in the Merensky Reef. These are, in order of decreasing abundance, pyrrhotite (FeS), pentlandite (Fe, Ni)S, chalcopyrite ($CuFeS_2$)[42, 56]. Minor sulphides include cubanite, mackinawite and pyrite which is more abundant in chromite-rich bands [42]. As the platinum minerals occur within and associated with these

sulphides, the Merensky Reef yields substantial copper and nickel as by-products, together with minor amounts of cobalt and selenium [56].

Extensive mineralogical studies show that seven PGMs are important in the Merensky reef although varieties occur in different areas and ore types. Those are braggite (Pt,Pd)S, cooperite (PtS), laurite (RuS_2), Pt-Fe alloy, sperrylite ($PtAs_2$), moncheite ($PtTe_2$), and kotulskite (PdTe) [42].

2.3.1.2 The Upper Group Chromitite Layer, UG2

Within the Critical Zone of the main Bushveld Complex, the chromitite layers are sequentially numbered in groups from the bottom upwards. These groups are named: lower group chromitite layer (LG), Middle group chromitite layer (MG), and the Upper group chormitite layer (UG). Each of these groups consists of a number of layers and different ratios of elements, i.e. chromium-to-iron ratio. The Upper group chromitite layers, UG1 and UG2, are allocated within the chromitite layer of the Upper Critical Zone [41].

The UG2 chromitite layer is a platiniferous chromitite layer which is developed some 20 to 400 metres below the Merensky Reef. The layer contains the highest PGM values in the BIC [41]. The UG2 consists predominantly of large amount of chromite ($FeCr_2O_4$) with lesser silicate minerals, and low concentrations of copper- and nickel-bearing sulphides [42]. The mineralogy of the platinum-group elements in UG2 chromitite varies significantly from locality to locality, both in terms of mode of occurrence and mineral assemblages [45, 49, 58].

2.3.1.3 Platreef

Th Platreef was discovered in the northern limb in 1924 [53, 59]. The northern limb rocks formed from a magma that was poorer in Mg, richer in Ca and Fe, and was Pd rather than Pt-dominant. The Platreef is geologically more complex than any of the PGE reefs in the eastern and western limbs [53].

The Platreef consists of a complex assemblage of pyroxenites, serpentinites and calc-silicates. Common base metal sulfides include pyrrhotite, pentlandite, chalcopyrite and pyrite, and high association of PGMs with silicate minerals is found in some areas. The Platreef silicates appear systematically more Fe-rich than their equivalents in the Merensky Reef [53]. The dominant PGM in the mined area of Platreef are sulphides, tellurides and arsenides [46].

The Platreef near Potgietersrus in South Africa contains the largest total PGE content of all of the mineralized layers in the Bushveld Complex, even though its grade is generally lower compared to Merensky and UG2 [47].

2.4 Mineral processing

Mining of platinum ore is either by opencast mining or underground operations mining. The former method being used on the more massive Platreef ores north of Potgietersrus in the northern limb [41, 56]. After mining, different platinum-group element deposits or ores should be treated with different recovery methods according to their mineralogical features and other factors [42].

The extraction of the valuable metals from the ore takes place in five distinct steps [41]:

- **Comminution and gravity concentration**: The ore is comminuted and a gravity concentrate is extracted [60].
- **Flotation**: The valuable sulphides are concentrated by flotation.
- **Smelting**: The flotation concentrates are smelted to produce a copper-nickle matte.
- **Separation**: Hydrometallurgical separation of the base metals from the precious metals.
- **Refining**: Finally, the concentrate is refined to separate the individual PGM and gold in their pure forms.

Each processing step is designed to increase the grade of the economic components of the original ore, while reducing the bulk of the products [41, 56].

For this particular project, we have only engaged with the flotation process, in order to prepare concentrate samples using the froth flotation method for the three ore types mentioned above. Therefore, the next section will discuss briefly the fundamentals of flotation.

2.4.1 Principles of flotation

The aim of the froth flotation process is to maximise recovery of PGM and sulphide minerals and minimise the amount of gangue minerals in concentrates [41]. In the laboratory flotation

process, milled ore mixed with water (pulp) is transfered to a flotation cell. Various chemicals are added to the pulp in a sequence that renders the valuable minerals hydrophobic (water-repellent) and the non-valuable minerals hydrophilic. Air is dispersed through the flotation cell and rises to the surface. The hydrophobic particles attach to the rising air bubbles and are removed from the main volume of pulp as a froth that contains the valuable minerals termed "concentrate", while the slurry that remains in the flotation cell (Fig 2.4) contains the unwanted minerals and is referred to as "tailings".

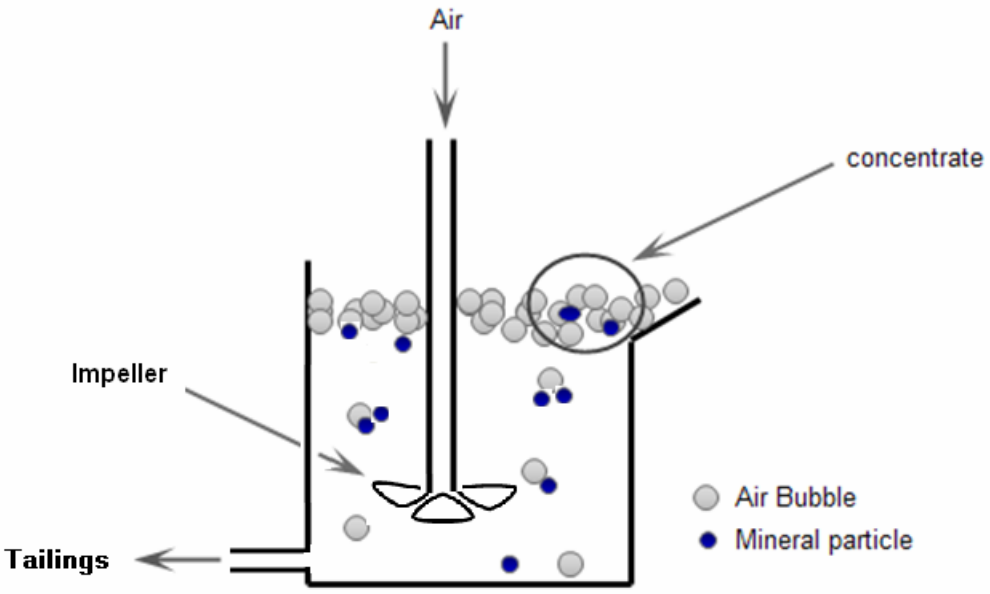

FIGURE 2.4: A simple froth flotation cell.

Recovery of minerals to the froth phase may occur through attachment to flowing bubbles (true flotation), which is selective, or by entrainment in water passing from the pulp phase to the froth phase (particles carried with the water between the bubbles), which is non-selective.

2.4.1.1 Flotation reagents

Flotation reagents are added to the pulp to manipulate mineral surface chemistry and thereby enhance differences in mineral hydrophobicity, facilitating separation of valuable minerals from gangue minerals [54]. The chemistry of the flotation process is particularly complex and there is a synergistic effect between the different reagents. Reagents used in the froth flotation of minerals can be classified into four types, collectors, frothers, depressants, and occasionally activators.

Collectors work to render the surface of valuable minerals hydrophobic. They are usually surface-active compounds (caustic alkali liquids), e.g. sodium isobutyl xanthate (SIBX), and sodium isopropyl xanthate (SIPX) are the most commonly used collectors in the mineral processing industry.

Activators enhance collector attachment to the valuable mineral. They are sometimes needed to further encourage the flotation of the desired mineral. The most commonly used activator is copper (II) sulphate pentahydrate ($CuSo_4.5H_2O$). Copper sulphate is used widely in the mineral processing industry as an activator for pyrrhotite.

Depressants ensure that minerals other than the valuable minerals do not float by enhancing the hydrophilic character of the gangue, and suppress the flotation of naturally hydrophobic gangue material. Industrial organic depressants fall into two main categories; Carboxmethyl-cellulose (CMC), and Guar Gum. To minimise the amount of floatable gangue minerals in the concentrate a high dose of depressant can be used.

One of the key stages in froth flotation is the formation of stable froth, which can retain the valuable minerals for further upgrading. Frothers are surface-active, usually non-ionic, molecules whose function in the flotation system is to enable a stable froth to be formed and efficiently concentrate the attached valuable mineral particles from the slurry, and ensure that a floated particle will not fall back into the flotation pulp before it can be removed. They help in bubble formation as well as stabilising the froth [61].

2.5 Analytical techniques for the determination of precious metals and their associates in geological and related materials

There is an increasing demand world wide for the platinum-group metals. This is mainly due to their wider applications in advanced technology, which has led the mining and mineral industries to improve the analytical methods in use for the determination of platinum-group elements as well as for gold, silver, copper, and nickel in geological matrices, from exploration soils and sediments through ores, concentrates, and final products [62, 63]. Recent years have shown a considerable development of the analytical techniques used in this field [44, 64]. A number of certified PGEs reference materials, which could be used to validate methodologies of laboratories, have been developed and distributed over the years for use in the mining industry [63].

In the case of ores the distribution of the PGE is inhomogeneous, requiring large samples (10 g and more) to provide representative analyses. Thus, a pre-concentration stage is necessary to extract the individual element from the host matrix prior to analysis by an instrumental analytical technique. On the other hand, in the case of concentrates, where the PGE are present at high concentrations, it is possible to use direct methods of analysis without chemical pre-concentration [63].

Common analytical techniques used are nuclear techniques such as X-ray fluorescence (XRF) [65], neutron activation analysis (NAA), and proton-induced X-ray emission (PIXE), which are generally considered as reference methods for many analytical problems [44]. Various instrumental techniques are also being used, such as flame atomic absorption spectrometry (FAAS), graphite furnace atomic absorption spectrometry (GFAAS), inductively coupled plasma atomic emission spectrometry (ICP-AES) and inductively coupled plasma mass spectroscopy (ICP-MS) [44, 63, 66].

Many studies have been focused on the determination of impurities in fine precious metals and their alloys. ICP-AES is used on a routine basis for the PGE analysis in these samples. Nevertheless, a brief review of the currently used final measurement techniques reveal that ICP-AES offers relatively poor sensitivity for the heavy elements [63]. On the other hand, ICP-MS and NAA offer superior detection limits and are widely used all over the world for the estimation of gold and PGEs [44].

In the field of mineral processing, there is an increasing trend in recent years towards the use of automated imaging techniques for the measurement of mineral composition and texture to help solve mineral processing problems [67]. A number of such techniques have been proposed including automated optical image analysis, automated electron microprobe and automated scanning electron microscopy [68]. Quantitative evaluation of minerals by scanning electron microscope (QEMSCAN or QEM*SEM) is widely used in studies relating to mineral processing [42, 68]. The applications of QEMSCAN range from plant studies to laboratory experiments aimed at improved understanding of the behaviour of composite particles [67].

Among all these techniques, neutron activation analysis provides high sensitivities attainable not only for the noble metals, but also for the determination of the less abundant and economically less important elements [62]. With the exception of inductively coupled plasma-mass spectrometry (ICP-MS) on liquid samples, NAA offers sensitivities that are superior to those possible by other analytical methods [30, 69]. As a general example, the role of

instrumental NAA in obtaining analytical data on some geological samples is shown in Fig 2.5. The following chapter will provide some details on neutron activation analysis.

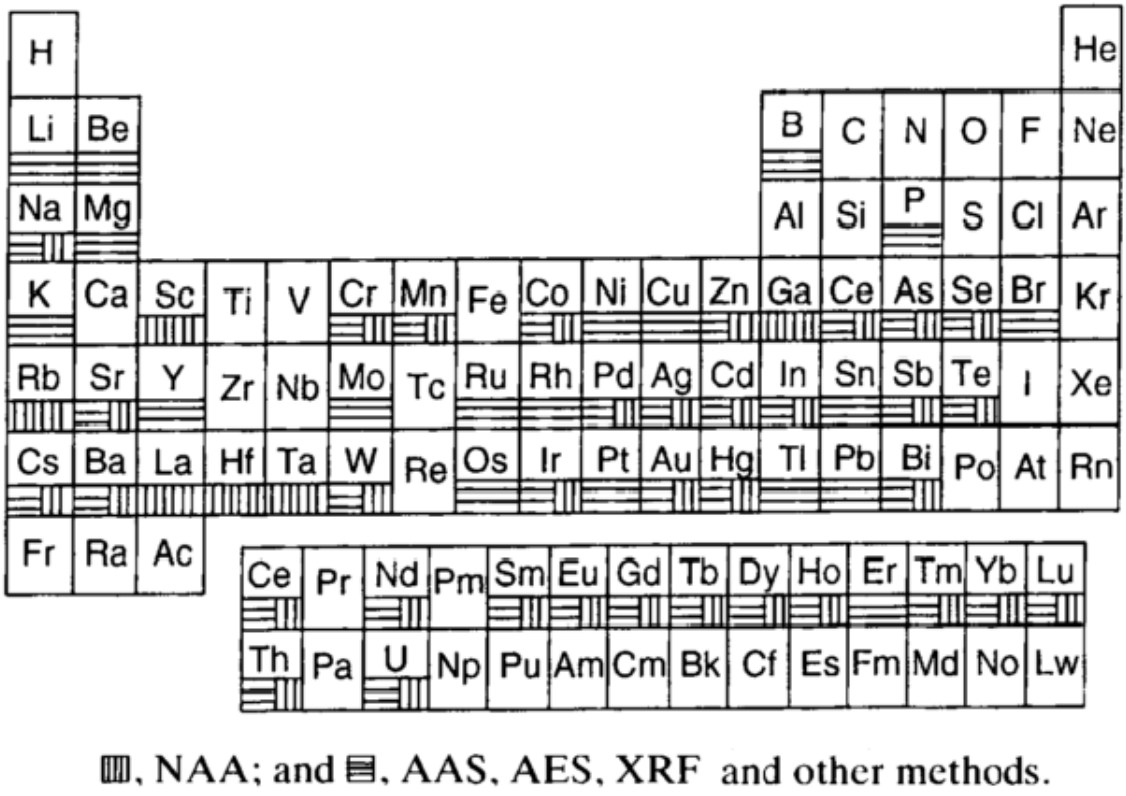

FIGURE 2.5: Analytical methods used in elemental determination of rocks (and soil) to the order of < 1 ppm, [24].

Chapter 3

Neutron Activation Analysis

3.1 Fundamentals of neutron activation analysis

The basic equipment required to carry out an analysis of samples by NAA are a strong source of neutrons and instrumentation suitable for measuring gamma-ray spectra.

3.1.1 Neutrons

Neutrons are electrically neutral, hence pass through nearly any material, and interact with the nucleus of the atom, rather than the electron shell. This allows the total elemental content of the sample to be observed regardless of its oxidation state, chemical form or physical state [39].

According to their energies, neutrons can be approximately classified as follows:

- **Thermal neutrons** have very low energies (0.025 eV) at room temperature (corresponding to a mean neutron velocity of 2200 m s^{-1}). They are produced when neutrons from any source are slowed down by elastic collisions with moderators, i.e. hydrogen-containing substances such as paraffin, water, or graphite [70].
- **Epithermal neutrons** have energies in the range of 0.5 eV to 10 keV.
- **Fast neutrons** have energies greater than 10 keV.

The choice of the neutrons, to activate a sample, depends on the amount of neutrons available from the source and the probability of an interaction to occur between the neutrons and the sample nuclei. The amount of neutrons available from a neutron source for irradiation is called the *neutron flux*, and is conventionally expressed in units of the number of neutrons passing through a squared centimetre per second (n cm^{-2} s^{-1}). For example, thermal neutron activation analysis requires at least a minimum neutron flux of 10^9 to 10^{10} n cm^{-2} s^{-1}. The probability for an incident neutron to be captured by a target nucleus, described by neutron capture cross-section (see Section 3.1.5), depends on the energy of the neutron and the nature of the target nucleus [71].

3.1.2 Neutron sources

There are three main sources of neutrons for activation analysis: nuclear reactors, particle accelerators, and radioisotopic neutron sources. Among these, the choice of the most suitable neutron source should be based on the specific requirements of the analysis [15]. Nuclear reactors provide high neutron fluxes and therefore permit very high sensitivities for the quantitative determination of various elements. Radioisotopic neutron sources provide neutron fluxes that are less intense than reactors. Accelerators will not be discussed here, as such discussion is irrelevant to this work.

3.1.2.1 Nuclear reactors for NAA

The spectrum of neutrons from a fission reactor can be broadly divided into three parts as illustrated in Fig (3.1). Under the appropriate conditions, these fission neutrons can promote a self-sustaining branching chain reaction [71]. Fast neutrons are produced in the fission, but they are rapidly moderated by collisions with atoms in the reactor.

Among the different types of research reactors, thermal reactors are the most common. An important characteristic of these reactors is the easy access to the neutrons in the core. They are usually supplied with tubes that permit samples to be inserted into the core and withdrawn without affecting other research work being carried out with the reactor. The samples are carried in little containers are called “rabbits” because of the speed at which they travel in and out of the reactor [7, 72].

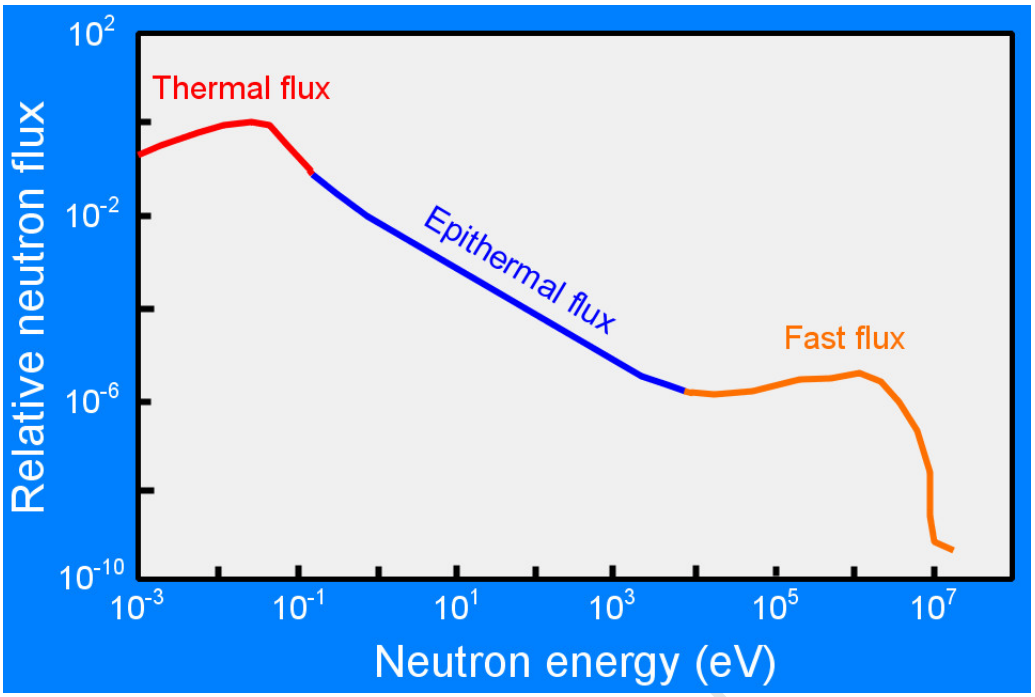

FIGURE 3.1: A typical neutron energy spectrum from a nuclear fission reactor. Image adopted from (http://serc.carleton.edu/).

3.1.2.2 Radioisotopic neutron sources for NAA

Radioisotopic neutron sources are small, portable, and easily maintained. However, they produce lower fast neutron fluxes, which limits their NAA applications to the determination of high-abundance, or high cross-sections elements [2, 13].

The radioisotopic neutron sources include spontaneous fission neutron sources (e.g ^{252}Cf), photoneutron sources based on (γ, n) reaction, and isotopic neutron sources [15, 72]. In the third type the neutrons are created in the (α, n) reactions, which occur in a carefully prepared mixture of beryllium and an alpha emitter, e.g.,^{241}Am-Be, ^{238}Pu-Be, ^{210}Po-Be. This nuclear reaction results in the emission of a neutron and the production of a stable carbon as follows [73]:

$$^{9}_{4}\mathrm{Be} + {}^{4}_{2}\mathrm{He} \longrightarrow {}^{1}_{0}\mathrm{n} + {}^{12}_{6}\mathrm{C} + 5.5\ \mathrm{MeV}. \tag{3.1}$$

^{241}Am-Be sources are the most commonly used isotopic neutron sources for routine laboratory work. The long half-life (433 years) of ^{241}Am provides an almost constant neutron flux [74].

3.1.3 Radioactive decay

The nuclei of atoms are characterized by their atomic and mass numbers. The atomic number, number of protons in a nucleus (Z), determines an element's identity; while the mass number, number of neutrons (N), usually determines whether or not that atom is radioactive or stable. However, there are some exceptions, a few elements are naturally radioactive and have no stable nuclei [75]. The stability of the nucleus is related to the neutron-to-proton ratio. An excess of protons will cause a Coulomb repulsion, whereas neutron excess decreases the nuclear forces.

The chart of nuclides, Fig 3.2, explains the stability of nuclides in terms of a plot of N versus Z. Stable nuclides occupy the bottom of a nuclear "stability valley". Nuclides on the high sides of this valley are unstable. The neutron-to-proton ratio in the stable nuclei varies from 1 for light stable nuclei to around 1.5 for heavier stable nuclei [76]. When a nucleus has a neutron-to-proton ratio too high for stability it tends to decrease the number of excess neutrons and to increase the number of protons by transformation of a neutron into a proton with the emission of an electron (β^-) and an anti-neutrino ($\bar{\nu}$). When a nucleus has a neutron-to-proton ratio too low for stability, it can decrease the number of excess protons by one of three processes: alpha emission, positron (β^+) emission, and orbital electron capture (K-capture) [77].

The mode of decay of a radioactive nuclei is universally agreed to be displayed in a form of "decay scheme". A complete decay will contain all the necessary information about the decay process, from the excited state of the nucleus to its ground state [70]. Fig 3.3, shows common representation of decay schemes. The energy levels are represented by horizontal lines, whereas arrows from parent to daughter energy levels show the energetically different decay modes. The electromagnetic transitions (gamma-rays) are represented by vertical arrows among energetic levels within the same nucleus. These gamma-rays are emitted from the excited daughter which stand as an indicator of the parent nucleus [77].

Radioactive nuclei, that produced by neutron capture reaction, almost always decay by emitting negatively charged beta particles usually accompanied by gamma rays. These decay modes may be associated with X-rays as well [32].

3.1.3.1 Interaction of gamma-rays with matter

Gamma rays consist of electromagnetic radiation, photons, emitted as a result of transitions between nuclear energy levels. According to their energies, Fig 3.4, gamma rays have no mass

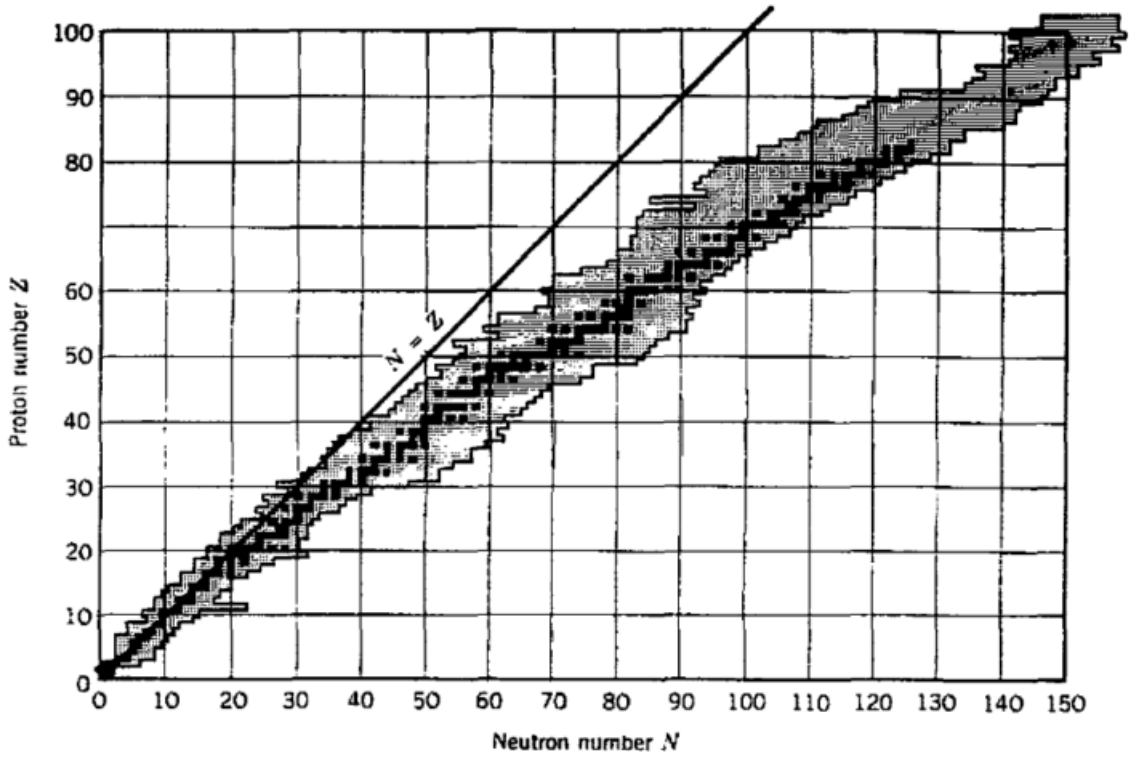

FIGURE 3.2: Nuclear Landscape, within the horizontal strip of isotopes, stable species are shown with a black background. adapted from [78].

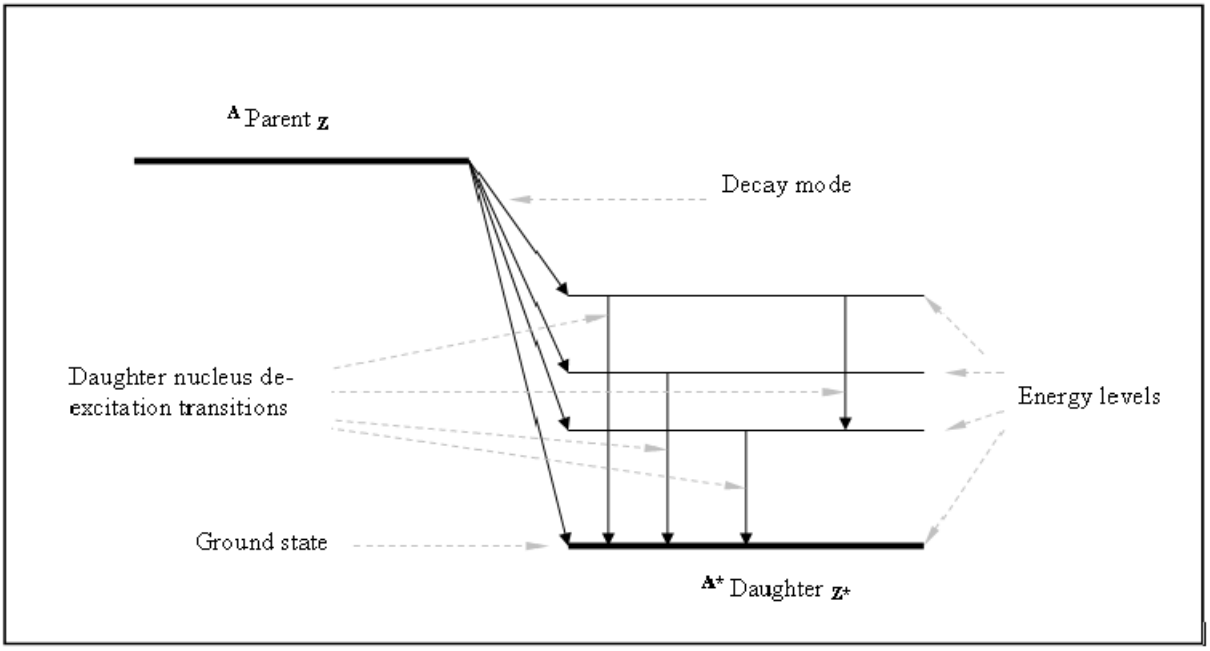

FIGURE 3.3: Graphical representation of a decay scheme. adopted from [77].

and no electric charge. Gamma-rays are emitted in the form of photons, discrete bundles of energy that have both wave and particle properties. Gamma-ray photons have the highest

energy in the electromagnetic radiation spectrum and consequently their waves have the shortest wavelength. These photons carry the energy released in a transition between states in a nucleus. The time characteristics of their emission represents the half-life time of the initial nuclear state, which is commonly a fraction of a second. Often gamma-ray emission occurs after β-decay. The time characteristics then reflect the lifetime of the β-decaying states and this may be very long, up to years. Gamma radiation is a very high-energy ionising radiation, implying that it has enough energy to remove tightly bound electrons from atoms. They interact with the matter via one of the following processes: Photoelectric effect, Compton effect, or pair production [79].

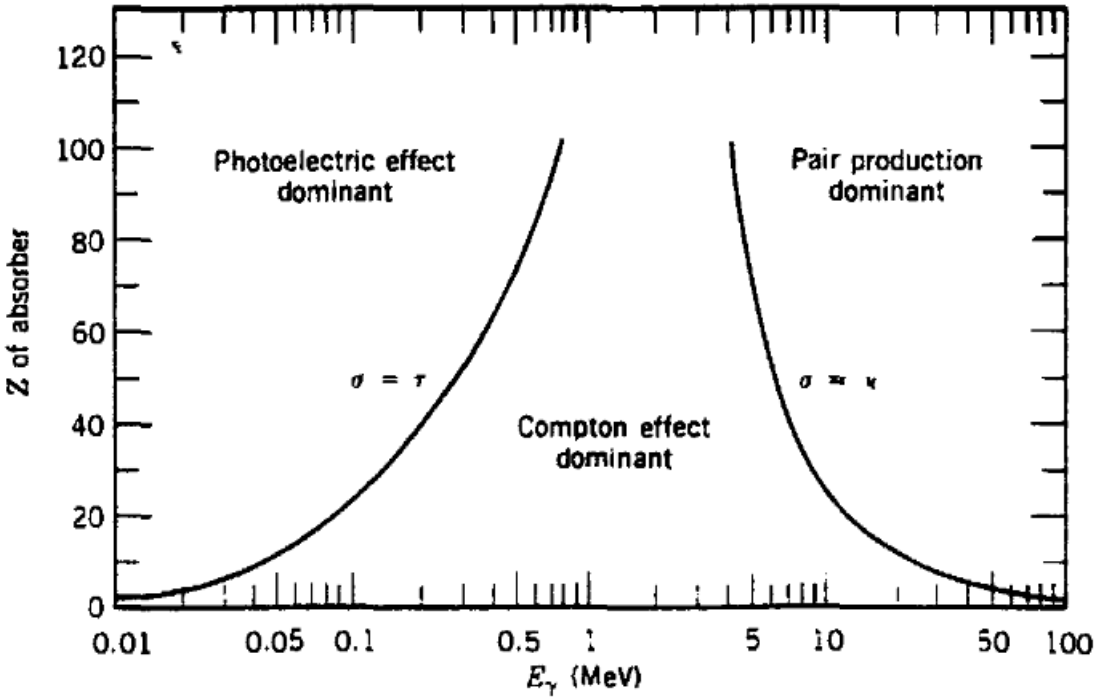

FIGURE 3.4: The three major gamma-ray interactions processes and their regions of dominance [79].

- Photoelectric effect: an interaction between a low-energy gamma-ray photon (E_γ= 60 KeV) and an inner orbital electron of an atom of the absorbing material. As a result of the interaction, the photon disappears and the electron is ejected with an energy equal to the photon energy minus the electron binding energy. Almost immediately the orbital electrons are rearranged and a characteristic X-ray, for the absorbing material, is emitted. Thus, photoelectric interactions always yield characteristic X-rays of the detector material.

  Energies of both ionized electron and X-ray are usually absorbed by further ionization of detector atoms. However, there is a possibility that the X-rays may escape from the

detector without further interaction in a form of "escapepeak". However, for incident radiation above 60 KeV, the probability of escape peak losses become negligible due to the decreasing probability of photon interaction with the detector by the photoelectric effect [71].

- Compton effect: results from an inelastic collision between a gamma-ray photon and an outer-orbital electron of an atom. This interaction occurs if the energy of the photon is of the order of KeV or more, while the binding energy of the electron is of the order of eV, i.e."free electron". e order of eV, i.e.free electron. During this collision, part of the gamma energy is transferred to the electron, whereas the gamma ray, which is now less energetic, is detected through an angle θ with respect to the incident direction , Fig 3.5.

  Maximum transfer of energy results from a head-on interaction following which the secondary gamma-ray is emitted at 180^o to the first. The energy of the gamma-ray after collision is a function of the scatter angle θ, and is given by

$$E_\gamma = \frac{E_o}{1 + (E_o/m_o c^2)(1 - cos\theta)} \tag{3.2}$$

  The secondary gamma photon can either be absorbed by further Compton or photo-electric interactions, or escape from the detector. Compton scattering is the main cause of the high background continuum below the energies of principal gamma photopeaks recorded on germanium detectors [71].

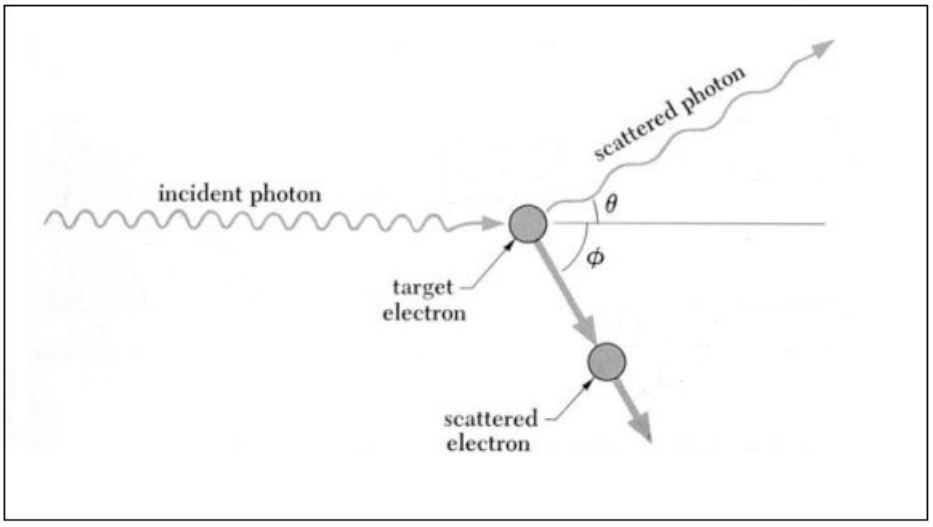

FIGURE 3.5: Compton scattering.

- Pair production: occurs only when incident gamma-rays exceed 1022 KeV. There is then a small probability that interaction in the intense electromagnetic field surrounding the nucleus will result in complete transmutation of gamma photon energy and give rise to an electron-positron pair. The gamma energy thus appears in the form of the rest mass of the two particles and as kinetic energy of the particles. Such particles lose their kinetic energy by further collision with atoms in the detector and then spontaneously annihilate to generate two 511 KeV back-scattered gamma rays. If one of these annihilation photons escapes from the detector, an event is detected at 511 KeV (single annihilation peak). If both are lost, double annihilation escape peak is detected at 1022 KeV line. A single annihilation peak will also be detected if pair production occurs in matter surrounding the detector. Pair production is not a significant interaction for incident radiation below 2000 KeV [71].

These interactions represent the main features of the gamma-ray spectrum. Fig 3.6 shows a typical gamma-ray spectrum of ^{28}Al.

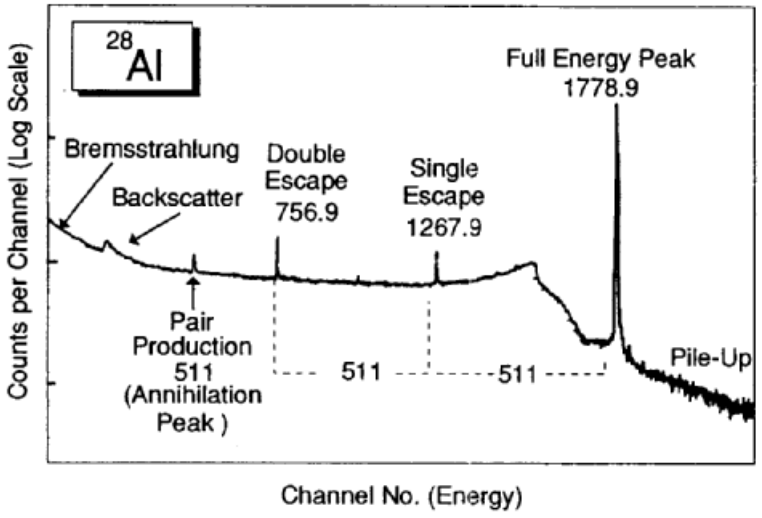

FIGURE 3.6: Nuclear Landscape, within the horizontal strip of isotopes, stable species are shown with a black background. adapted from.

3.1.3.2 Interaction of neutrons with matter

The neutrons interact with nuclei through the strong nuclear interaction, but have to pass close to a nucleus for an interaction to occur. The neutron interact with a target nucleus in one of two ways: scattering or absorption. Scattering reactions are either elastic or inelastic (Fig 3.7). In elastic scattering, a neutron collides with a nucleus without changing the

structure of the target nucleus. However, the neutron changes direction and speed, and the nucleus recoils. Thus, the total kinetic energy of the system is unchanged, but the neutron transfers some of its energy to the target nucleus. In case of a collision with a light nucleus, the neutron's loss of kinetic energy is relatively high resulting in the neutron being moderated. In inelastic scattering, the target nucleus is left in an excited state, and decays to the ground state with the emission of one or more γ-rays [80].

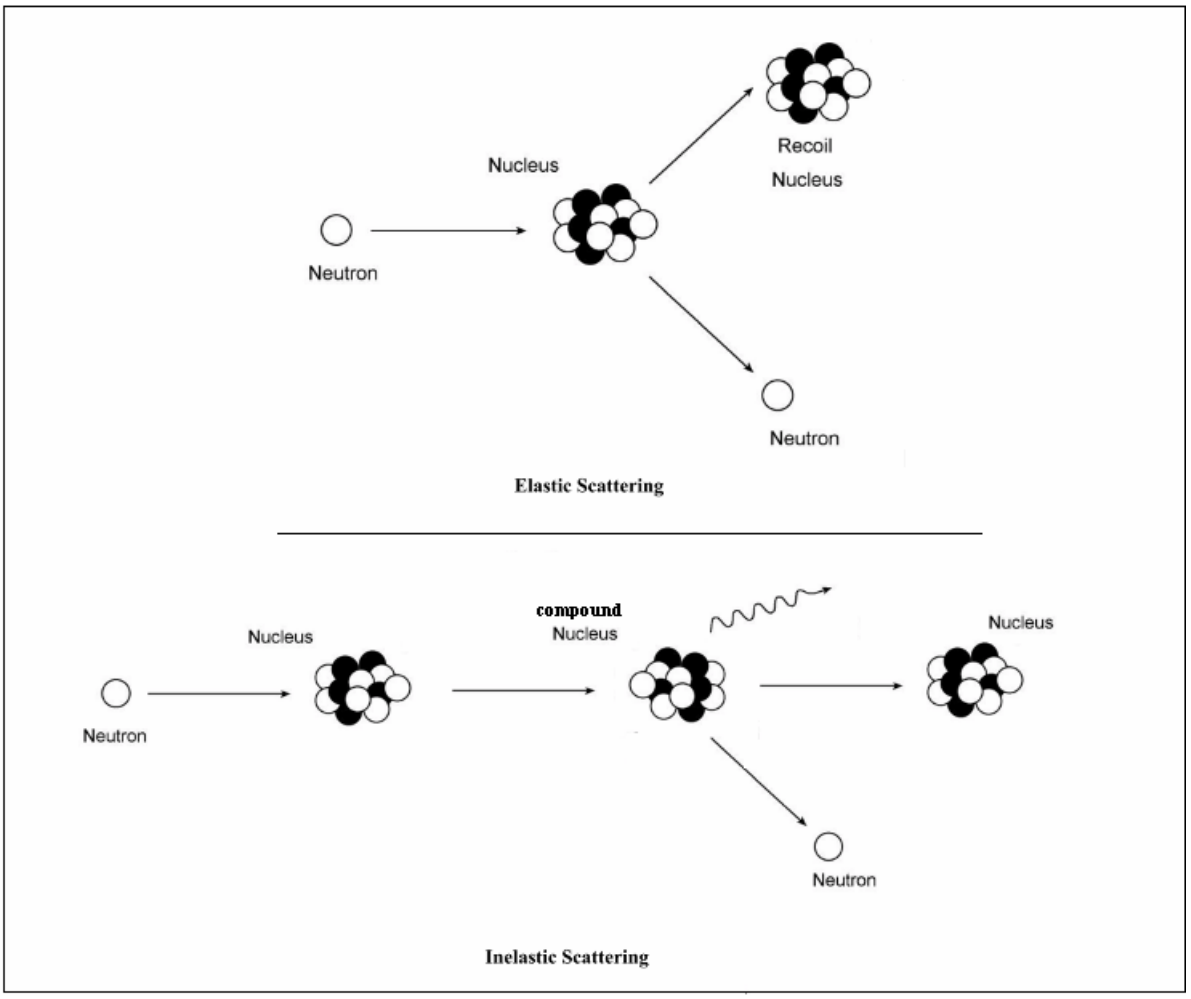

FIGURE 3.7: Neutron scattering interactions. Image adopted from [81].

In an absorption reaction, the neutron is captured in the targeted material, producing one or more reaction particles [12, 72]. The neutron capture reaction is the main form of interaction of thermal neutrons with matter. In this case, the capture of the neutron creates a nucleus with an atomic weight of one more unit than the parent [75]. The ability of a nucleus to capture a neutron depends on the type of nucleus as well as the neutron energy. Thus, not all elements are suitable for (n, γ) reactions. Some of the elements may be determined by (n,p), (n,α), (n,n') or (n,2n) reactions with fast neutrons [15].

When a nucleus undergoes a neutron capture reaction (Fig 3.8) the compound nucleus rearranges its internal structure to a more stable configuration by emitting one or more characteristic "prompt" γ-rays (typically within 10^{-12} s). In most cases, this will be followed by β^- decay associated by characteristic "delayed" γ-rays, [3, 72]. These decay modes may also produce X-rays [10]. In principle either the prompt or delayed γ-rays can be used for both qualitative and quantitative analysis, but the majority of NAA applications are based on the measurement of the delayed γ-rays [12].

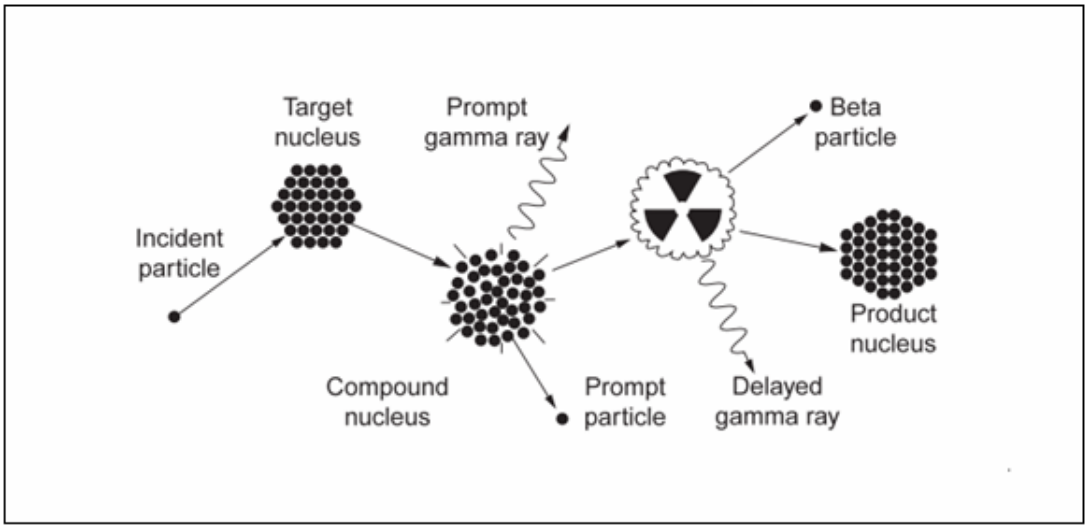

FIGURE 3.8: Neutron capture reaction [30].

Generally β^- particles are not useful for analytical purposes because in β^- decay the total energy is shared between the beta particle and the anti-neutrino ($\bar{\nu}$):

$$n^0 \longrightarrow p^+ + \beta^- + \bar{\nu}. \tag{3.3}$$

On the other hand, gamma rays accompanying β^- decay have characteristic energies which make them suitable for identification of the emitting radioisotope and thus the parent element [82]. The technique of gamma spectrometry for NAA is based on the uniqueness of gamma energies in the characterisation of radioactive species, and the high precision with which such energies can be measured [76].

3.1.4 Analysis of gamma-ray spectra

Complex gamma-ray spectra require treating each peak, its background, and its interferences individually [15]. Calculation of the amount of an element activated in a sample involves the determination of the area of the peak in the gamma-ray spectrum. A peak area can be found by summing data points within the peak or by fitting it to a functional form [30].

For each peak, the net peak area (N_P) is determined by subtracting an estimated background (N_B) from the total number of counts under the peak (N_T) as follows:

$$N_P = [N_T - N_B]\,. \tag{3.4}$$

The standard deviations in the gross counts in the peak (σ_T) and the counts in the background (σ_B) propagate to give the standard deviation in the net counts (σ_P) as below

$$\sigma_P = \sqrt{{\sigma_T}^2 + {\sigma_B}^2} \tag{3.5}$$

$$= \sqrt{N_T + N_B} \tag{3.6}$$

$$= \sqrt{N_P + 2N_B}. \tag{3.7}$$

The uncertainty in the net peak area is reported by calculating the relative standard deviation in per cent (% σ_P):

$$\%\ \sigma_P = \left(100\ \sqrt{N_P + 2N_B}/N_P\right). \tag{3.8}$$

The limit of detection for a peak depends on how well the background is known. The usual definition for the detection limit is based on the two-sigma (around 95%) probability that a peak should be observed above the background [30].

Activity concentrations could be determined as follows:

$$A_c(Bq/kg) = \frac{counts}{Br\ \epsilon\ LT\ m} \tag{3.9}$$

where *counts* represent the full-energy peak content corrected for continuum, Br the branching ratio (that is the percentage of the decay of the nuclide that will proceed via the emission of a particular gamma-ray), ϵ the detector's efficiency, LT the live time (in s) for spectrum acquisition and m (in kg) the sample mass.

3.1.5 Neutron cross-sections

The probability that a neutron will interact via a certain process with a given nucleus is described by the "microscopic cross-section" or "reaction cross-section". For a given reaction, microscopic cross-section can be thought of as the effective cross-sectional area which the

target nucleus presents to the neutron for the reaction, and depends on the kind of the nucleus as well as the energy of the neutron involved [80, 83].

Dependence of the neutron cross-section on the energy of the neutron is shown in Fig (3.9). On average, at neutron energies less than about 0.5 eV, neutron cross-section are smooth functions of energy. As neutron energies increase above 0.5 eV, the cross-sections for most target nuclides are characterised by a number of resonance peaks. The energies of the resonance peaks coincide with the excited states of the compound nucleus [30]. At higher neutron energies, the cross-sections for (n, γ) reactions are very small, and nuclear reactions that result in the ejection of one or more particles (n,p), (n, α), (n, n'), and (n,2n) reactions dominate [30].

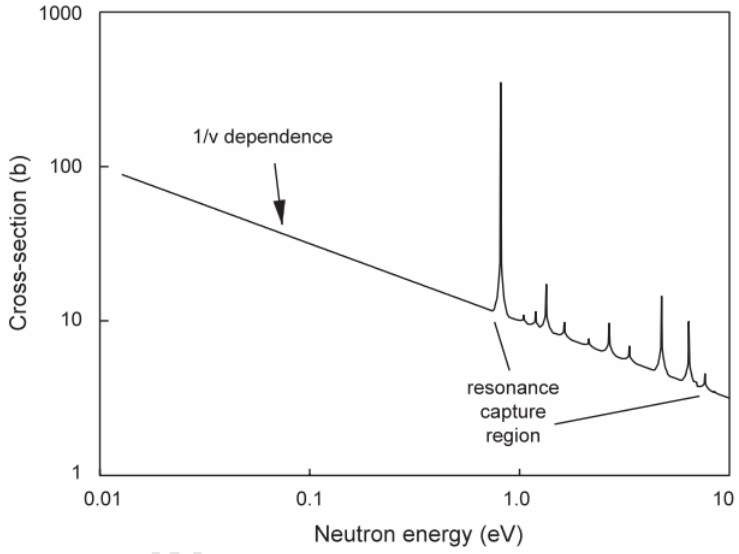

FIGURE 3.9: Schematic of neutron capture cross-section versus energy for a common neutron capture reaction involving thermal and epithermal neutrons [30].

For example, Figs 3.10 and 3.10 show illustrations of the neutron capture reaction with ^{23}Na nucleus and ^{152}Sm nucleus, respectively.

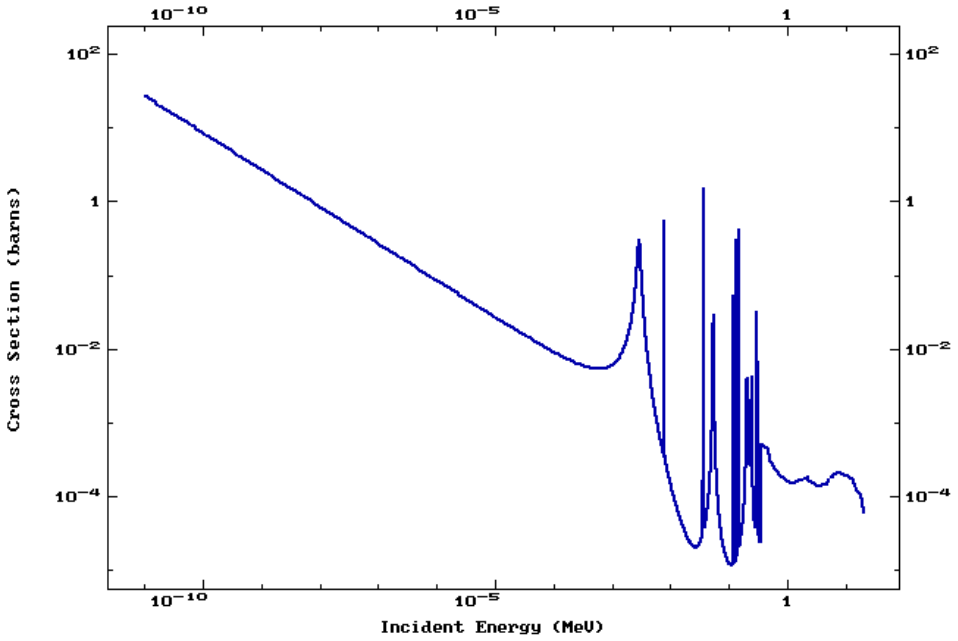

FIGURE 3.10: Neutron capture cross-section for ^{23}Na [84].

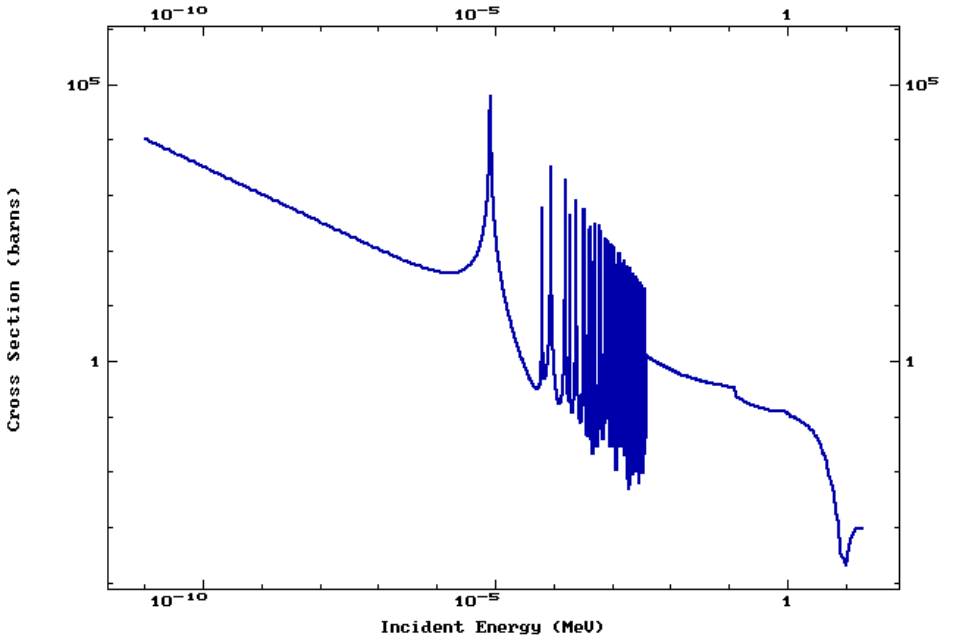

FIGURE 3.11: Neutron capture cross-section for ^{152}Sm [84].

The scattering cross-section (σ_s) and absorption cross-section (σ_a) are usually distinguished from one another; each of these cross-sections is composed of partial cross-sections such as elastic and inelastic scattering, neutron capture, etc. The sum of all partial cross-sections is called the total cross-section (σ_t):

$$\sigma_t = \sigma_s + \sigma_a. \tag{3.10}$$

Whether a neutron will interact within a certain volume of material depends not only on the microscopic cross-section of the individual nuclei but also on the number of nuclei within that volume. Therefore, it is suitable to introduce the macroscopic cross-section $\Sigma(\mathrm{m}^{-1})$, which is the probability that the neutron is scattered or absorbed per unit length [83, 85]. The macroscopic cross-section ,Σ (m^{-1}) is related to the microscopic cross-section σ (m^2) as a function of neutron energy (E) by the expression

$$\Sigma(E) = N\sigma(E) \tag{3.11}$$

where the atom density N (m^{-3}) is the number of atoms per unit volume of the material and can be obtained by

$$N = \frac{\rho}{M} N_A \tag{3.12}$$

where ρ ($\mathrm{kg\ m}^{-3}$) is the density of the material, N_A (mol^{-1}) is Avogadro's number and M ($\mathrm{kg\ mol}^{-1}$) the atomic weight.

Microscopic cross-sections represent an effective target area that a single nucleus presents to a bombarding particle, while a macroscopic cross-section represents the effective target area presented by all nuclei contained in a unit volume of the material [79]. The average distance traveled by a neutron before interaction, known as the mean free path λ (m), is related to the macroscopic cross-section by

$$\lambda = \frac{1}{\Sigma}. \tag{3.13}$$

The neutron flux ϕ ($\mathrm{m}^{-2}\mathrm{s}^{-1}$) can be defined as the total path length traveled by all neutrons per unit volume during one second

$$\phi = n\nu \tag{3.14}$$

where the neutron density n (m^{-3}) is the number of free neutrons moving through a unit volume of material with average velocity ν (ms^{-1}).

The initial intensity (I_o) of the neutron beam will decrease exponentially when traversing a material with thickness d. This exponential attenuation is given by

$$I = I_o e^{-\Sigma_{tot} d} \tag{3.15}$$

where Σ_{tot} is the total macroscopic cross-section for all processes occurring in the material, and I is the final intensity [79]

$$\Sigma_{tot} = \Sigma_{inelastic-scattering} + \Sigma_{elastic-scattering} + \Sigma_{capture} + \dots \tag{3.16}$$

In addition, given a mixture of nuclides, with atom densities $N_1, N_2, \dots$, and microscopic cross-sections $\sigma_1, \sigma_2, \dots$, for any type reaction, the macroscopic cross-section for the mixture can be calculated as

$$\Sigma_{tot} = \Sigma_1 + \Sigma_2 + \dots \tag{3.17}$$

$$= N_1\sigma_1 + N_2\sigma_2 + \dots \tag{3.18}$$

The rate R_x ($\mathrm{m^{-3}s^{-1}}$) at which a particular nuclear reaction (x) will occur will thus depend on the neutron flux, the cross-section for the interaction (σ_x) and the atom density of the target

$$R_x = \phi\,(N\sigma_x) \tag{3.19}$$

$$= \phi\ \Sigma_x. \tag{3.20}$$

3.1.6 Basic equations of growth and decay of radioactivity

Considering a simple case where a sample containing N_x nuclei of the stable isotope X, which has undergone neutron activation with a neutron flux ϕ, and decayed producing a radioactive nucleus Y that decay to a stable nucleus Z:

$$\mathrm{X} \xrightarrow{n,\gamma} \mathrm{Y} \xrightarrow{\lambda_y} \mathrm{Z\ (stable)}$$

During irradiation, the net rate of change of the radioactive atoms N_y is equal to the difference between the rate of formation and the rate of decay; that is,

$$\frac{dN_y}{dt} = N_x\phi\sigma - \lambda_y N_y \tag{3.21}$$

where λ_y ($\mathrm{s^{-1}}$)is the decay constant of radioisotope Y, $\lambda = 0.693/\mathrm{t}_{1/2}$, ϕ ($\mathrm{m^{-2}s^{-1}}$) is the neutron flux, and σ ($\mathrm{m^2}$)is the neutron cross section. Initially, before the beginning of the irradiation, there is no formation of radioactive nuclei. Integrating Eq 3.21 and substituting the initial conditions where $t = 0$ and $N_y = 0$ gives

$$N_y = \frac{N_x\phi\ \sigma}{\lambda_y}\left[1 - e^{-\lambda_y t}\right]. \tag{3.22}$$

The induced activity (A_y) at any time during irradiation is therefore

$$A_y = \lambda_y \mathrm{N}_y \tag{3.23}$$

$$= N_x \phi\ \sigma \left[1 - e^{-\lambda_y t}\right]. \tag{3.24}$$

The factor within the brackets of Eq (3.24) is the "saturation factor" (S), which is seen to vary between zero and unity. Thus, Eq (3.24), can be re-written as

$$A_y = N_x \phi \sigma S. \tag{3.25}$$

At a very long irradiation time, the saturation factor S approaches unity. This is the point where further irradiation no longer increases the number of radioactive atoms present in the target [71, 86]. After an irradiation time greater than about six half-lives of Y, the activity of Y reaches the limiting value "saturation activity".

If the irradiation ends at time t_{irr}, the activity at this time is [3, 8]:

$$A_{y,t_{irr}} = N_x \phi\ \sigma \left[1 - e^{-\lambda_y t_{irr}}\right] \tag{3.26}$$

and if the sample is not measured immediately after the end of the irradiation, and left to cool and decay for time t_d, the activity of the sample will then be [3, 8]

$$A_{y,(t_{irr}+t_d)} = N_x \phi\ \sigma \left[1 - e^{-\lambda_y t_{irr}}\right] e^{-\lambda_y t_d}. \tag{3.27}$$

The principal uncertainties that arise in NAA are due to self-shielding, uncertainties for some of the parameters, e.g. unsteady neutron flux, and errors in counting due to absorption, scattering and differences in sample-to-detector geometry [4, 13]. These mistakes are often reduced by using comparator standards containing known amounts of the element of interest, which are irradiated simultaneously with the samples [87, 88] . The percentage of an element in an unknown sample can be determined by comparing the activity induced in a standard of known weight, with that of the unknown. The direct ratio between the amount of element and the activity of the sample is shown in the following equation:

$$\frac{\text{Weight of the element in unknown}}{\text{Weight of the element in standard}} = \frac{\text{Activity in unknown}}{\text{Activity in standard}}. \tag{3.28}$$

This procedure does not include any nuclear data (except the half-life for the decay correction) [89, 90].

3.2 Sensitivity of NAA

Sensitivity in this case means how small an amount of an unknown element can be detected. Neutron activation methods promise possibilities of high sensitivity, which exceeds that of other methods for many elements by a factor of 100 or more, as little as microgram amounts of elements can typically be detected [4].

The sensitivity of NAA varies in practice with a number of practical as well as theoretical factors. These include the properties of the particular nucleus, the half-life of the daughter radionuclide produced, the duration of neutron irradiation, the flux of neutrons available for irradiation, the efficiency of the counting apparatus, possible interferences, type of the radiations accompanying the decay of the daughter radionuclides, and duration of counting [7, 39, 91]. Given NAA's excellent sensitivities, analysis is possible for nearly 70 elements. Under the appropriate experimental parameters, more than 30 elements can be analysed on a simultaneous basis [12].

3.3 Detectors suitable for gamma-ray measurement

The common detectors in the NAA laboratory are the sodium iodide thallium activated scintillation type detector (NaI(Tl)), the lithium-drifted germanium semiconductor detector (Ge(Li)), and the intrinsic or high-purity-germanium (HPGe) semiconductor detector (Fig 3.12) [13]. Intrinsic germanium detectors have the advantages of high relative efficiency and high resolution, and excellent peak-to-Compton ratio, which make the use of NaI(Tl) less essential for NAA. However, the NaI(Tl) detector, having the lowest energy resolution but the highest detection efficiency, is an attractive detector for field applications, as it works well at room temperature [82, 92]. On the other hand, the efficiency of the HPGe detector decreases as the gamma-ray energy increases, but the requirement of high resolution is much more important than high efficiency [77]. Fig 3.12 shows a comparison between the two detectors in terms of energy resolution.

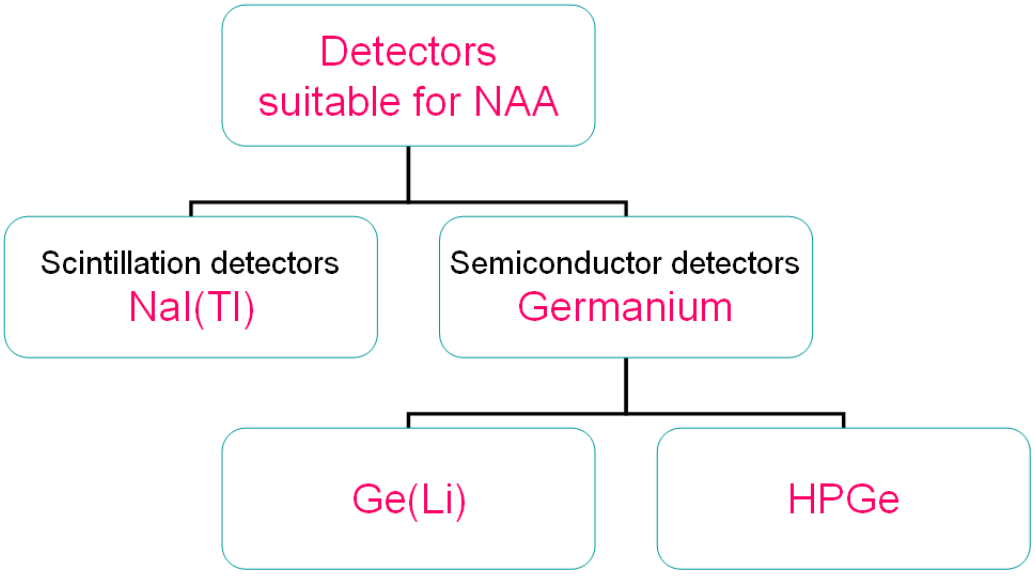

FIGURE 3.12: Detectors suitable for NAA.

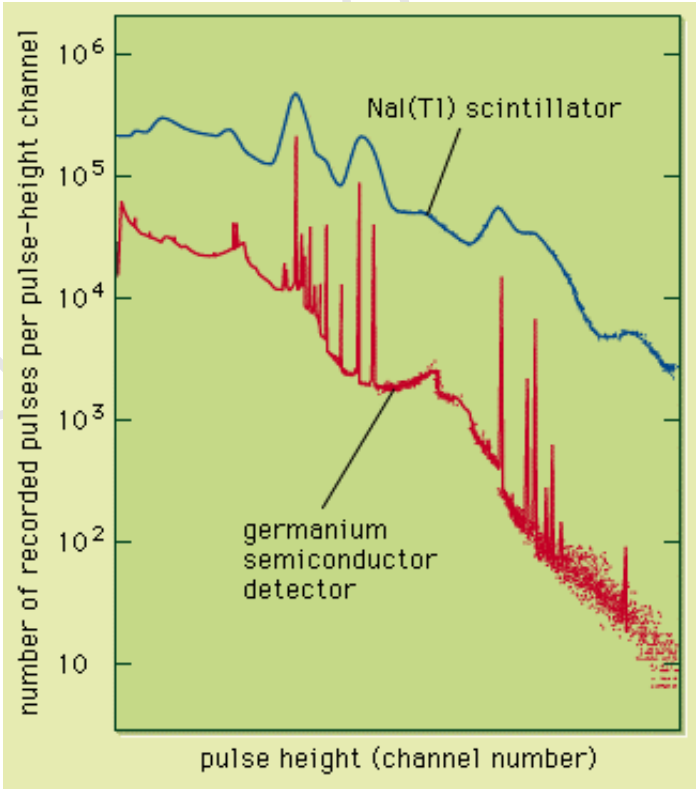

FIGURE 3.13: Comparison between spectra measured by NaI(Tl) and germanium. The superior energy resolution of the germanium detector is evident from the much narrower peaks.

3.3.1 Background radiation

When setting a detection system to detect radiation from a measured sample, and before introducing this sample to the detector, it is common to measure background radiation from the surrounding environment observed by the detector. The background in a spectrum can generally be classified as [73]:

- **Background in the presence of a source**: The background due to the source itself is essentially the continuum generated by Compton scattering and by bremsstrahlung.
- **Background in the absence of the source**: In the absence of the source, background radiation may be detected from both cosmic rays and the decay of naturally-occurring radioactive isotopes (uranium and thorium) present in the environment, especially in building materials. A significant reduction in background counts can be achieved by surrounding the detector with a thick shielding of lead, which decreases the probability of interaction with high-energy cosmic radiation [71].

3.4 Forms of neutron activation analysis

NAA is a useful method for the identification and determination of almost all the elements in the periodic table. The variation of the neutron cross-section of the elements leads to the need of using varying neutron fluxes and energies for irradiating the samples.

3.4.1 Thermal neutron activation analysis

The decay of radionuclides formed by neutron capture reaction involves the emission of prompt and delayed gamma rays. Thus, there are two main approaches to thermal NAA [12, 71]:

- **Prompt gamma neutron activation analysis(PGNAA)**. Neutron induced prompt gamma-ray activation analysis (PGNAA) is based on the detection of instantaneous gamma radiation following the absorption of thermal neutrons [93, 94]. Measurements of prompt gamma spectrum is performed while the sample is being irradiated. It is particularly useful for the determination of light elements such as hydrogen, boron, cadmium, or gadolinium, and elements with low delayed gamma-ray intensities [95, 96].

- **Delayed gamma neutron activation analysis (DGNAA)**. This approach involves the measurement of delayed radiations from the decay of the product radionuclide. This process may be purely instrumental neutron activation analysis (INAA) or may involve radiochemical separations (RNAA).

  Instrumental Neutron Activation Analysis (INAA) is the most common form of neutron activation analysis for individual and multi-elemental analysis. This technique involves the measurement of delayed gamma-rays. The word "instrumental" indicates that the technique is non-destructive, no chemical pre-treatment is performed on the sample before or after the irradiation process [95]. This reduces the contamination risk of samples by impurities in the reagents to the minimal. The samples are simply packaged, irradiated for the specified length of time, allowed to decay, then counted. Table (3.1) lists the approximate sensitivities for determination of elements via instrumental neutron activation analysis, assuming interference free spectra [11]. Fig (3.14) shows the elements, in the periodic table, that are effectively analysed by INAA.

  Unlike INAA, Radiochemical Neutron Activation Analysis (RNAA) is a destructive technique based on the measurement of an indicator radionuclide, chemically separated from a neutron-activated sample. The radiochemical separation carried out during the decay period is characteristic of RNAA. It serves to reduce or eliminate unwanted radionuclides interfering with the measurement of the indicator, and therefore to minimize the uncertainty associated with the determination of a particular element. This procedure is time-consuming and involves specialised laboratory facilities for manipulation of radioactive material [13, 97].

3.4.2 Epithermal Neutron Activation Analysis

This method involves placing the samples into filters of high-cross sections materials, such as cadmium metal or boron containing containers for irradiation. The reason of using cadmium or boron filters is to shield the sample from thermal neutrons, thus the sample is exposed to neutrons with higher energies [13, 15].

3.4.3 Fast Neutron Activation Analysis

Fast Neutron Activation Analysis (FNAA) is usually done with neutron generators producing 14 MeV neutrons, as well as radioisotopic sources, and sometimes the fast component in the

reactor neutron energy spectrum. FNAA is used mainly for lighter elements not amenable to thermal NAA and for elements present at major and minor levels [13, 39].

Sensitivity (picograms)	**Elements**
1	Dy, Eu
1-10	In, Lu, Mn
10-100	Au, Ho, Ir, Re, Sm, W
100-1E3	Ag, Ar, As, Br, Cl, Co, Cs, Cu, Er, Ga, Hf, I, La, Sb, Sc, Se, Ta, Tb, Th, Tm, U, V, Yb
1E3-1E4	Al, Ba, Cd, Ce, Cr, Hg, Kr, Gd, Ge, Mo, Na, Nd, Ni, Os, Pd, Rb, Rh, Ru, Sr, Te, Zn, Zr
1E4-1E5	Bi, Ca, K, Mg, P, Pt, Si, Sn, Ti, Tl, Xe, Y
1E5-1E6	F, Fe, Nb, Ne
1E7	Pb, S

TABLE 3.1: Estimated detection limits for INAA using decay gamma rays, assuming irradiation in a reactor neutron flux of 10^{13} n cm^2 s^{-1} [11].

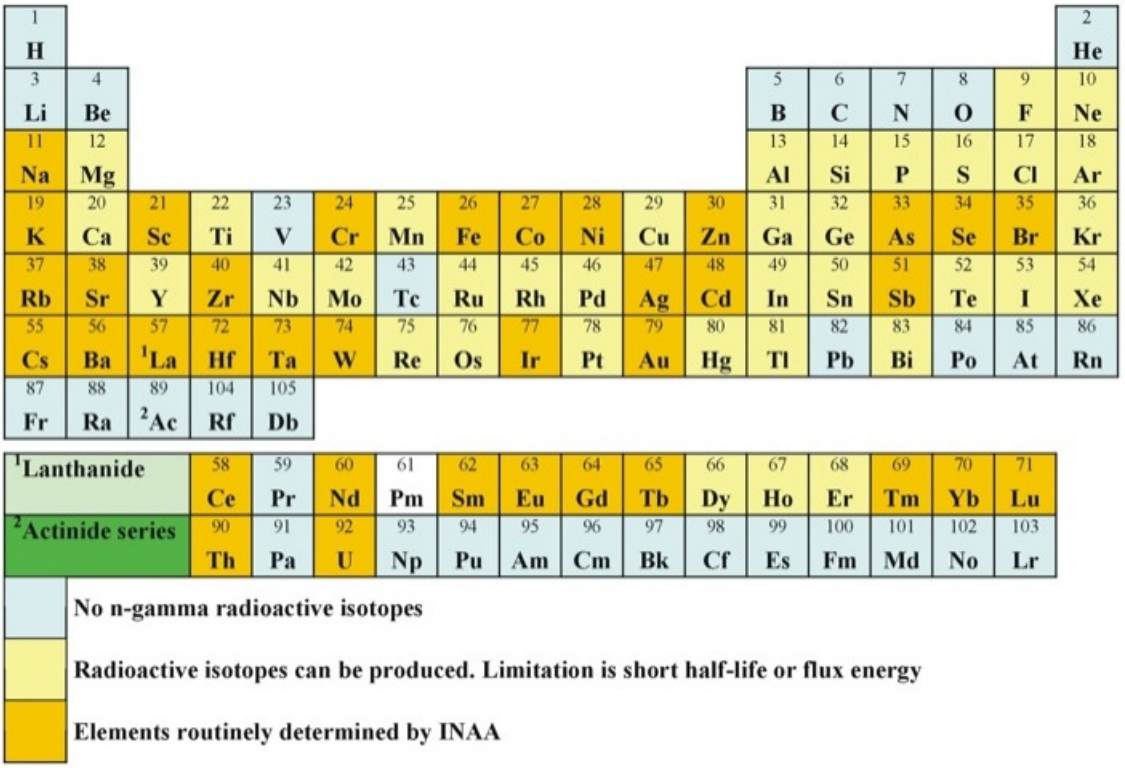

FIGURE 3.14: Periodic table showing elements that can be analyzed by INAA [98].

3.5 Neutron activation analysis of rocks, ores and minerals

Undoubtedly, the most significant contribution of early NAA to modern geo- and cosmochemistry was the work dealing with the distribution of the rare earth elements, REEs (La, Ce, Nd, Sm, Eu, Tb, Yb, Lu) in meteorites, rocks [99] and sediments. REEs play an important role in geochemical studies, since their distribution in the earth's crust and mantle contributes to elucidate evolutionary processes of geological cycles, which provides information on formation and dating of igneous rocks [17]. In particular, instrumental NAA utilises small amounts of material for analysis, which makes it very adequate for the study of separate mineral phases [15].

3.5.1 NAA of platinum group elements

Neutron activation analysis has proved to be of increasing importance in noble metals geochemistry since its application by Vincent and Smales in 1956 [100] to the determination of Pd and Au in basic and ultrabasic rocks.

Noble metals are usually inhomogeneously distributed in parts per million (ppm) or parts per billion (ppb) levels in rocks and ores, thus preconcentrations and radiochemical separation procedures have had to be used with neutron activation analysis. The purpose of performing separation procedures before or after irradiation is the isolation of a single element or group of elements from the sample in order to enhance the sensitivity of the analysis [13].

Much work has been done in the past decades to determine the PGEs in rocks and minerals using NAA [33, 101–103]. The determinations were done, generally, by applying neutron activation analysis associated with radiochemical separation [14, 87], or pre-concentration procedures for extraction for the individual noble metals. These procedures involved fire assay (e.g. lead bead [26, 104, 105] and nickel sulfide (NiS) [106]), cupellation, volatilization, ion exchange [107, 108], solvent extraction and final precipitation of individual noble metals [16, 109]. These methods provide very good sensitivities with the disadvantages of length of time and potential losses during the radiochemical procedures.

Several investigations have been carried out to evaluate the possibility of applying neutron activation analysis without using wet chemical operations. For example, Turkstra et al [62] have used instrumental reactor activation analysis and a Ge(Li) detector to investigate the nondestructive determination for noble metals in platinum-bearing ores, lead beads, and matte. In the case of platinum-bearing ores, weighed samples (500 mg) of typical South African ores were analysed. The irradiation times varied according to the elements to be determined, and the samples were irradiated together with suitable standards. Copper was determined by irradiating a standard and an ore sample (packaged in polyethylene containers) for 10 seconds in the pneumatic facility of SAFARI I, an ORR-type reactor, in a thermal neutron flux of 1.2×10^{13} n cm^{-2} s^{-1}. Gamma spectrometry of the irradiated samples and the standards was done within 25 seconds after each irradiation using Ge(Li) detector. Copper was measured using the 1039 keV photopeak of ^{66}Cu. Subsequently, for the determination of gold, iridium, platinum, and nickel, each ore sample and standards (sealed in separate quartz ampoules), were irradiated for 4 hours in the hydraulic facility of SAFARI I, in a thermal neutron flux of 4.4×10^{13} n cm^{-2} s^{-1}. The 411.8 keV photopeak of ^{198}Au was measured after 6 days of decay. Ten days after irradiation the 468 keV, 158.4 keV, and 810.5 keV photopeaks of ^{192}Ir, ^{199}Au(daughter of ^{198}Pt), and ^{58}Co were used for measuring iridium, platinum and nickel, respectively (Fig 3.15). On figure 3.15, very strong photopeaks of ^{51}Cr and ^{46}Sc are observed, which indicate their high abundances in the platinum-bearing ore. The more intense photopeaks of ^{192}Ir (295.5 keV, 308.4 keV, and 316.5 keV) are completely obscured by the very strong 319.8 keV photopeak of ^{51}Cr. As a result of the excess activities of scandium and chromium, the percentage standard deviations

for the analyses were between 10 to 20% and thus not too satisfactory. No traces of long-lived activities from silver, ruthenium and osmium were observable. To determine ruthenium and osmium, three samples of each ore were also subjected to 30 hours of irradiation and left to decay for 6 weeks before counting.

Turkstra et al [62] have concluded that the technique is more successful when dealing with matte and lead beads, but for ore samples as such, the technique is less successful. Nevertheless gold, platinum, iridium, copper, and nickel can be determined, although not with high precision due to excess activities from other abundant matrix elements [62].

Target Isotope	**Abundance** (%)	**Cross-section** (barn)	**Product radionuclide**	**Half-life**	**Gamma-ray photopeak(s) measured (keV)**
^{102}Ru	31.61	1.2	^{103}Ru	39.6 d	497
^{103}Rh	100	140	^{104}Rh	43 sec	555.5
^{108}Pd	26.71	0.07	^{109}Pd ^{109m}Pd	13.47 hr 40 sec	497 87.7
^{109}Ag	48.65	89	^{110}Ag	24.4 sec	657.6
^{184}Os	0.018	200	^{185}Os	94 d	645.8
^{191}Ir	38.5	700	^{192}Ir	74.2 d	295.9 308.4 316.5 468
^{193}Ir	627	110	^{194}Ir	17.4 hr	328.5
^{198}Pt	7.2	4	^{199}Pt ^{199}Au	30 min 3.15 d	 158.4 208.2
^{197}Au	100	98	^{198}Au	2.698 d	411.8
^{65}Cu	30.91	2.3	^{66}Cu	5.1 min	1039
^{58}Ni	67.88	0.8	^{58}Co	71.5 d	810.5

TABLE 3.2: Nuclear data for radionuclides produced from noble metals, nickel, and copper by irradiation in thermal reactor [62].

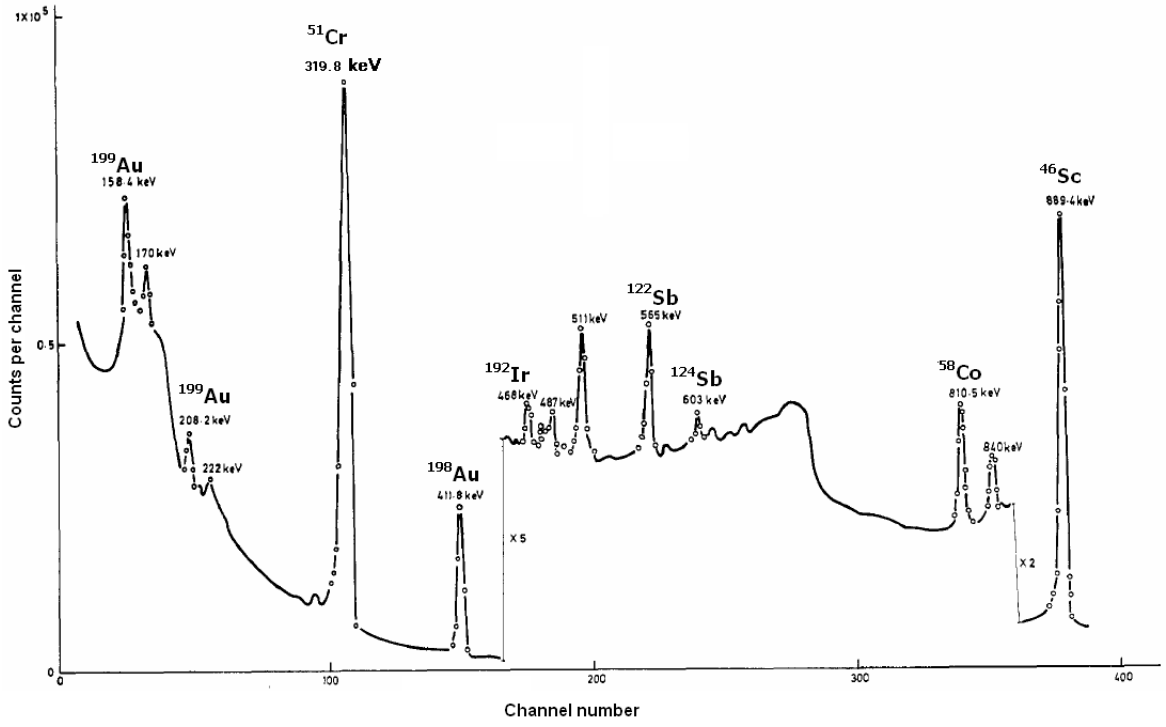

FIGURE 3.15: Gamma-ray spectrum of platinum-bearing ore, irradiated for 4 hours in the hydraulic facility of SAFARI-I and measured 10 days after irradiation [62].

Chapter 4

Experiments

4.1 Introduction

In this work, neutron activation analysis has been used to determine the elemental signatures of platinum ore, concentrate, feed, and tailing samples. All the samples were irradiated without any chemical treatment before or after irradiation. Two sets of irradiations were performed. The first set of irradiations was undertaken using fast neutrons from an isotopic source at iThemba LABS (Section 4.3), while the second set was done with thermal neutrons from the SAFARI-I nuclear reactor at NECSA (Section 4.5). The irradiations were followed by measurements of the emitted gamma rays and analyses of the measured gamma-ray spectra. It should be mentioned that these experiments were conducted without using comparator standards, which were not required for the work.

Moreover, ore samples were also analysed to measure the activities from natural radioactive emitters. These experiments were also performed at iThemba LABS.

4.2 Samples collection and preparation

Bulk samples of platinum-bearing ores were obtained from Lonmin mines, Platreef (PPL), which is from the northern limb of the Bushveld Complex, and Merensky (MRY) and UG2 which are from the western limb of the Bushveld Complex in South Africa. Upon arrival at the mineral processing unit of the Centre of Minerals Research (CMR) in the Chemical Engineering Department at the University of Cape Town (UCT), the ore samples were

divided into 10 kg piles. These were further divided using a rotary splitter into 1 kg samples and packed into plastic bags, which were divided into two groups. Some were used as ground ore samples and the others were floated to prepare concentrate samples.

Preparation of the concentrate samples involved milling of the ore to prepare slurries, flotation of the slurries and collection of the concentrate froth. The slurry was prepared by milling 1 kg of ore sample mixed with synthetic plant water using a stainless steel rod mill. The synthetic plant water is a mixture of distilled water with certain chemical salts. Different ores have different milling times due to the particular properties of the ore. The milling time should achieve 60% passing of the mixture using a 75 μm sieve.

The milled slurry was then transferred to the flotation cell, which consists of a vertical rotator and an air rotameter (Fig 2.4). At the beginning of the flotation process a "feed" sample of 5 ml was collected from the slurry using a syringe, then the flotation started by setting the impeller speed at 12 rpm. The air was switched on the slurry after 10 minutes, and the reagents were added to it during the process as shown in Table 4.1. Different reagents are added to the flotation process to achieve specific functions that enable the separation of valuable minerals from gangue minerals on the basis of the difference in their surface properties [54]. The slurry level was kept fixed during the flotation process by manually adding synthetic plant water.

		MRY		UG2		PPL	
Reagents	**Conditioning time** (min)	**Type**	**Dosage** (g/t)	**Type**	**Dosage** (g/t)	**Type**	**Dosage** (g/t)
Activator	5	$CuSO_4$	55	$CuSO_4$	170	none	none
Collector	2	SNPX	200	SNPX	155	SIBX	250
Depressant	2	Dep267	220	KU11	80	KU11	200
Frother	1	DOW200	40	DOW200	40	DOW200	40

TABLE 4.1: Conditioning time for the flotation procedures for concentrate samples, showing the reagents added and their dosages.

The froth formed on the surface was scraped frequently, and four concentrates were collected at 2 min, 4 min, 6 min, and 8 min after switching the air on, respectively. These concentrates were then combined in one concentrate sample. At the end of the flotation process, the remaining slurry in the cell, which represent the tailings samples, was drained into a container.

The concentrates, feeds, and tailings were then filtered and left to dry overnight in a $\pm 90\ ^{o}$C oven, then weighed before analysis.

We have been involved in all the preparation steps of the samples with the help of the CMR technicians.

4.3 Experiment I (a): Fast neutron activation analysis at iThemba LABS

4.3.1 Irradiation

These experiments were undertaken at iThemba LABS. Only concentrate samples were irradiated in this experiment. The three different concentrates ($\sim$ 160 g) and the empty container ($\sim$ 20 g) were irradiated using an ^{241}AmBe isotopic source. The activity of the source was 220 GBq which yields 1.5×10^{7} neutrons s^{-1}, which provided about 10^{5} neutrons per second irradiating the sample.

A small facility ($\sim$ 1 m^3) was built using wax bricks to moderate the neutrons emitted by the americium-beryllium source (Fig 4.1). The sample was placed close to the source, about 3 cm apart, and each sample was irradiated for one hour. The counting of the activated sample was started immediately after the end of the irradiation and counted for about 30 minutes.

4.3.2 Counting the emitted gamma-rays

The counting system consisted of a solid-state high purity germanium gamma-ray detector (HPGe), and a PC computer running Canberra Genie-2000 software.

The activated sample was placed on the face of the detector (sample-to-detector distance approximately 1 cm). The counting was split into three runs. In this experiment we have decided to do the irradiation for 1 hour for each sample and then take the sample to the detector in the other side of the lab, which about 5 minutes to reach there and adjust the sample and the detector and then start counting. The counting was done on nine runs as in Table 4.2.

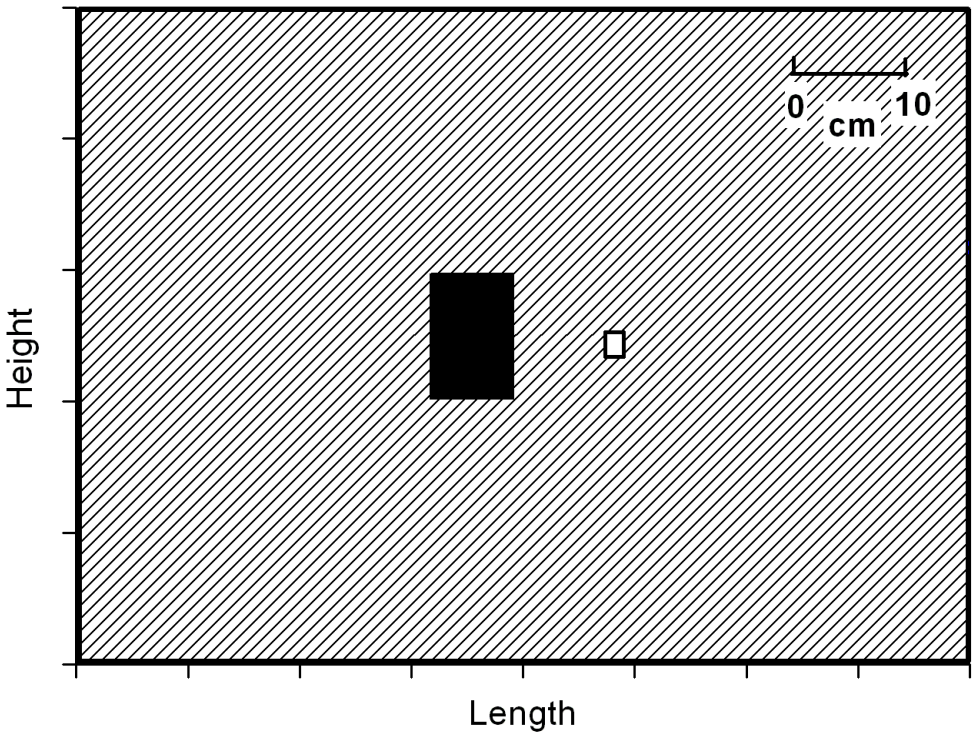

FIGURE 4.1: Cross-section of the irradiation arrangement at iThemba LABS. The black square represents the irradiated sample, the shaded area represents the wax bricks, and the small white square represents the radioactive source.

In between these runs there was a "waiting time" of about 1 minute to save the run and then start the next run. (This of course will affect the acquired gamma spectra). These runs were reconstructed as in Table 4.3. The length of the first run (Run 1) was 15 min , the second run (Run 2) was 25 min, and the third run (Run 3) was 35 min. Further discussion of the results will be provided in Chapter 5.

Run	Time
Run1	2 minutes
Run2	2 minutes
Run3	2 minutes
Run4	2 minutes
Run5	2 minutes
Run6	5 minutes
Run7	5 minutes
Run8	5 minutes
Run9	10 minutes

TABLE 4.2: Time table of the nine counting runs.

Run	Renamed as	Time
Run1 to Run6	Run 1	15 minutes
Run7 to Run9	Run 2	25 minutes
Run1 to Run9	Run 3	35 minutes

TABLE 4.3: Addition of the runs for the purpose of the analysis.

Prior to counting, the detection system was calibrated using several standard radioactive sources of well known gamma-ray energies (Table 4.4). The energy calibration consists of determining the linear relationship (it is generally a linear relationship but it is not always the case) between the channel number (C), and the gamma-ray energy (E). The energy calibration was performed by plotting the channel number against the corresponding energy, then a least square fitting was performed (Fig 4.2). In practice, the calibration line might not pass through the origin, since the detector system might have an offset. Fig 4.3 shows the measured gamma-ray spectra of the calibration sources.

Radioactive isotope	**Decay process**	**Daughter**	**Gamma-ray Energy (keV) (keV)**
^{60}Co	β^-	^{60}Ni	1332 1173
^{137}Cs	β^-	^{137}Ba	32(X) 661
^{22}Na	β^+	^{22}Ne	511(A) 1274

TABLE 4.4: Calibration gamma-ray energies. where, β^- = emission of an electron or beta particle, β^+= emission of a positron, A= annihilation, and X= X-rays.

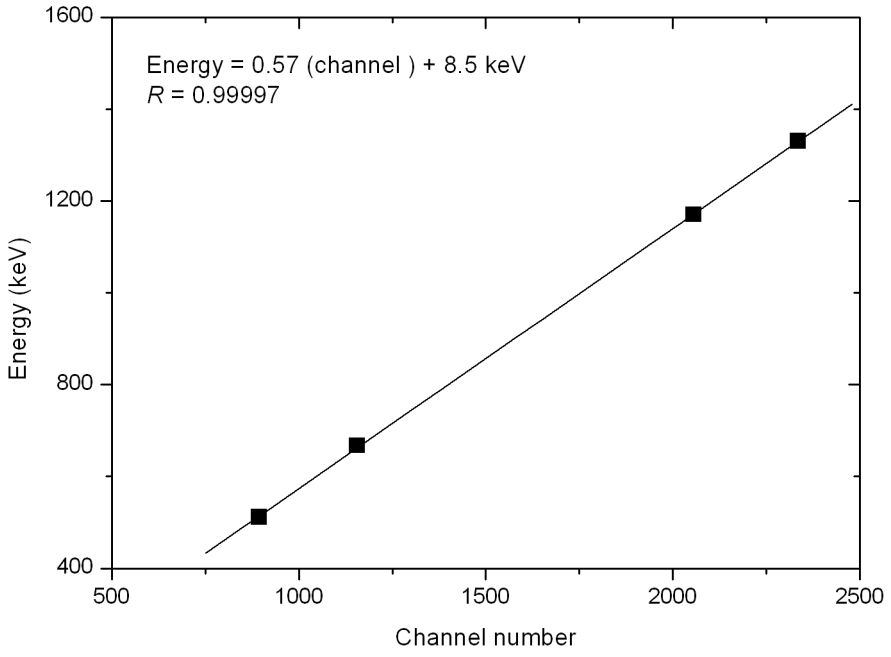

FIGURE 4.2: Energy calibration of the HPGe detector. R is the linear regression factor.

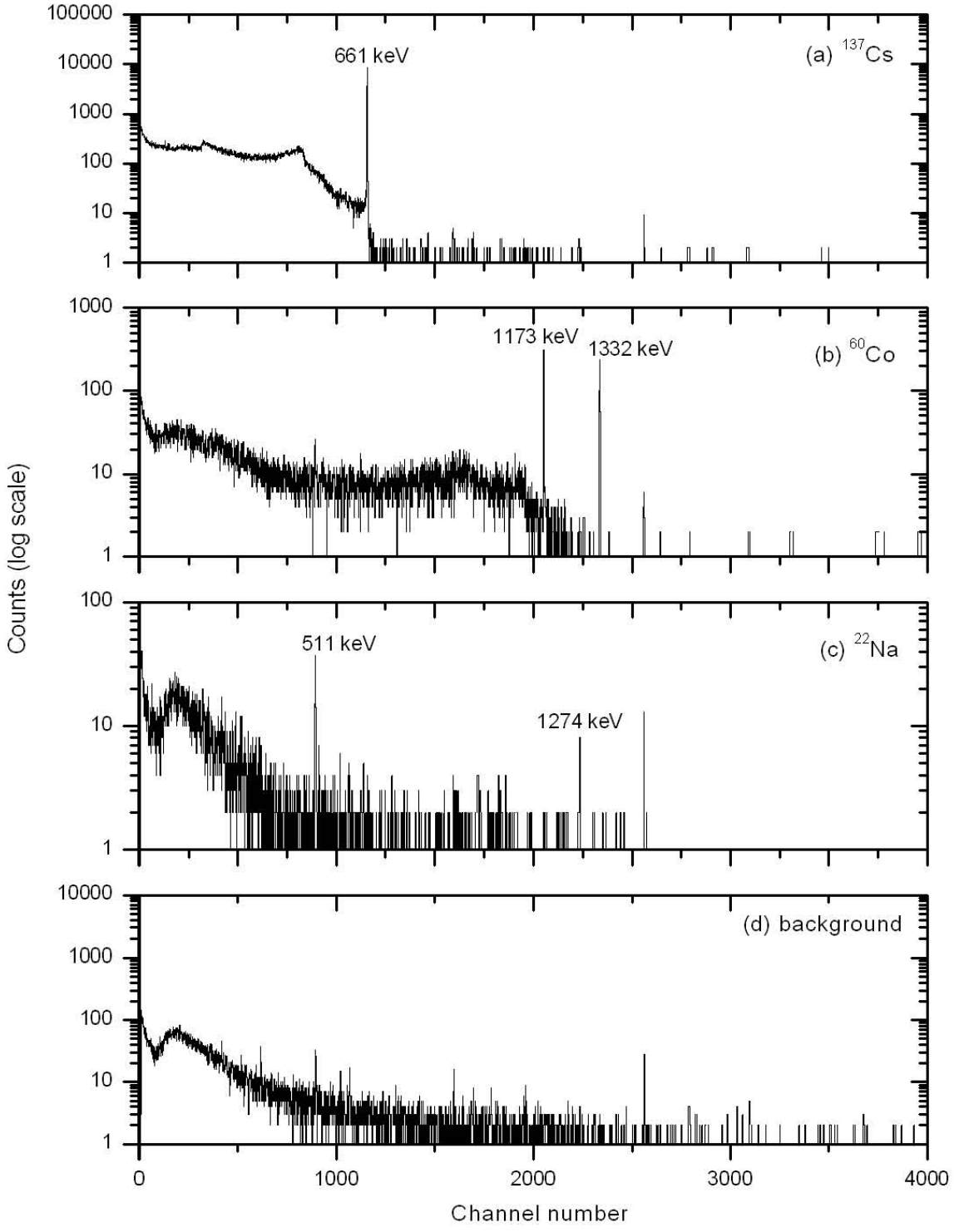

FIGURE 4.3: Gamma spectra of the calibration standards, labeled with the photopeaks energies.(a) ^{137}Cs, (b) ^{60}Co, (c) ^{22}Na and (d) background radiation measured with the detection system in the absence of the radioactive sample.

To determine the resolution of the detector used in this experiment, the photopeaks of the calibration standards (Table 4.4) were fitted using OriginPro70 software (Fig 4.4). The resolution (R) of the detector was determined by finding the full width of the photopeak at half the maximum amplitude (FWHM) which is expressed as a percentage as follows:

$$R = \frac{\delta E}{E} \times 100\%. \tag{4.1}$$

After that a graph of resolution versus gamma energy was plotted (Fig 4.5).

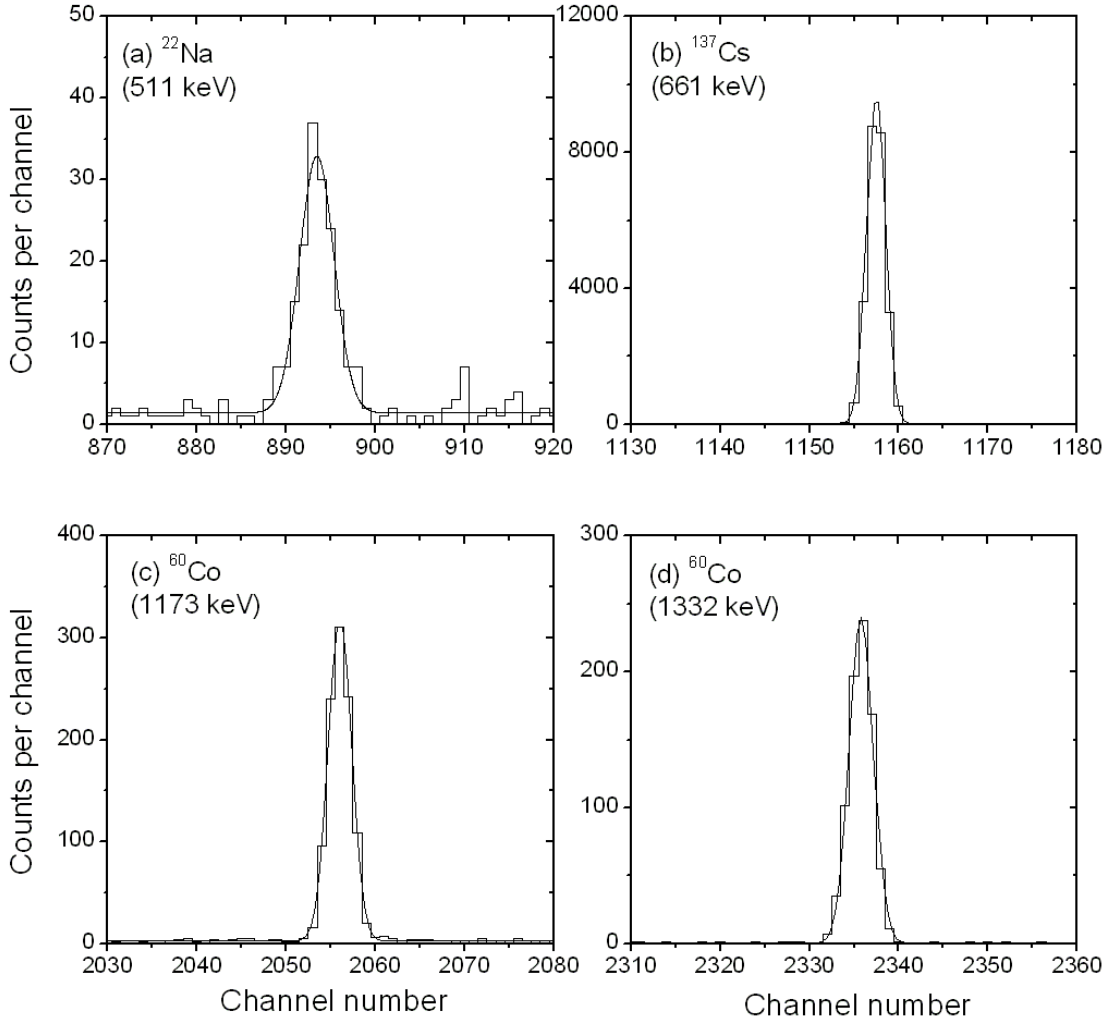

FIGURE 4.4: Fitting of the well known photopeaks of the calibration standards.

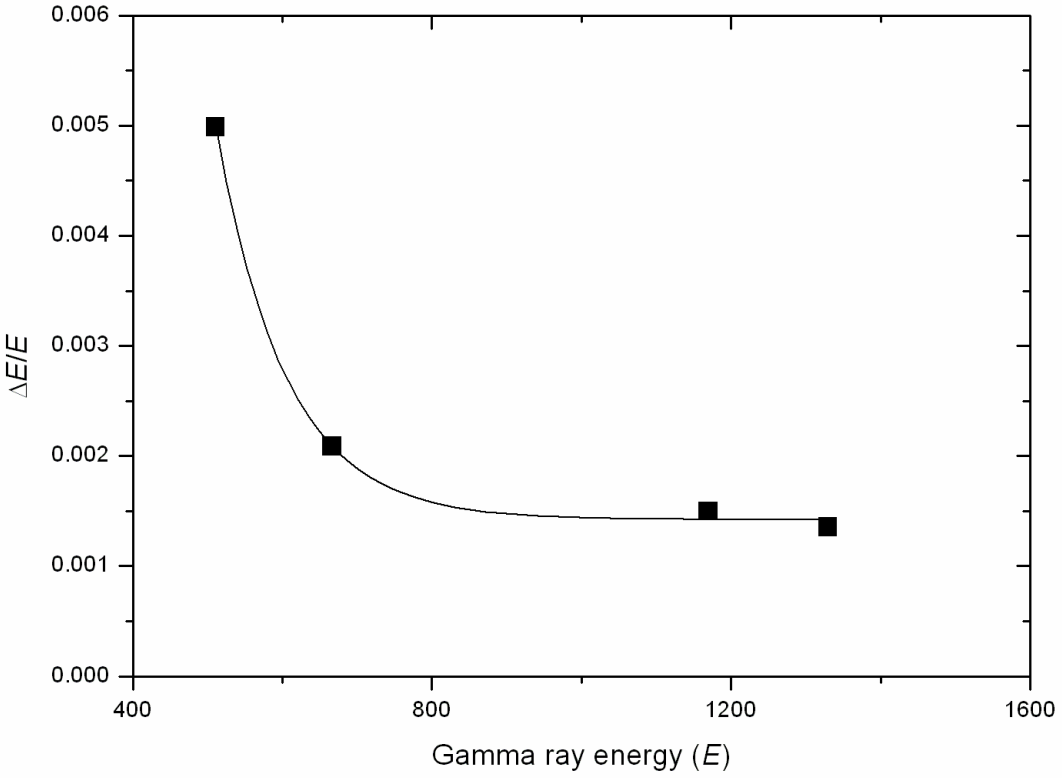

FIGURE 4.5: Resolution of the detector as a function of gamma energy.

The energy calibration and energy resolution data were used in the analysis of the gamma-ray spectra of the samples. A discussion of the results and analysis of the samples will follow in Chapter 5.

The probability that an emitted gamma ray will interact with the detector and produce a count is the *efficiency* $\epsilon(\%)$ detector. In general, the efficiency of larger detectors is higher than smaller detectors.Relative efficiency values are often used for germanium detectors, and compare the efficiency of the detector at 1332 keV to that of a 3 in $\times$ 3 in NaI detector. The energy of the gamma rays being detected is an important factor in the efficiency of the detector. An efficiency curve can be obtained by plotting the efficiency at various energies. This curve can then be used to determine the efficiency of the detector at energies different from those used to obtain the curve. High-purity germanium (HPGe) detectors typically have higher sensitivity. The full-energy peak efficiency of the coaxial HPGe detector (38 cm^3), as shown in Fig(4.6), was provided by the manufacturers and modeled according to the equation [110]

$$\epsilon = \left(\frac{a_1}{E}\right)^{a_2} + a_3 e^{-a_4 E} + a_5 e^{-a_6 E} \tag{4.2}$$

Where

$$a_1 = 4.41$$
$$a_2 = 0.425$$
$$a_3 = 115$$
$$a_4 = 5.06$$
$$a_5 = 11.1$$
$$a_6 = 0.673$$

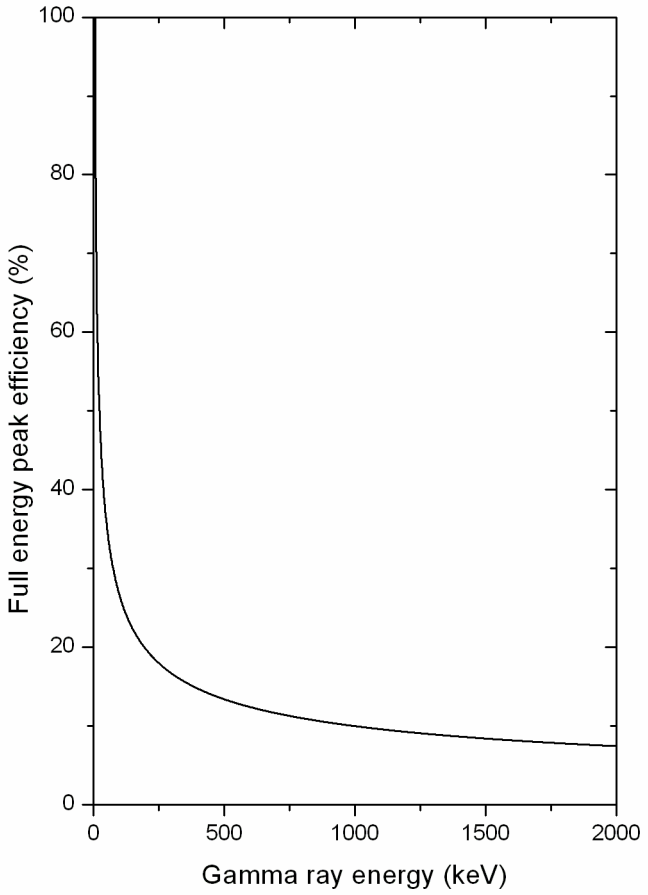

FIGURE 4.6: Full-energy peak efficiency calibration curve as a function of gamma energy.

4.4 Experiment I (b): Radiometric inspection of ore samples at iThemba LABS

The minerals that carry uranium and thorium are generally associated with felsic intrusions; they are found much less frequently in mafic rocks or in volcanics. The uranium and thorium content of rocks generally increases with acidity, with the highest concentrations found in pegmatites. The potassium content of rocks also increases with acidity. In general, potassium is concentrated in micas and feldspars.

Gamma-ray spectrometry is widely used to studying natural radioactivity because it provides a fast, multielemental and non-destructive method of radioactivity measurement. However, it does not permit direct determination of U-238 and Th-232 because both are very weak gamma-emitters; usually, U-238 and Th-232 concentrations are determined from their decay products assuming secular equilibrium between parents and daughters.

Measuring the variation of naturally emitted radiation from the ore samples might be used to identify the ores in terms of origin of extraction. The soil samples were open to the air, in unsealed plastic containers prior to being sealed in 1.0 litre (polypropylene) Marinelli beakers. The samples were then measured, one day after sealing in the beakers, by means of gamma-ray spectroscopy using Closed-end coaxial ERL-HPGe detector (p type, 45% relative efficiency, 2 keV FWHM resolution at 1.33 MeV) system. The detector is encased in a 10 cm thick lead castle fitted with a 2.0 mm thick copper inner lining in order to reduce the background in the sample spectra. The three samples were measured for about 24 hours (each sample) and the computer dead times during data acquisition were less than 1%. The spectra analyses follow in Chapter 5.

4.5 Experiment II: Thermal neutron activation analysis measurements at NECSA

Experiments were undertaken at SAFARI-1 (20 MW) research reactor, at South African Nuclear Energy Corporation (NECSA) in Pelindaba (Pretoria, South Africa), where concentrate, feed, and tailing samples of the three ore types (MRY, UG2, and PPL), were analyzed. The samples were prepared at UCT, then taken to NECSA for irradiation. Weighed samples of platinum concentrates, feeds, and tailings (Table 4.5), were sealed in small High Density Polythylene capsules (HDPE). These were sealed in a large HDPE capsule, and were

irradiated near the core of the reactor for 10 seconds. The neutron flux was approximately 10^{14} n cm^2 s^{-1} (epithermal to thermal ratio approximately 1). After irradiation the smaller capsule was removed from the larger for analysis. The activated samples were left to decay before measuring the emitted radiation. The spectra were planned to be acquired after one day, 3 days, and 16 days. Unfortunately, the acquisition after one day decay was not done due to a failure in the sample changer. However, the spectra after 3 days and 16 days of decay were acquired successfully, where the activated samples were measured for 30 min, in both cases.

The analyses of the measured gamma-ray spectra are shown and discussed in Chapter 6.

Label	**Description**	**Sample mass (mg)**
MRY	Concentrate	1.400E-003
PPL	Concentrate	1.430E-003
UG2	Concentrate	1.280E-003
MRY	Feed	1.470E-003
PPL	Feed	1.440E-003
UG2	Feed	1.480E-003
MRY	Tailings	1.460E-003
PPL	Tailings	1.070E-003
UG2	Tailings	1.560E-003

TABLE 4.5: The samples irradiated at NECSA.

Chapter 5

Results from experiments at iThemba LABS

5.1 Introduction

Following the irradiations and measurements of the three concentrate samples (Section 4.3), the acquired gamma-ray spectra via germanium detectors were analyzed for identification of spectral components. This procedure involved comparing observed peak energies against a list of known energies to determine the radionuclides present in the particular spectrum. Further consultation of the available tables of isotopes was needed to confirm the presence of a certain radionuclide.

5.2 Analysis of gamma-ray spectra

Geological samples consist of a large number of elements which, when irradiated, produce complex gamma-ray spectra with different groups of gamma-rays [15]. The gamma-ray spectra were analysed first to determine the energies of the photopeaks present in each spectrum in order to identify the parent isotopes, and second to calculate the areas of selected peaks. All the experimental data have been tabulated and analysed by using MS Excel, and OriginPro70 programs.

5.2.1 Identification of radionuclides in the gamma-ray spectra

The gamma-ray spectra (Run 1, Run 2, Run 3) of the three concentrate samples and empty container (Fig 5.2, Fig 5.3, and Fig 5.4),were analyzed. The empty plastic container represented the background for the concentrates (full plastic containers).

The peaks in the empty plastic container spectra are associated with natural radioactive sources, earlier addressed (Subsection 3.3.1). The 1460 keV peak of ^{40}K is predominant in the spectra. Radon (^{222}Rn) is usually found to be concentrated in closed rooms. The characteristic gamma-rays of ^{222}Rn daughters, ^{214}Pb and ^{214}Bi, are frequently found in background spectra [73]. Table 5.1 presents some of the background peaks together with their gamma-ray energies and intensities.

Element	**Energy (keV)**	**Intensity (%)**
^{40}K	1460.8	10.67
^{208}Tl	583.19	84.50
^{212}Pb	238.6	43.60
^{214}Pb	295.2	19.30
	351.9	35.60
^{214}Bi	609.3	46.10
	1120.3	15.10
	1764.4	15.40
^{228}Ac	794.4	4.8
	911.2	25.80
	968.8	15.80

TABLE 5.1: The most prominent background peaks observed [3].

The gamma-ray spectra measured for the three concentrates show many peaks with different intensities. The shape of each spectrum varies as a function of the gamma-ray energy, number of counts, and decay mode of the emitter. These parameters are governed by the probabilities of the absorption of the photons in the detector. Furthermore, the presence of any material around the detector also has a significant influence on the spectra [77]. The main features observed in the concentrates spectra are the full energy peaks, and the rapid rise of the background under the peaks toward lower energies ($E_\gamma < 500$ keV) where many peaks are crowded together.

The identification of all the peaks within each gamma-ray spectrum was not necessary for this work, hence only a few lines were selected. The only criterion of the selection was that the peaks are distinctly identified. Accordingly, four radionuclides with six gamma-ray peaks were chosen: ^{24}Na , ^{27}Mg, ^{28}Al, and ^{56}Mn, which are radionuclides formed by the neutron capture reaction (n, γ). These elements are of high abundances on the earth's crust and represent, among a few others, the major elements that could be found in igneous rocks. Fig 5.1 shows an example gamma-ray spectrum of a concentrate sample labeled with the selected gamma-ray peaks, while Table 5.2 gives these radionuclides with their corresponding nuclear data.

Other important features of gamma-ray spectra caused by the different absorption processes include: single escape peaks, double escape peaks, and sum peaks. All these features have been encountered in the gamma-ray spectra of the concentrates, but were not regarded in the analysis.

Element	**Radionuclide measured**	**Photopeak(s) used in determination (keV)**	**Intensity (%)**	**Cross-section (barn)**	**Half-life**	**Product isotope**
Na	^{24}Na	1368	99.99	0.53	14.9 hr	^{24}Mg
Mg	^{27}Mg	843 1014	71.8 28	0.063	9.4 min	^{27}Al
Al	^{28}Al	1778	100	0.21	2.2 min	^{28}Si
Mn	^{56}Mn	846 1810	98.9 27.2	13.3	2.5 hr	^{56}Fe

TABLE 5.2: Nuclear data for the selected radionuclides identified in the gamma-ray spectra of the concentrates [111, 112].

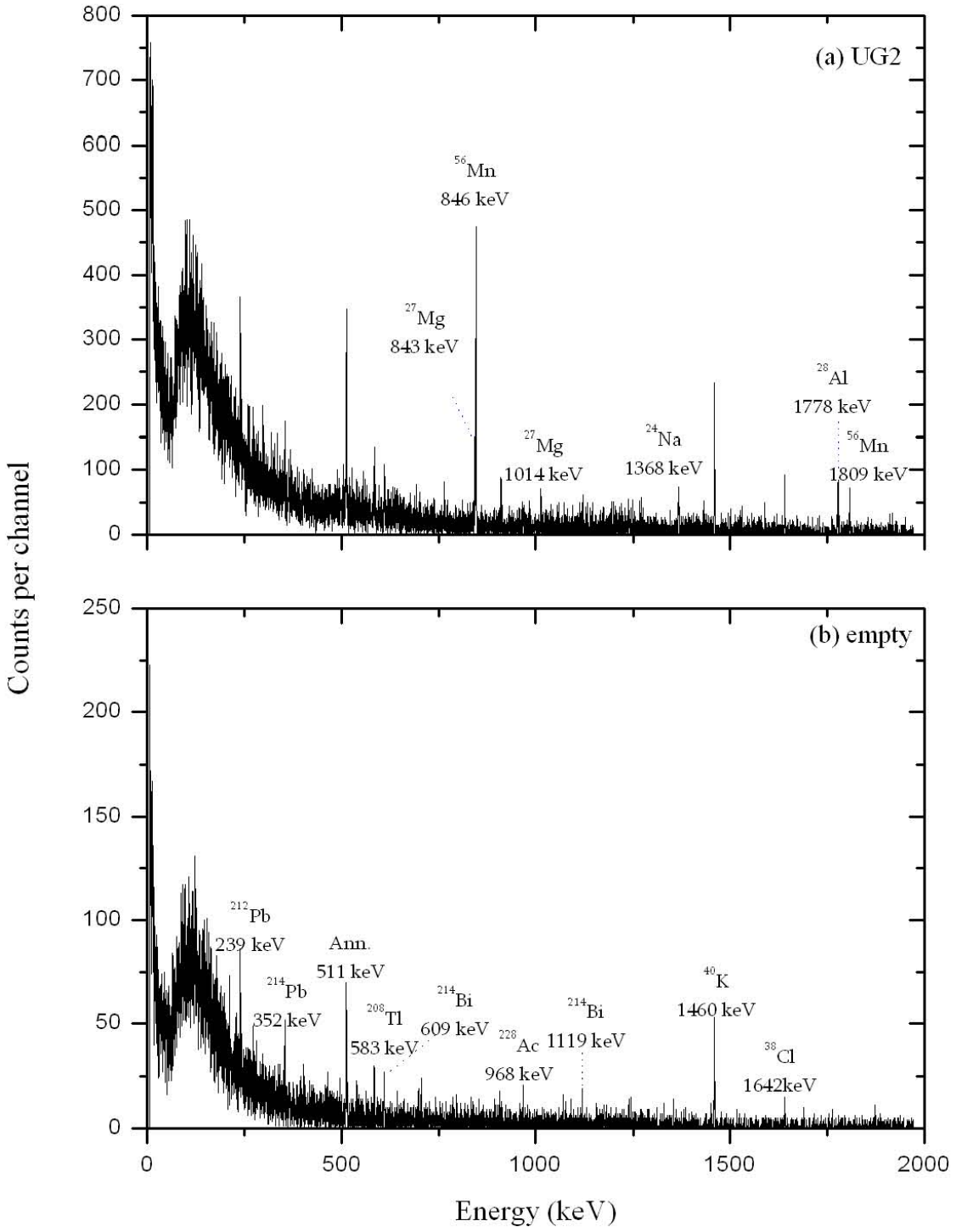

FIGURE 5.1: Gamma-ray spectrum of a UG2 concentrate (layer above) counted for 15 minutes (Run 1). The selected peaks are labeled with radioisotope and energy. The bottom figure is for an empty container (Run 1) labeled with the background radiations.

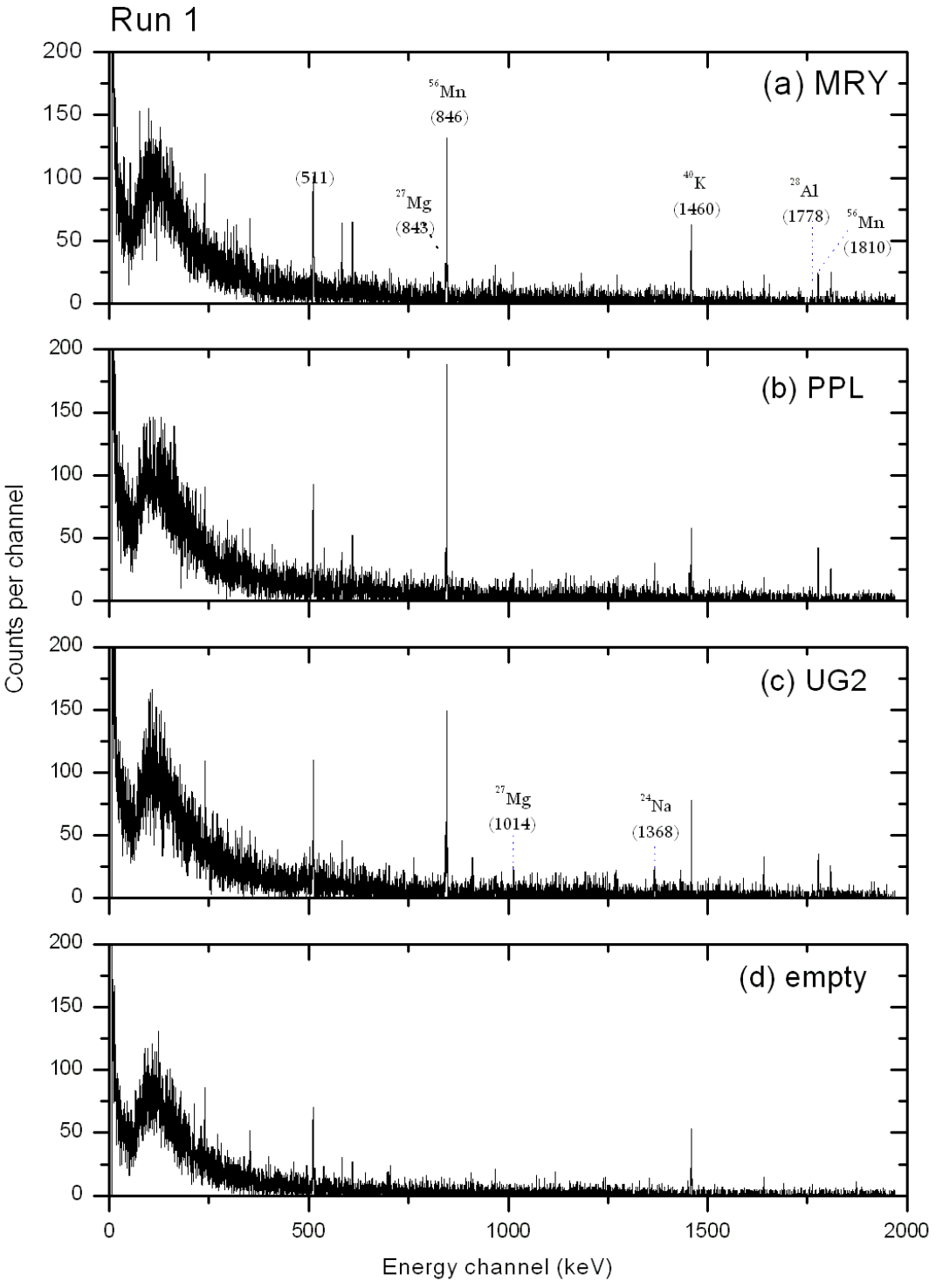

FIGURE 5.2: Gamma-ray spectra for the three concentrate samples and the empty container, counted for 15 min (Run 1).

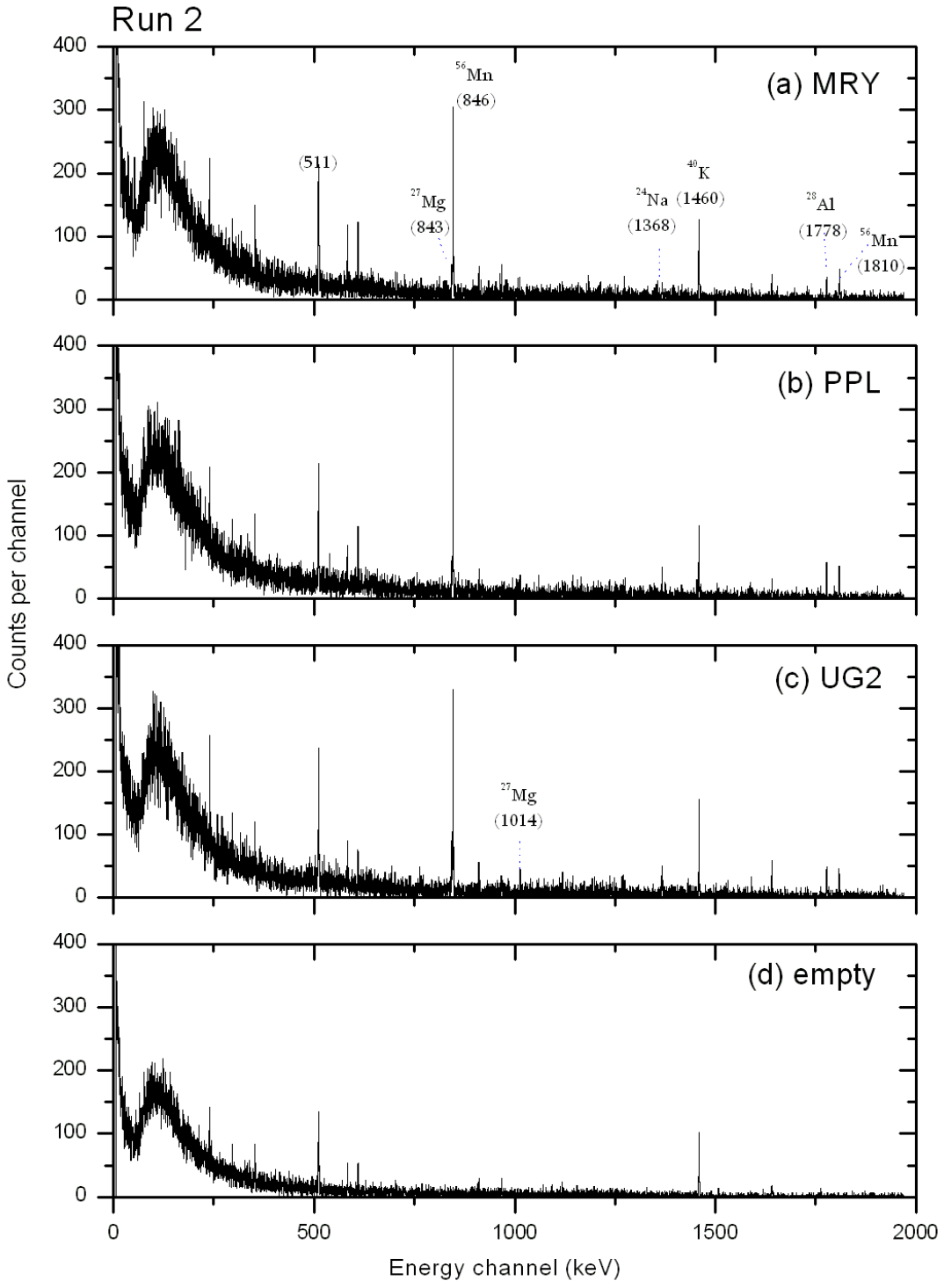

FIGURE 5.3: Gamma-ray spectra for the three concentrate samples and the empty container, counted for 25 min (Run 2).

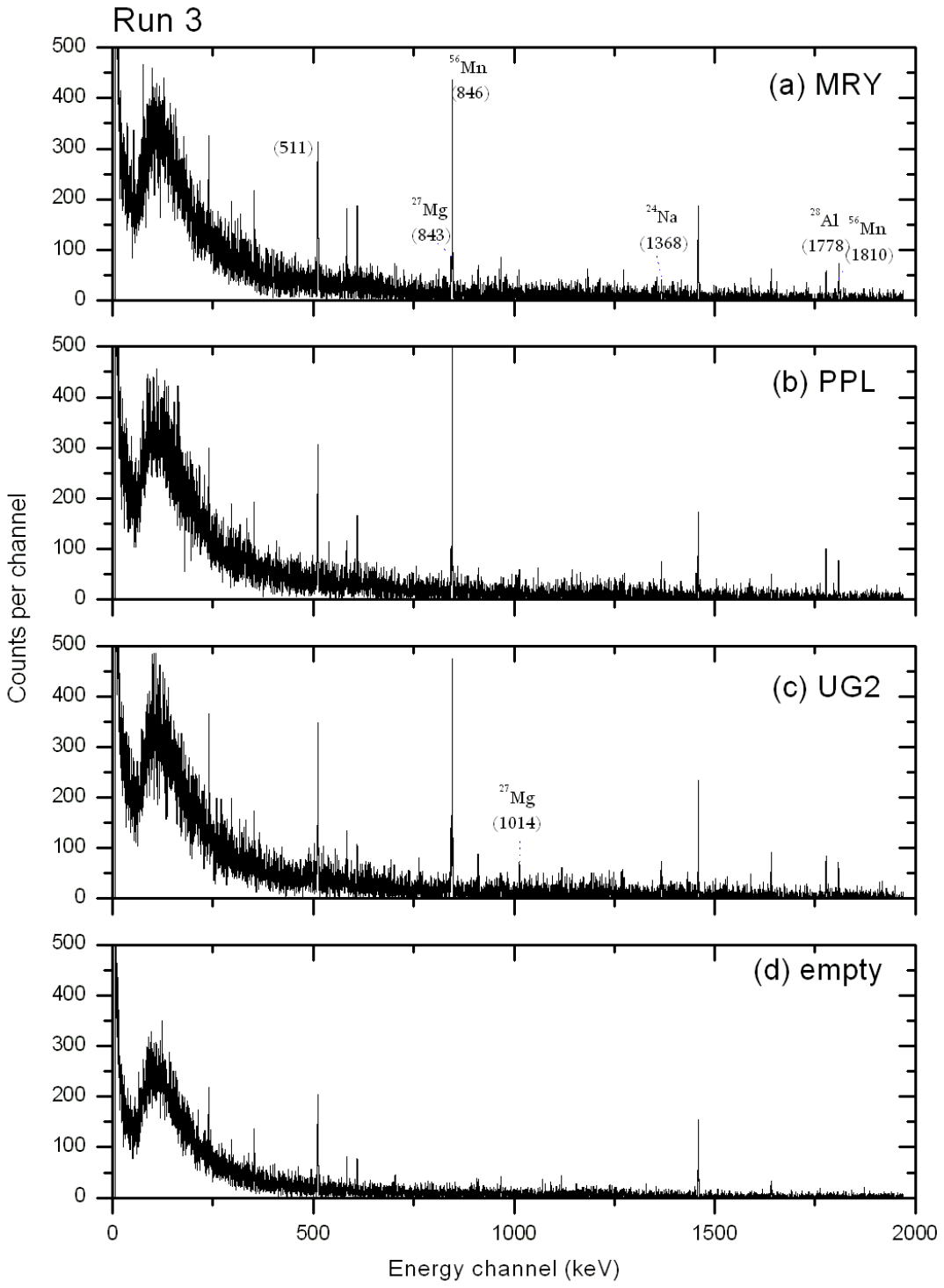

FIGURE 5.4: Gamma-ray spectra for the three concentrate samples and the empty container, counted for 35 min (Run 3).

5.2.2 Calculation of element concentrations in gamma-ray spectra

Complex gamma-ray spectra require treating each peak, its background, and its interferences individually [15]. Calculation of the amount of an element activated in a sample involves the determination of the area of the peak in the gamma-ray spectrum. A peak area can be found by summing data points within the peak or by fitting it to a functional form [30].

Gaussian fitting was performed, using OriginPro70 software, for the six selected gamma-ray peaks in all the spectra measured. An example of the fitting is shown in Fig 5.6. The calculations, as in Subsection 3.1.4, were carried out for the three concentrate samples, and tabulated as shown in Tables 5.3, 5.4 and 5.5. The continuum contributions were incorporated in the calculations. On the other hand, multiple Gaussian fitting for closely spaced peaks was avoided due to the high uncertainty associated with it, e.g Fig 5.5.

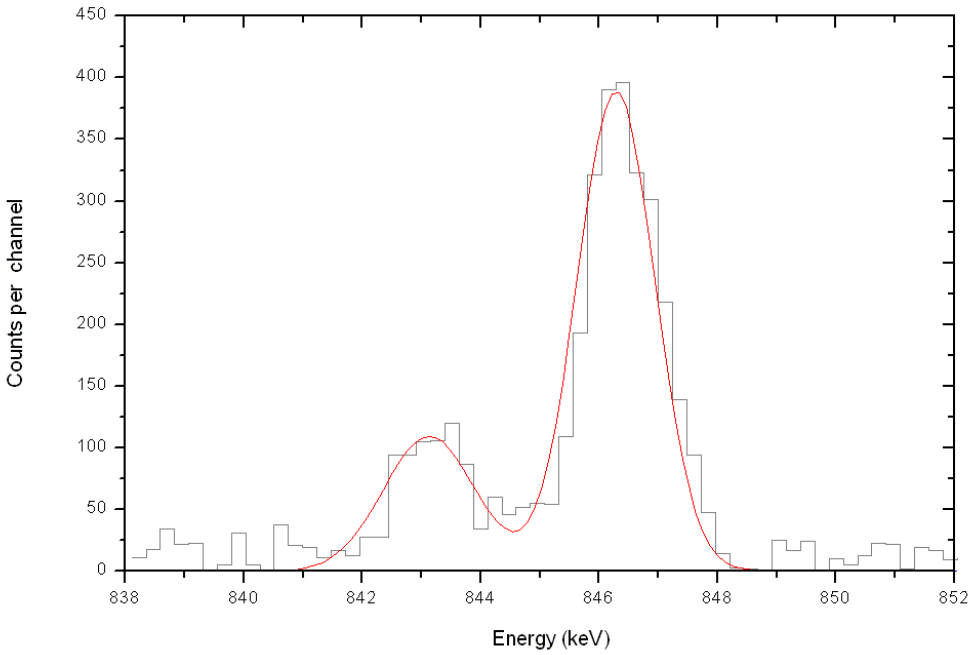

FIGURE 5.5: Multiple Gaussian fitting, using the peak fitting module (PFM) of OriginPro7 software, for two close peaks (843 keV of ^{27}Mg and 846 keV of ^{56}Mn)in a UG2 concentrate sample (Run 3).

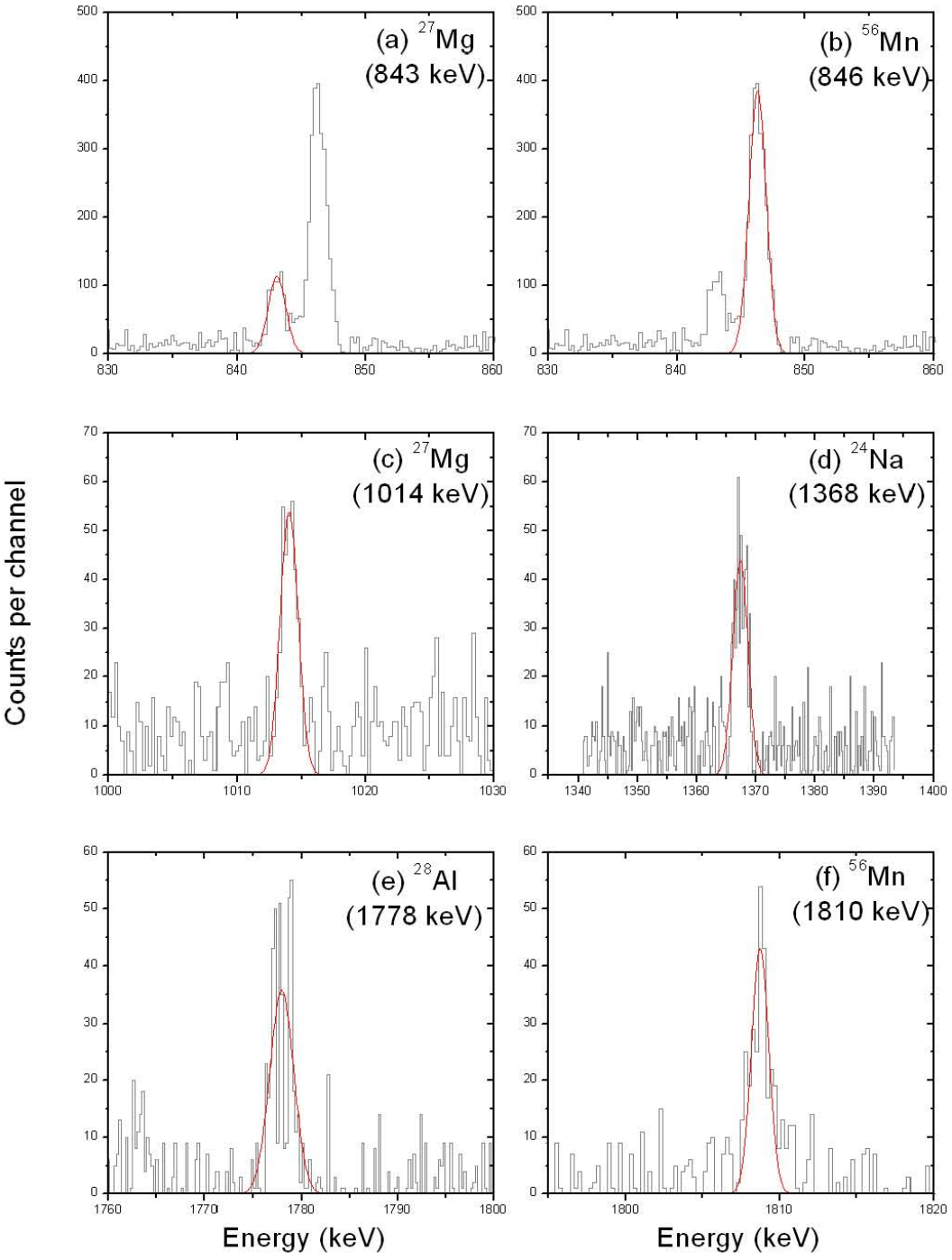

FIGURE 5.6: Gaussian fitting, using OriginPro7 software, for the six peaks in a UG2 concentrate sample (Run 3).

Several radionuclides show up in the gamma-ray spectra with more than one line. Since the efficiency of the HPGe detector is known the count rates can be converted to activity

Radionuclide	**Energy(keV)**	**MRY** $N_P \pm \sigma_P$	**PPL** $N_P \pm \sigma_P$	**UG2** $N_P \pm \sigma_P$
^{24}Na	1368	5 ± 2	5 ± 4	20 ± 5
^{27}Mg	843	17 ± 7	32 ± 7	23 ± 11
	1014	7 ± 3	10 ± 3	25 ± 5
^{28}Al	1778	19 ± 5	31 ± 7	29 ± 6
^{56}Mn	846	128 ± 14	212 ± 15	136 ± 14
	1810	15 ± 4	21 ± 5	14 ± 4

TABLE 5.3: The net peak area (N_p) and the uncertainty (σ_P) for the concentrate samples (Run 1).

Radionuclide	**Energy(keV)**	**MRY** $N_P \pm \sigma_P$	**PPL** $N_P \pm \sigma_P$	**UG2** $N_P \pm \sigma_P$
^{24}Na	1368	24 ± 5	28 ± 6	48 ± 8
^{27}Mg	843	26 ± 8	22 ± 8	37 ± 9
	1014	5 ± 3	32 ± 5	23 ± 7
^{28}Al	1778	18 ± 4	19 ± 5	15 ± 5
^{56}Mn	846	213 ± 17	362 ± 21	262 ± 18
	1810	31 ± 6	43 ± 7	26 ± 6

TABLE 5.4: The net peak area (N_p) and the uncertainty (σ_P) for the concentrate samples (Run 2).

concentrations previously discussed in Subsection 3.1.4(Eq 3.9), which for each radionuclide should be the same. Calculation of activity concentrations for the concentrate samples, irradiated at iThemba LABS, are shown in Tables 5.6, 5.7, and 5.8.

Radionuclide	**Energy(keV)**	**MRY** $N_P \pm \sigma_P$	**PPL** $N_P \pm \sigma_P$	**UG2** $N_P \pm \sigma_P$
^{24}Na	1368	32 ± 6	42 ± 8	70 ± 9
^{27}Mg	843	36 ± 11	52 ± 11	87 ± 14
	1014	9 ± 4	24 ± 6	63 ± 8
^{28}Al	1778	38 ± 7	62 ± 9	69 ± 9
^{56}Mn	846	296 ± 24	571 ± 26	343 ± 24
	1810	53 ± 8	60 ± 9	40 ± 7

TABLE 5.5: The net peak area (N_p) and the uncertainty (σ_P) for the concentrate samples (Run 3).

				MRY		**UG2**		**PPL**	
Radionuclide	**Energy** (keV)	**Efficiency** (%)	**Br** (%)	**Counts rate** (Counts/s)	**Activity** (Bq/Kg)	**Counts rate** (Counts/s)	**Activity** (Bq/Kg)	**Counts rate** (Counts/s)	**Activity** (Bq/Kg)
^{24}Na	1368	8.73	1	5.56E-03	3.98E-03	5.56E-03	3.98E-03	2.22E-02	1.59E-02
^{27}Mg	843	10.73	1	1.89E-02	1.10E-02	3.56E-02	2.07E-02	2.56E-02	1.49E-02
	1014	9.92	1	7.78E-03	4.90E-03	1.11E-02	7.00E-03	2.78E-02	1.75E-02
^{56}Mn	846	10.71	0.98	2.11E-02	1.25E-02	3.44E-02	2.03E-02	3.22E-02	1.90E-02
	1810	7.75	0.27	1.42E-01	4.22E-01	2.36E-01	6.98E-01	1.51E-01	4.48E-01
^{28}Al	1778	7.81	1	1.67E-02	1.33E-02	2.33E-02	1.87E-02	1.56E-02	1.24E-02

TABLE 5.6: Calculation of the activity concentration for gamma-ray spectra of concentrate samples acquired for 15 minutes (Run1).

				MRY		**UG2**		**PPL**	
Radionuclide	**Energy** (keV)	**Efficiency** (%)	**Br** (%)	**Counts rate** (Counts/s)	**Activity** (Bq/Kg)	**Counts rate** (Counts/s)	**Activity** (Bq/Kg)	**Counts rate** (Counts/s)	**Activity** (Bq/Kg)
^{24}Na	1368	8.73	1	1.60E-02	1.15E-02	1.87E-02	1.34E-02	3.20E-02	2.29E-02
^{27}Mg	843	10.73	1	1.73E-02	1.01E-02	1.47E-02	8.55E-03	2.47E-02	1.44E-02
	1014	9.92	1	3.33E-03	2.10E-03	2.13E-02	1.34E-02	1.53E-02	9.66E-03
^{56}Mn	846	10.71	0.98	1.42E-01	8.38E-02	2.41E-01	1.42E-01	1.00E-02	5.90E-03
	1810	7.75	0.27	2.07E-02	6.13E-02	2.87E-02	8.50E-02	1.75E-01	5.18E-01
^{28}Al	1778	7.81	1	1.20E-02	9.60E-03	1.27E-02	1.01E-0.2	1.73E-02	1.39E-02

TABLE 5.7: Calculation of the activity concentration for gamma-ray spectra of concentrate samples acquired for 25 minutes (Run2).

				MRY		UG2		PPL	
Radionuclide	**Energy** (keV)	**Efficiency** (%)	**Br** (%)	**Counts rate** (Counts/s)	**Activity** (Bq/Kg)	**Counts rate** (Counts/s)	**Activity** (Bq/Kg)	**Counts rate** (Counts/s)	**Activity** (Bq/Kg)
^{24}Na	1368	8.73	1	1.52E-02	1.09E-02	2.00E-02	1.43E-02	3.33E-02	2.39E-02
^{27}Mg	843	10.73	1	1.71E-02	9.99E-03	2.48E-02	1.44E-02	4.14E-02	2.41E-02
	1014	9.92	1	4.29E-03	2.70E-03	1.14E-02	7.20E-03	3.00E-02	1.89E-02
^{56}Mn	846	10.71	0.98	1.41E-01	8.32E-02	2.72E-01	1.60E-01	1.63E-01	9.64E-02
	1810	7.75	0.27	2.52E-02	7.48E-02	2.86E-02	8.47E-02	1.90E-02	5.65E-02
^{28}Al	1778	7.81	1	1.81E-02	1.45E-02	2.95E-02	2.36E-02	3.20E-02	2.63E-02

TABLE 5.8: Calculation of the activity concentration for gamma-ray spectra of concentrate samples acquired for 35 minutes (Run3).

5.3 Observations and comparative analysis of the gamma-ray spectra of the concentrate samples

The net counts in peaks of each element in the gamma-ray spectrum was determined by performing a gaussian fitting on the peak and the calculated value was quoted as the (net count in peak ± standard deviation).

The standard deviation is expressed as one sigma "1σ" which corresponds to 68% level of confidence. For expanding the level of confidence, the standard uncertainty is re-scaled using the coverage factor (k). The coverage factor, k, is the number which is multiplied by the combined standard uncertainty (equivalent to one standard deviation) to give an expanded uncertainty for a particular level of confidence. For normal distribution, some of the coverage factors are: $k = 1$ for a confidence level of approximately 68%, $k = 2$ for a confidence level of approximately 95%, $k = 2.58$ for a confidence level of 99%, and $k = 3$ for a confidence level of 99.7% [113].

In this work, the reported uncertainties are based on the standard uncertainty multiplied by a coverage factor $k = 2$, which gives standard uncertainty of 2σ, and defines an interval having a level of confidence of approximately 95%. Thus, the results of the amount of each element in the samples were quoted as (net count in peak $\pm 2\sigma$). These results were compared, by taking two samples at a time, and the overlapping between the results was studied. In the cases where two results do not overlap within the 95% confidence level, the ratio of the net counts in peak for these results were determined.

A comparison between the three concentrate samples was performed by plotting the net counts in peaks of the chosen radioisotopes in the concentrates gamma-ray spectra (Fig 5.7). A comparative discussion of the observation for each element is as follows:

- **Sodium** was identified with 1368 keV peak of ^{24}Na ($t_{1/2}$ = 14.9 hr). Na levels are consistently higher in the UG2 sample. However, the results of ^{24}Na in the three concentrate samples overlapped over the 95% confidence level.

- **Magnesium** was identified using ^{27}Mg ($t_{1/2}$ = 9.4 min), which is the product nuclide from the neutron capture reaction ^{26}Mg (n, γ) ^{27}Mg. The two gamma-rays peaks 843 keV and 1014 keV, were observed in the three concentrates gamma-ray spectra. The results of ^{27}Mg in the three concentrate samples overlapped over the 95% confidence level.

- **Aluminum** was identified using ^{28}Al ($t_{1/2}$=2.24 min), which is produced from the neutron capture reaction on ^{27}Al. The ^{28}Al nucleus decays via β^- emission into the 1778 keV excited state of the daughter nucleus ^{28}Si.

  The line of aluminum is relatively weak, which may indicate the low existence of this element in the concentrate samples. All the concentrate samples contain similar amounts of ^{28}Al.

- **Manganese** main activity is due to the short-lived ^{56}Mn ($t_{1/2}$ = 2.5 hr). The 846 keV is the most dominant peak in the concentrates spectra. The existence of manganese in the samples is confirmed with the second peak at 1810 keV.

  The results of ^{56}Mn in the MRY and the UG2 concentrates were overlapped over the 95% confidence level. PPL concentrate shows higher contents of ^{56}Mn compared to MRY and UG2. The ratio of PPL to UG2 is 1.66 to 1, and the ratio of PPL to MRY is 1.9 to 1. Results for 846 keV line show a distinct traingle pattern. However, the differences in results for the 1810 keV line are marginal.

These observations are illustrated in Fig 5.8, where the selected gamma-ray spectra were subtracted from each other and the resultant difference spectra are shown.

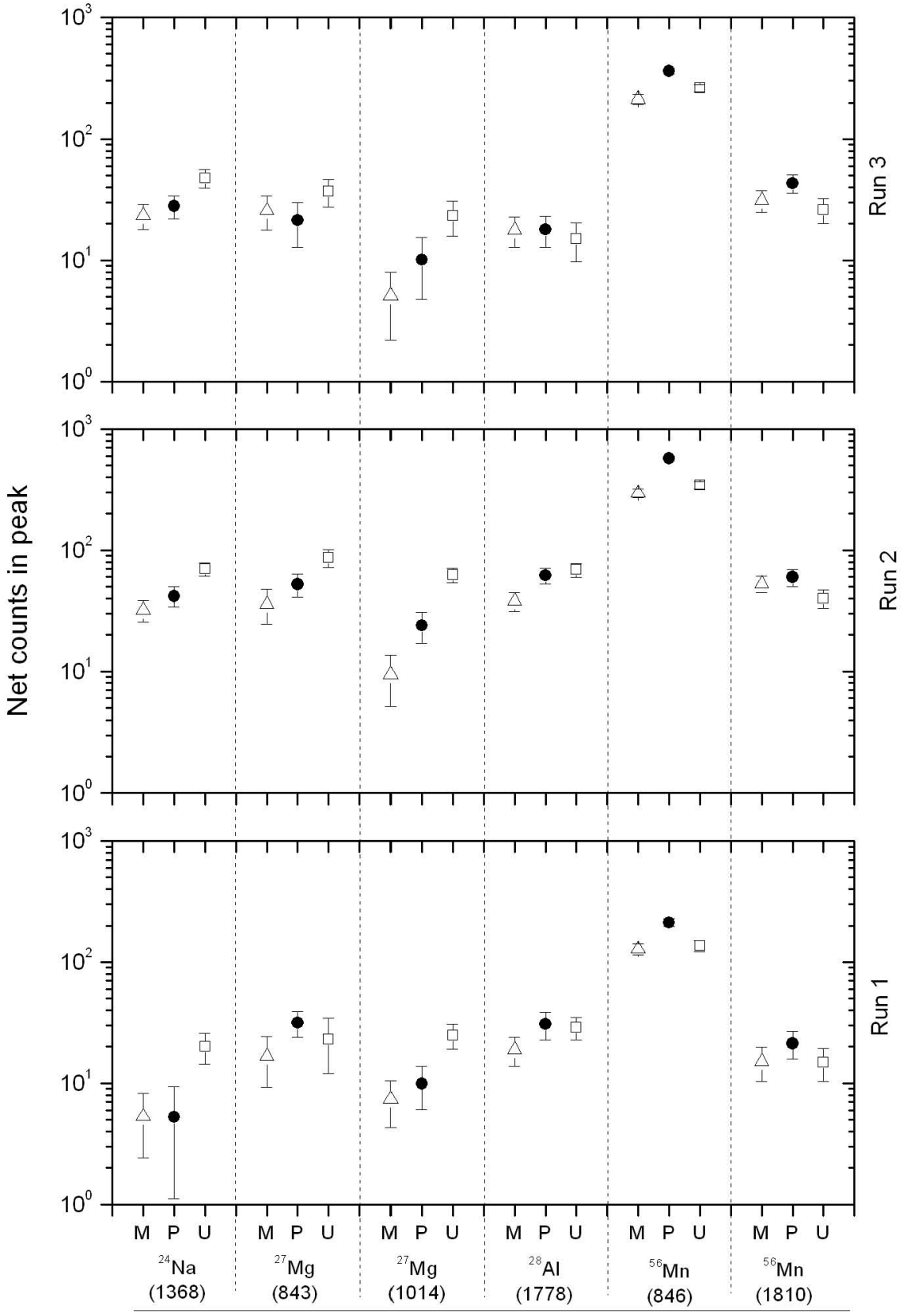

FIGURE 5.7: The net counts in the selected peaks of the radionuclides observed in the gamma-ray spectra of the concentrates for MRY (M; Δ), PPL (P; •), and UG2 (U; □).

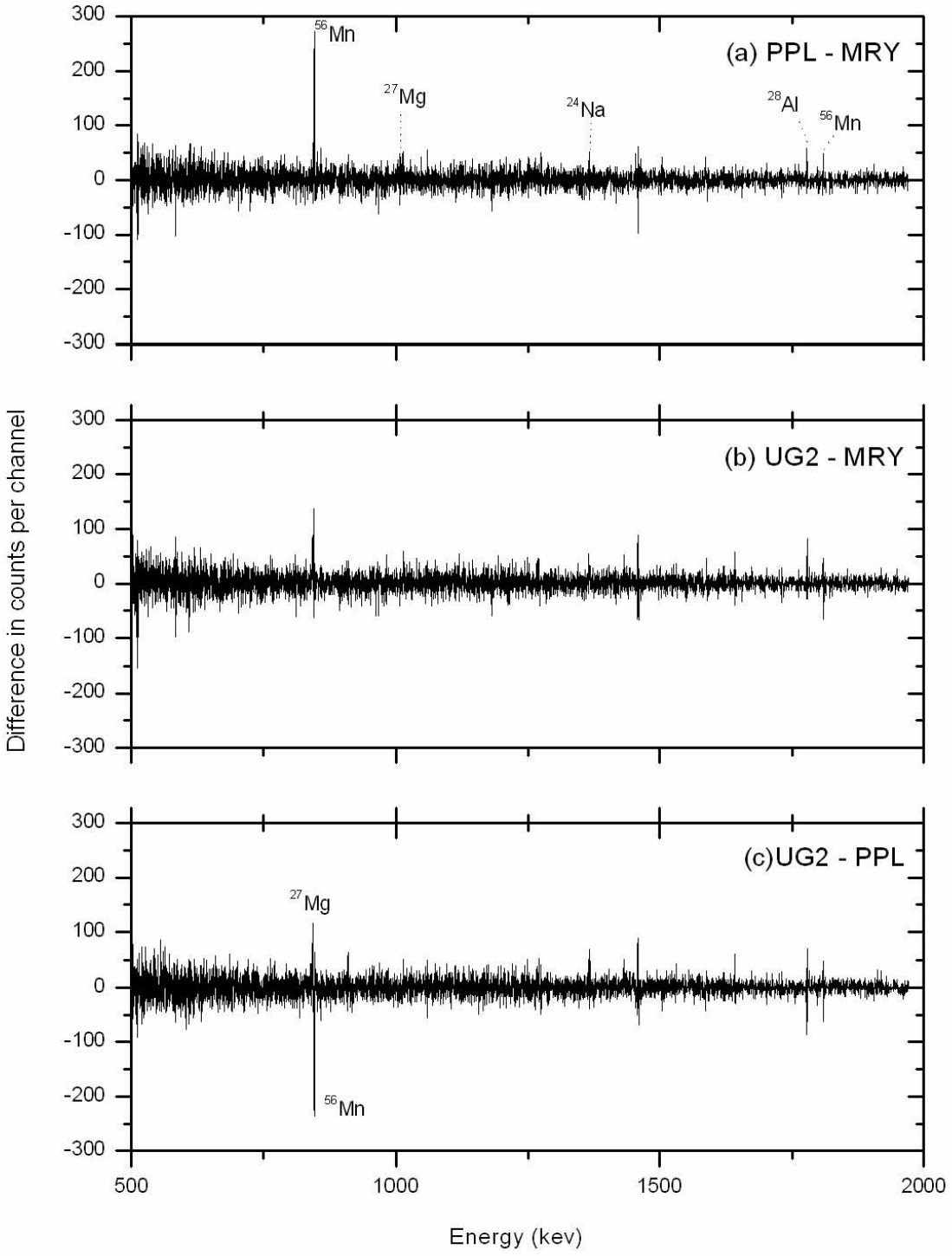

FIGURE 5.8: Differences between the gamma-ray spectra for the 3 concentrates (Run 3).

5.4 Results of the radiometric inspection of the ore samples

As previously discussed in Subsection 4.4, the variation of naturally emitted radiation from the three soil (ore) samples was measured by means of gamma-ray spectroscopy. The three samples were measured for about 24 hours (each sample). Table 5.9 shows the total count rates for the background and soil samples. The data are based on the total number of counts in the entire spectrum divided by live time of acquisition. The sample data as presented in the table, and the figures (Figs 5.9 and 5.10), are not corrected for background.

Sample description	**Total count rate (cps)**
Empty Marinelli Beaker	2.093 ± 0.003
Deionised water	2.127 ± 0.003
PPL sample	11.487 ± 0.012
MRY sample	4.851 ± 0.007
UG2 sample	5.369 ± 0.008

TABLE 5.9: The total count rates per second for the background and ore samples.

In the figures shown (Figs 5.9 and 5.10), all the soil samples spectra presented are superimposed over a background spectrum (empty Marinelli beaker). It is noticeable that the differences in intensities for each sample are relative to the background spectrum. The scan across shows that the gamma-ray energy signals are similar to natural radionuclides, dominated mainly by the uranium-series and thorium-series radionuclides, plus the ^{40}K gamma-ray energy signal at 1460 keV.

In the thorium series (^{232}Th, $t_{1/2} = 1.9 \times 10^{10}$ yr), gamma-ray peaks of ^{228}Ac ($t_{1/2} = 6.1$ hr), ^{212}Pb ($t_{1/2} = 10$ hr), and ^{208}Tl ($t_{1/2} = 3.1$ min) were observed. While, in the high relative abundance uranium series (^{238}U, $t_{1/2} = 4.4 \times 10^{8}$ yr), the observed gamma-ray peaks were for ^{234}Th ($t_{1/2} = 24.1$ d), ^{226}Ra ($t_{1/2} = 1600$ yr), ^{214}Pb ($t_{1/2}$= 26.6 min), and ^{214}Bi ($t_{1/2}$= 19.9 min).

The net counts in some of the most intense peaks in the ore gamma-ray spectra were extracted with Origin software (Table 5.10), then a comparison between the three ore samples was performed by plotting the net counts in peaks (Fig 5.11).

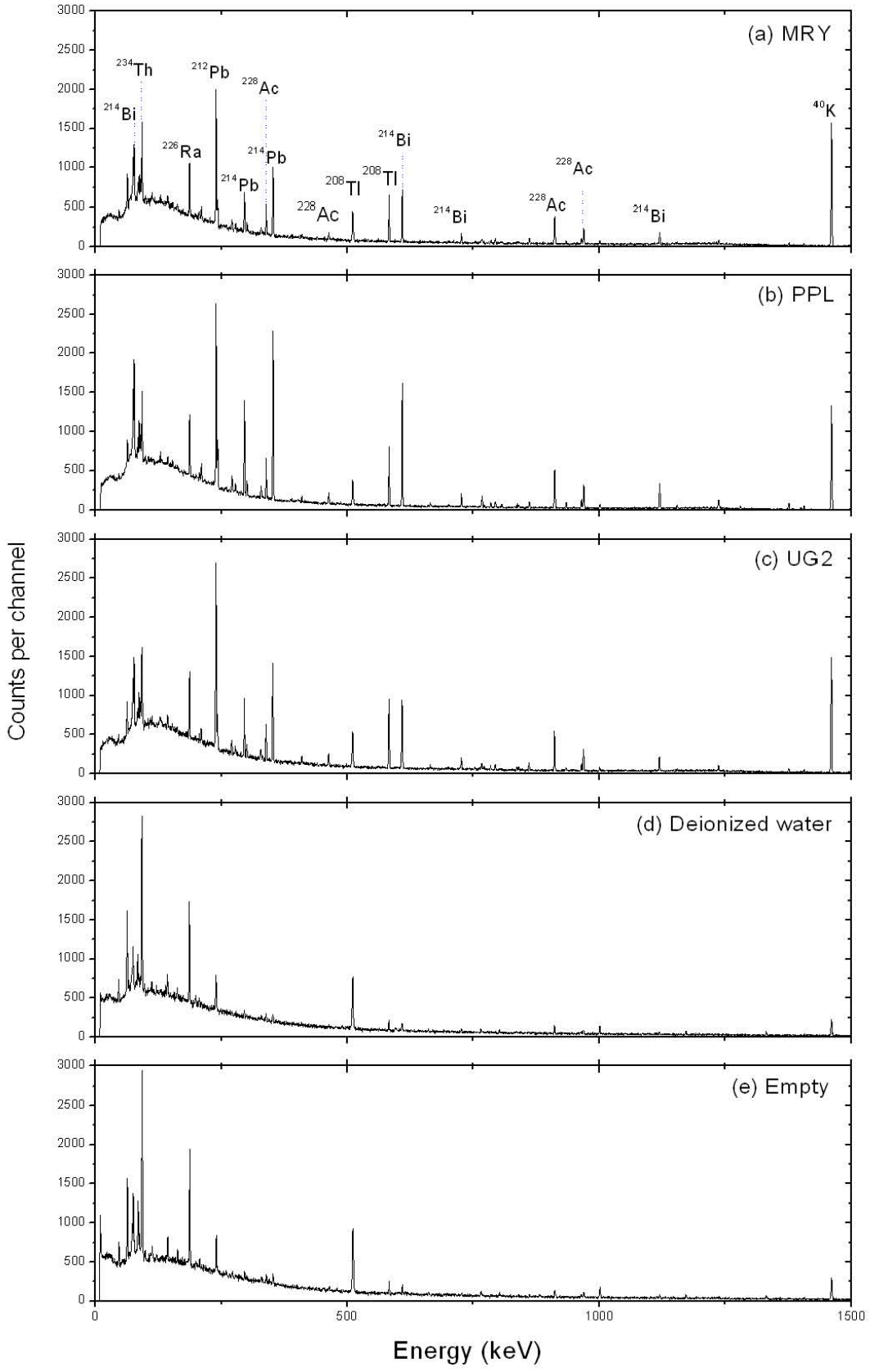

FIGURE 5.9: Gamma-ray spectra for ore samples, deionized water and empty beaker. Gamma energy range from 0 to 1500 keV.

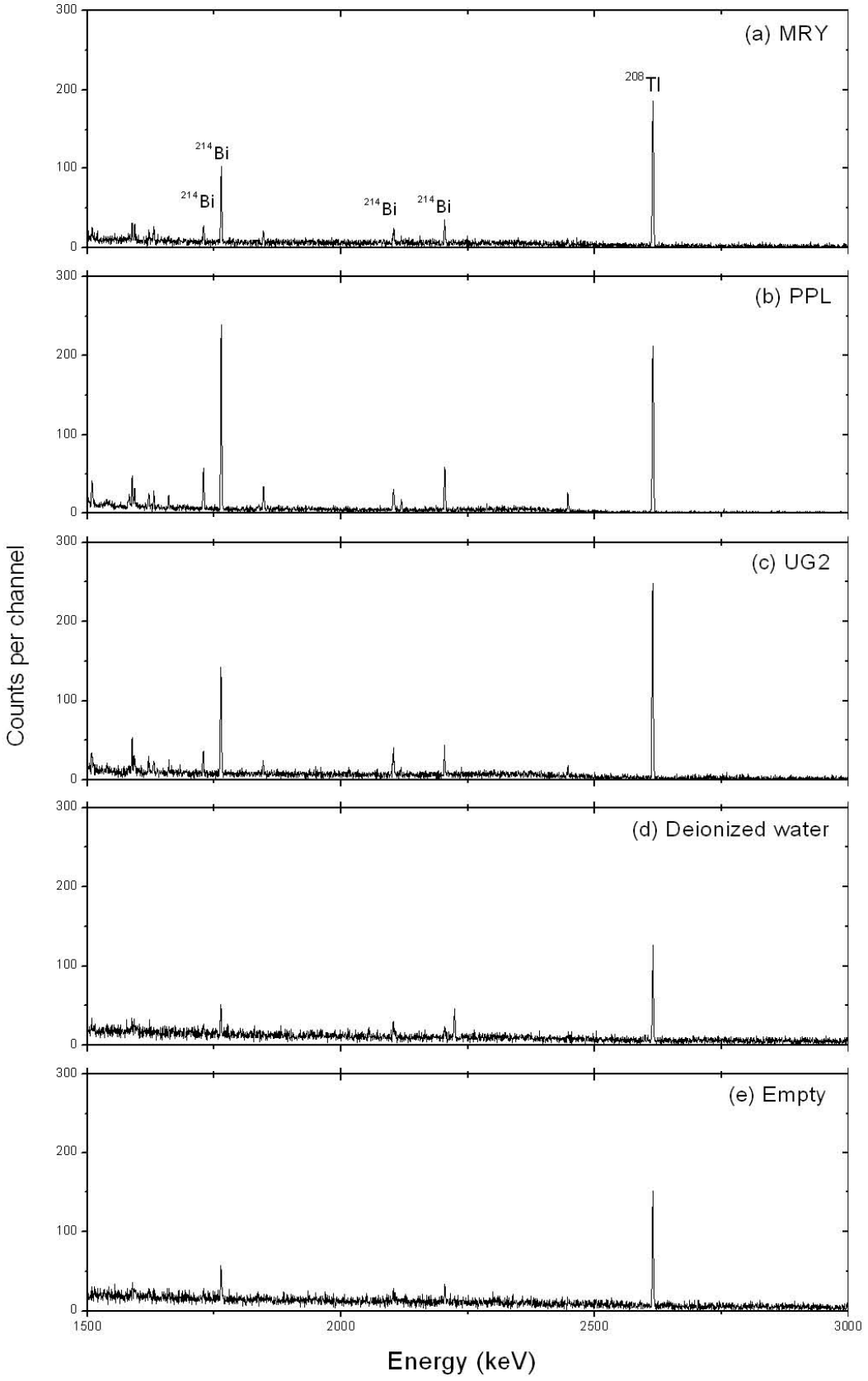

FIGURE 5.10: Gamma-ray spectra for ore samples, deionized water and empty beaker. Gamma energy range from 1500 to 3000 keV.

Isotope	**Energy(keV)**	**MRY** $N_P \pm \sigma_P$	**PPL** $N_P \pm \sigma_P$	**UG2** $N_P \pm \sigma_P$
^{40}K	1460	7469 ± 87	6069 ± 56	6779 ± 83
^{208}Tl	510	2399 ± 60	1931 ± 38	2906 ± 63
	582	2321 ± 55	2854 ± 43	3383 ± 62
	2614	1027 ± 33	1180 ± 25	1303 ± 36
^{212}Pb	238	9282 ± 116	8997 ± 77	12112 ± 128
^{214}Pb	296	2538 ± 66	4324 ± 56	3368 ± 71
	352	3737 ± 72	7737 ± 69	5414 ± 84
^{214}Bi	77	9035 ± 137	11642 ± 105	8566 ± 124
	609	2632 ± 57	5727 ± 58	3690 ± 65
	726	764 ± 34	789 ± 25	723 ± 32
^{226}Ra	186	4010 ± 88	4653 ± 65	4613 ± 91
^{228}Ac	338	1947 ± 55	2141 ± 41	2466 ± 62
	911	1593 ± 44	1987 ± 35	2151 ± 50
	968	1020 ± 36	1180 ± 29	1227 ± 39
^{234}Th	93	7632 ± 122	4670 ± 67	5810 ± 101

TABLE 5.10: The net peak area (N_p) and the uncertainty (σ_P) for the ore samples.

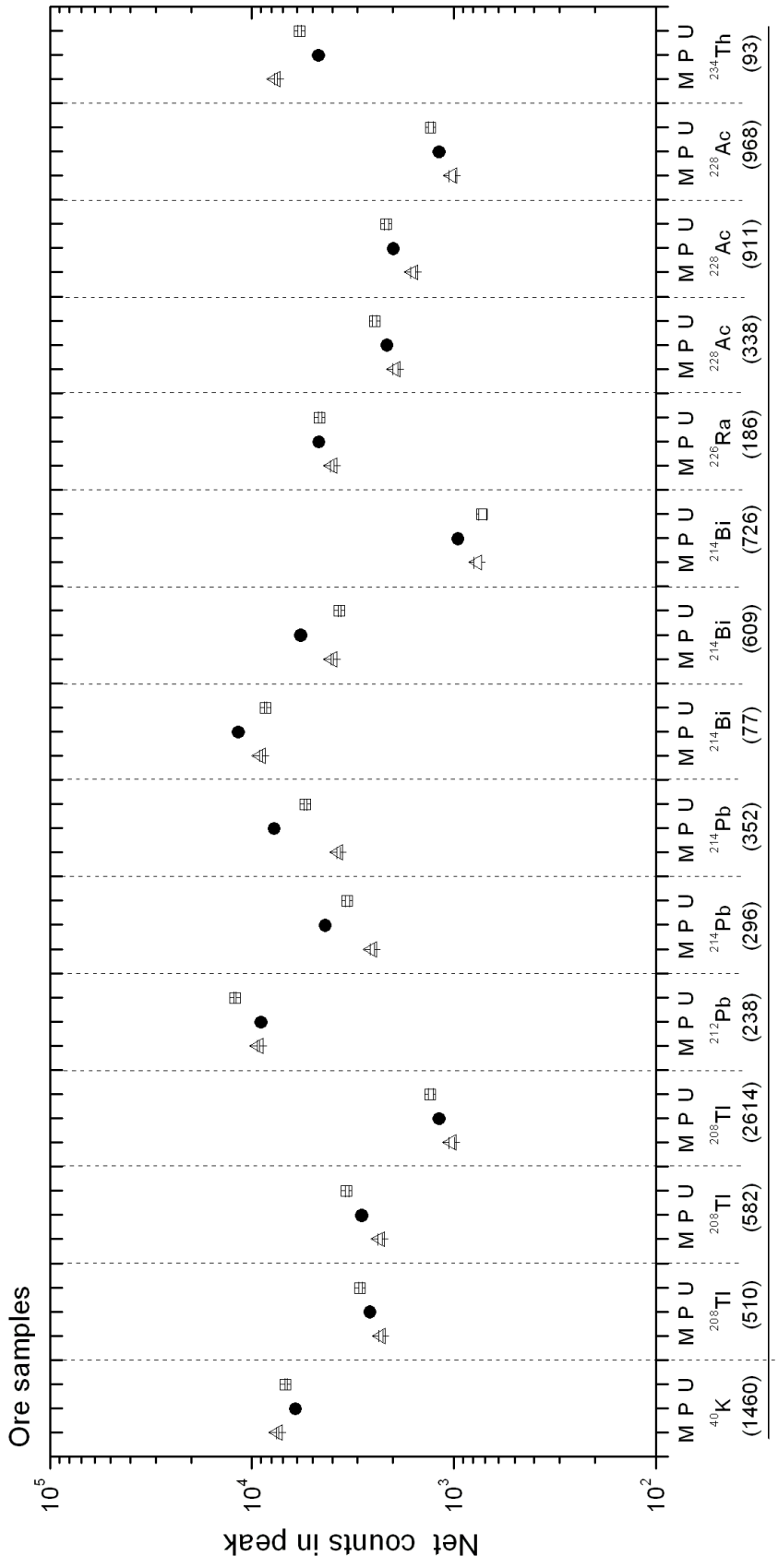

FIGURE 5.11: The net counts in the peaks of the natural radionuclides observed in the gamma-ray spectra of the ore samples. MRY (M; Δ), PPL (P; •), and UG2 (U; □).

Chapter 6

Results from experiments at NECSA

6.1 Introduction

Many types of geological samples, after irradiations in a thermal neutron reactor, show intense peaks of ^{24}Na, ^{28}Al, ^{42}K, ^{46}Sc, ^{51}Cr, ^{56}Mn, ^{59}Fe and ^{140}La, formed by neutron capture reactions [114]. Nevertheless, in a nuclear reactor, activation not only occurs with thermal neutron fluxes, but also with epithermal and fast neutrons. On the other hand, a convenient choice of the optimum irradiation, decay and counting times allow the identification of different groups of elements in the samples according to the elements' half-lives, and helps to avoid relative spectral interferences in the measured spectra.

The experiments were undertaken at the SAFARI-1 nuclear reactor at NECSA (Section 4.5). The nuclear-physics properties of the identified elements in the gamma-ray spectra of the samples analysed are listed in Table 6.1.

6.1.1 Spectra acquired after three days decay

The decay period of 3 days after the end of the irradiation gives the opportunity for shorter lived (half-lives in the order of a few seconds or minutes) radionuclides to decay, and allows the identification of intermediately lived radionuclides. For example, one of the most prominent activities present is for ^{24}Na ($t_{1/2}$ = 14.9 hr), which has the most intense photopeaks and usually dominate the gamma-ray spectrum from 2 to 8 days after irradiation [115]. The gamma-ray spectra were counted for 30 minutes for the three concentrates (Fig 6.1), feeds

Element	Daughter radionuclide measured	Photopeak(s) used in determination (keV)	Intensity (%)	Cross-section (barn)	Half-life	Product isotope
Na	^{24}Na	1368 1732 2243	99.99	0.53	14.9 hr	^{24}Mg
K	^{42}K	1524	18.08	1.459	12 hr	^{42}Ca
Sc	^{46}Sc	889 1120 2010	99.98 99.98	27.16	83 d	^{46}Ti
Cr	^{51}Cr	320	9.91	15.92	27 d	^{51}V
Ni	^{58}Co	811	99.45	...	70 d	^{58}Fe
Fe	^{59}Fe	192 1100 1292	3.08 56.5 43.2	1.149	44 d	^{59}Co
Co	^{60}Co	1173 1332	99.85 99.98	37.17	5.2 yrs	^{60}Ni
Cu	^{64}Cu	1346	0.475	4.470	12 hr	^{64}Ni
As	^{76}As	559 657	45.0 6.2	4.501	1.07 d	^{76}Se
Mo	^{99}Mo	140	4.52	0.13	65 hr	^{99}Ru
La	^{140}La	487 1596	45.5 95.4	9.041	1.6 d	^{140}Ce
Sm	^{153}Sm	103	29.25	206	46 hr	^{153}Eu
Pt	^{199}Au	158	40	...	3.1 d	^{199}Hg
Au	^{198}Au	411	95.58	...	2.6 d	^{198}Hg

TABLE 6.1: Nuclear data for radionuclides identified by thermal reactor activation.

(Fig 6.2), and tailings (Fig 6.3) samples. The 0-300 keV data were measured on a separate ADC to the data above 300 keV, which made no difference to the results. The analyses of these spectra is tabulated in Tables 6.2, 6.3, and 6.4. The deadtimes during HPGe measurements were always below 10%

These samples were prepared as mentioned earlier (see Section 4.2). To prepare the concentrate sample, a feed is prepared by mixing an ore sample with plant water and milling the mixture for a certain length of time ($\sim$ 15 minutes). The feed is then transfered to the flotation cell and floated with the addition of suitable reagents to help recover the valuable elements to the concentrate froth. While the unwanted elements are quantitatively retained in the flotation cell (Tailings sample). Therefore, it is expected to find high contents of certain elements (such as platinum group elements and base metal sulfides (BMS): copper, nickel and cobalt) in the concentrate samples that are not present, or present but in very low amounts in the tailing samples, depending on the quality of the flotation process. This has to do with the care in handling the reagents and their conditioning time as well as the trained worker who is conducting the flotation. Thus in this manner, NAA could also be used to evaluate the quality of the froth flotation process via analysing the concentrates, feeds and tailings.

The elements identified in this process include sodium (indicator is ^{24}Na), samarium (indicator is ^{153}Sm), molybdenum (indicator is ^{99}Mo), arsenic (indicator is ^{76}As), copper (indicator is ^{64}Cu), lanthanum (indicator is ^{140}La), platinum (indicator is ^{198}Au), and gold (indicator is ^{199}Au). Further discussion is given in Subsection 6.1.2.

Some other lines were also observed and identified in all the samples, but they were too small to measure. The lower the concentration of an element in a sample, the less precise the analytical data [3]. On the other hand, it was not necessary to consider all the observed lines in the analysis, because we were not attempting to determine the overall composition of the sample.

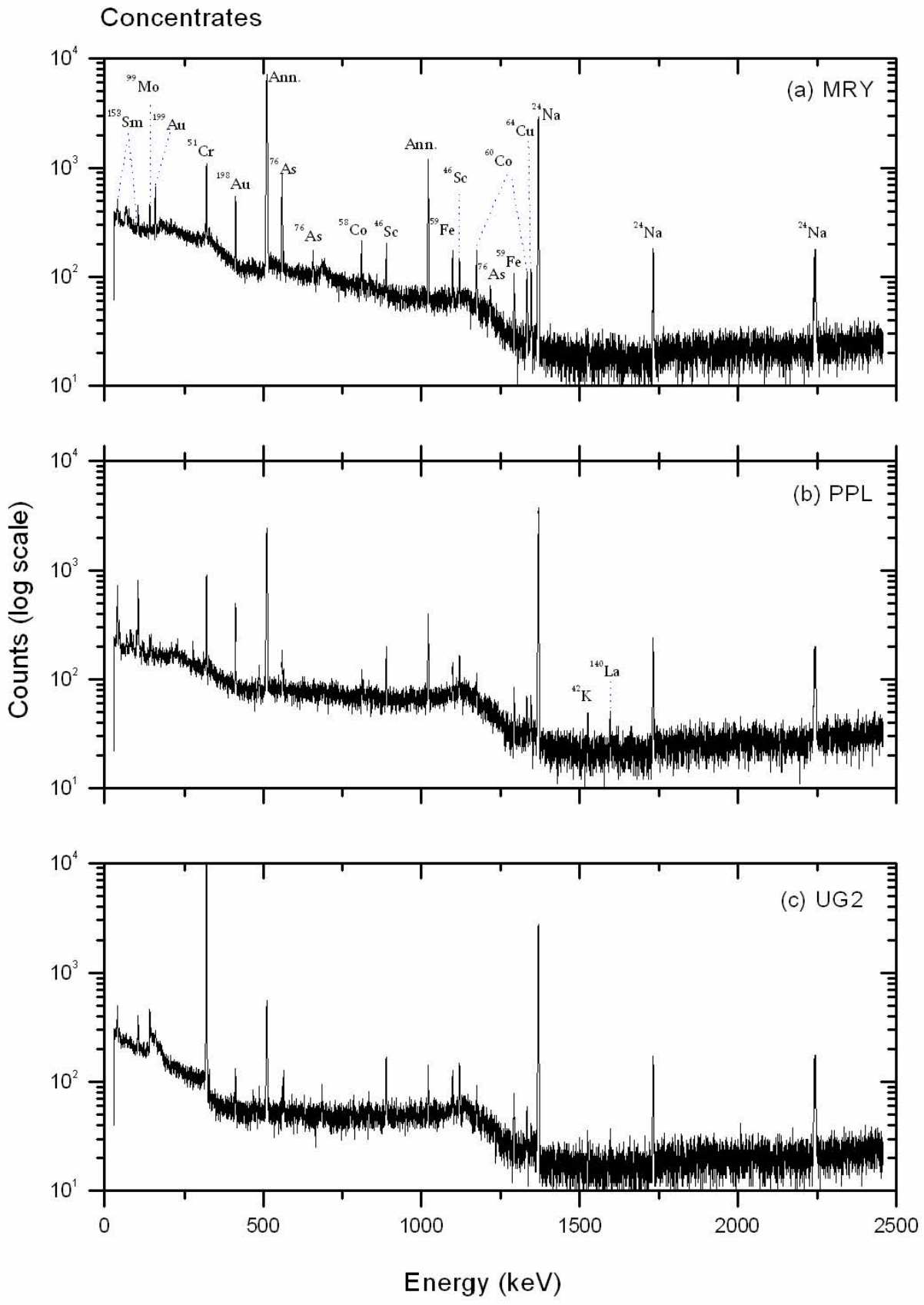

FIGURE 6.1: Gamma-ray spectra of the three concentrates: (a) Merensky (MRY), (b) Platreef (PPL), and (c) Upper group chromite (UG2), acquired after 3 days decay. The photopeaks are labeled with the identified radionuclides in panel (a).

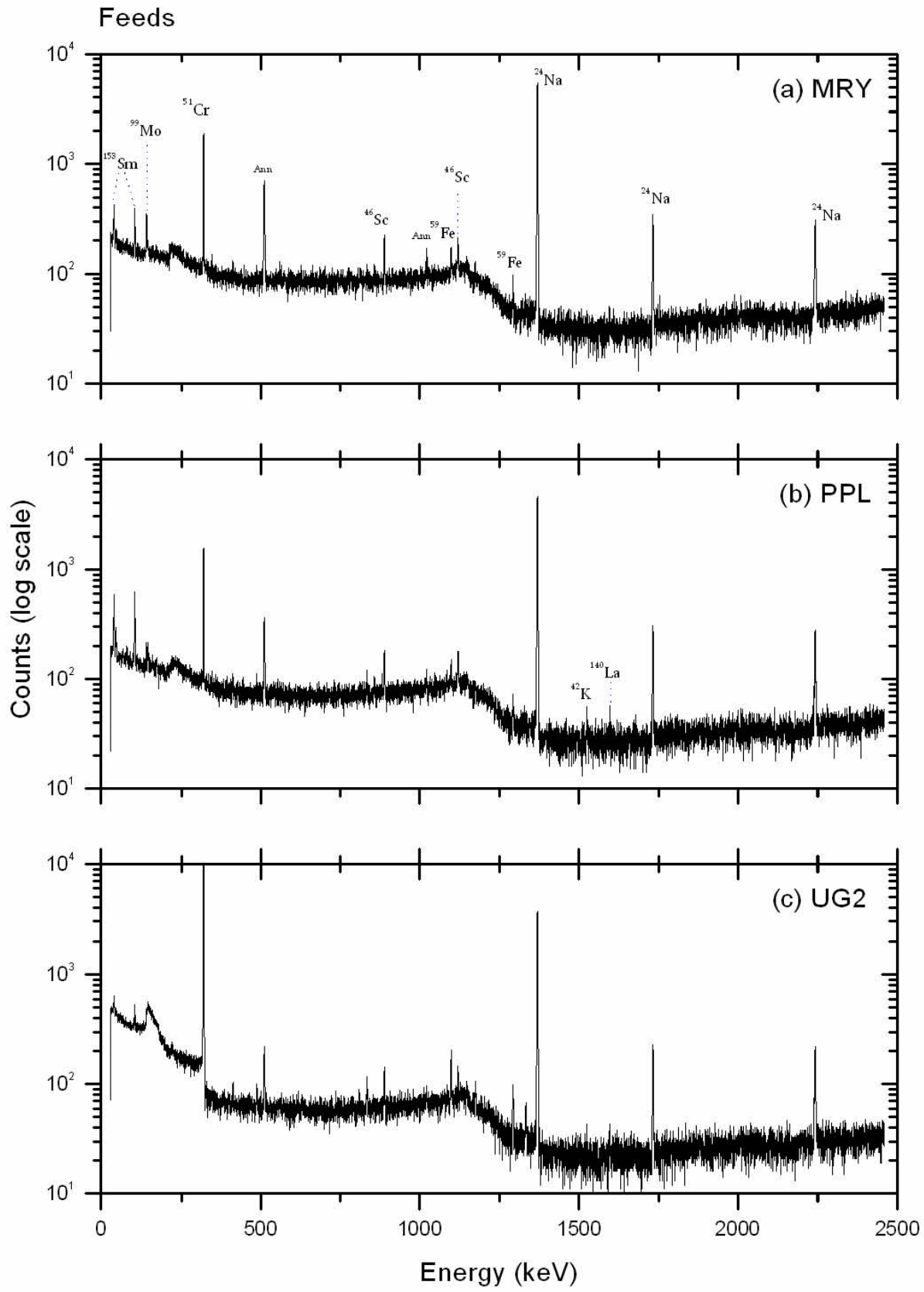

FIGURE 6.2: Gamma-ray spectra of the three feeds: (a) Merensky (MRY), (b) Platreef (PPL), and (c) Upper group chromite (UG2), acquired after 3 days decay. The photopeaks are labeled with the identified radionuclides in panel (a). The UG2 spectrum was counted for 60 minutes in the energy range 0-300 keV (in error).

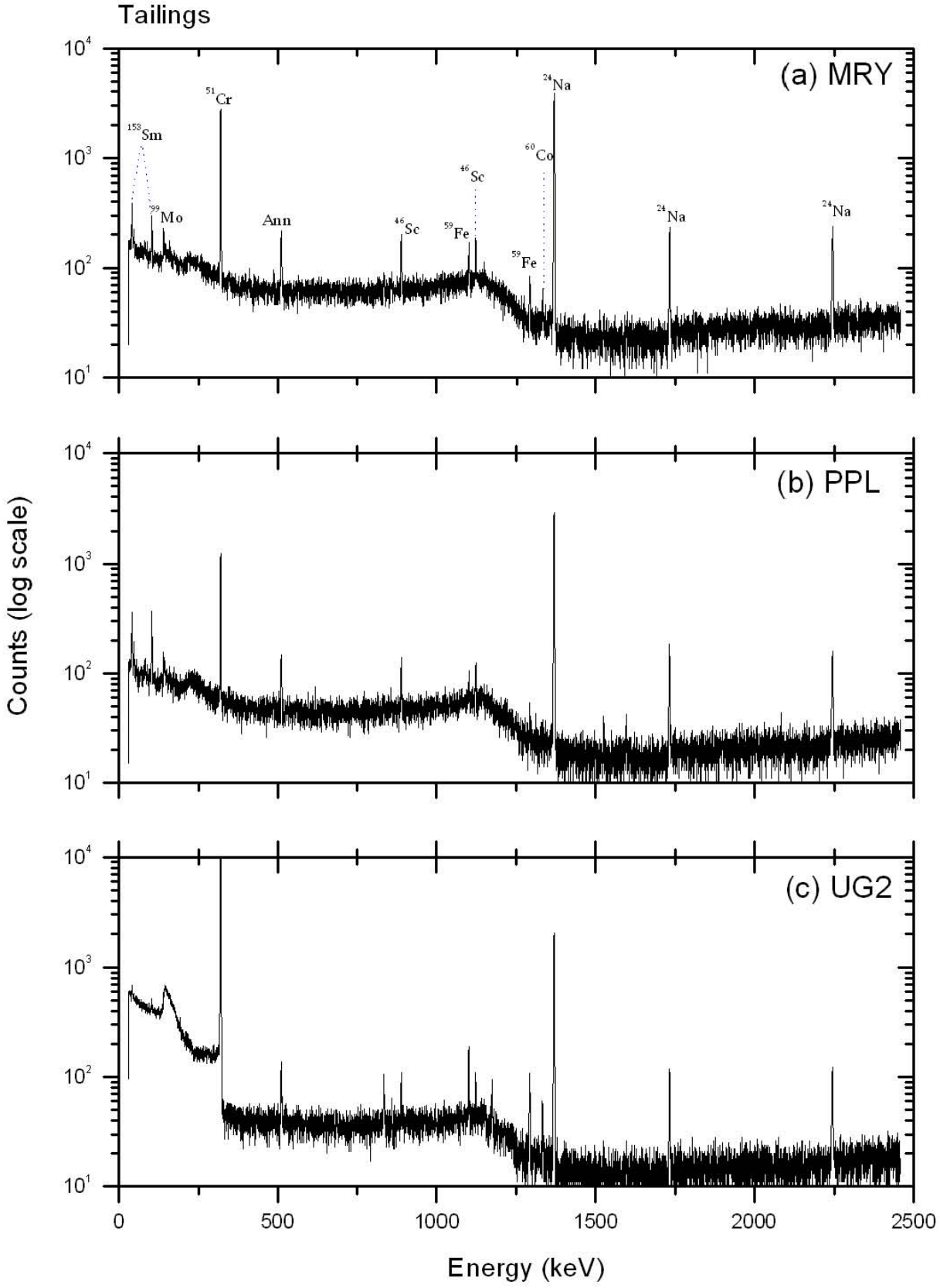

FIGURE 6.3: Gamma-ray spectra of the three tailings: (a) Merensky (MRY), (b) Platreef (PPL), and (c) Upper group chromite (UG2), acquired after 3 days decay. The photopeaks are labeled with the identified radionuclides in panel (a). The PPL spectrum was counted for 60 minutes in the energy range 0-300 keV (in error).

radionuclide	**Energy** (keV)	**MRY** $N_P \pm \sigma_p$	**PPL** $N_P \pm \sigma_p$	**UG2** $N_P \pm \sigma_p$
^{24}Na	1368	26984 ± 172	33813 ± 192	25279 ± 166
	1732	1605 ± 57	909 ± 65	1467 ± 58
	2243	1890 ± 67	2444 ± 74	1794 ± 63
^{42}K	1524	—	167 ± 39	—
^{46}Sc	889	778 ± 66	913 ± 69	1054 ± 73
	1120	563 ± 72	659 ± 82	782 ± 71
	2010	—	—	116 ± 34
^{51}Cr	320	6541 ± 159	5862 ± 128	86329 ± 489
^{58}Co	811	688 ± 78	110 ± 53	—
^{59}Fe	1099	915 ± 82	498 ± 62	573 ± 60
	1292	609 ± 48	352 ± 49	424 ± 49
^{60}Co	1173	851 ± 68	321 ± 65	387 ± 67
	1332	630 ± 52	291 ± 46	247 ± 42
^{64}Cu	1346	777 ± 57	358 ± 50	—
^{76}As	559	5812 ± 130	611 ± 74	—
	657	540 ± 89	—	—
	1216	330 ± 61	—	—
^{99}Mo	140	1210 ± 147	192 ± 96	1370 ± 105
^{140}La	487	—	315 ± 65	169 ± 48
	1596	—	222 ± 41	119 ± 38
^{153}Sm	40	1484 ± 145	4107 ± 265	1557 ± 137
	102	1283 ± 121	5826 ± 188	1357 ± 124
^{198}Au	411	3038 ± 103	3036 ± 101	335 ± 57
^{199}Au	158	2878 ± 152	—	—
Ann+	511	78997 ± 305	26960 ± 188	5746 ± 104
Ann+	1022	8972 ± 123	2813 ± 88	543 ± 56

TABLE 6.2: Results for the gamma-ray spectra of the three concentrate samples acquired after 3 days decay.

radionuclide	**Energy** (keV)	**MRY** $N_P \pm \sigma_p$	**PPL** $N_P \pm \sigma_p$	**UG2** $N_P \pm \sigma_p$
^{24}Na	1368	50292 ± 234	42981 ± 217	34315 ± 194
	1732	2945 ± 79	2538 ± 74	2015 ± 65
	2243	3475 ± 92	3010 ± 85	2429 ± 77
^{46}Sc	889	1202 ± 83	968 ± 84	806 ± 75
	1120	698 ± 77	803 ± 94	453 ± 70
^{51}Cr	320	13384 ± 153	11241 ± 134	183404 ± 440
^{59}Fe	1099	603 ± 83	—	896 ± 78
	1292	369 ± 57	192 ± 50	594 ± 56
^{60}Co	1173	—	—	344 ± 66
	1332	—	—	345 ± 57
^{99}Mo	140	1347 ± 112	376 ± 42	—
^{140}La	1596	—	165 ± 39	—
^{153}Sm	40	1622 ± 121	3345 ± 245	1504 ± 185
	102	1543 ± 110	3124 ± 111	1347 ± 160
Ann+	511	6988 ± 123	3553 ± 100	1625 ± 80
Ann+	1022	560 ± 85	—	—

TABLE 6.3: Results for the gamma-ray spectra of the three feeds acquired after 3 days decay.

radionuclide	**Energy** (keV)	**MRY** $N_P \pm \sigma_p$	**PPL** $N_P \pm \sigma_p$	**UG2** $N_P \pm \sigma_p$
^{24}Na	1368	36368 ± 199	26909 ± 171	19104 ± 145
	1732	2113 ± 68	1506 ± 56	1125 ± 50
	2243	2554 ± 78	1821 ± 67	1337 ± 57
^{42}K	1524	—	118 ± 30	—
^{46}Sc	889	1226 ± 77	688 ± 63	529 ± 55
	1120	930 ± 76	512 ± 70	324 ± 56
^{51}Cr	320	20619 ± 166	8962 ± 117	267895 ± 527
^{59}Fe	1099	571 ± 76	250 ± 63	1109 ± 60
	1292	362 ± 49	144 ± 37	808 ± 45
^{60}Co	1173	—	—	317 ± 50
	1332	—	—	362 ± 38
^{99}Mo	140	420 ± 91	244 ± 68	—
^{153}Sm	40	1427 ± 113	2113 ± 196	—
	102	1338 ± 105	1800 ± 90	509 ± 139
Ann+	511	1536 ± 86	1027 ± 69	974 ± 64

TABLE 6.4: Results for the gamma-ray spectra of the three tailings acquired after 3 days decay.

6.1.2 Observations and statistical analysis of the gamma-ray spectra acquired after three days decay

The samples show variations in their elemental content, and some radioisotopes appeared in some of the gamma-ray spectra and not in others. Some rare earth elements, such as ^{153}Sm and ^{140}La, were observed. There is a presence of a 144 keV line in the PPL feed gamma-ray spectrum, which might be an indication of the existence of cerium (^{141}Ce, $t_{1/2} = 32.5$ d). Nuclear reactions other than neutron capture are found to occur, for example ^{58}Co results from the (n,p) reaction on ^{58}Ni and is used to determine nickel.

For the analysis of the results of this experiment the uncertainties were reported as 2σ (as in Section 5.3) which defines an interval having a level of confidence of approximately 95%. The results of the analyses were plotted for the three concentrates (Fig 6.4), feeds (Fig 6.5), and tailings (Fig 6.6).

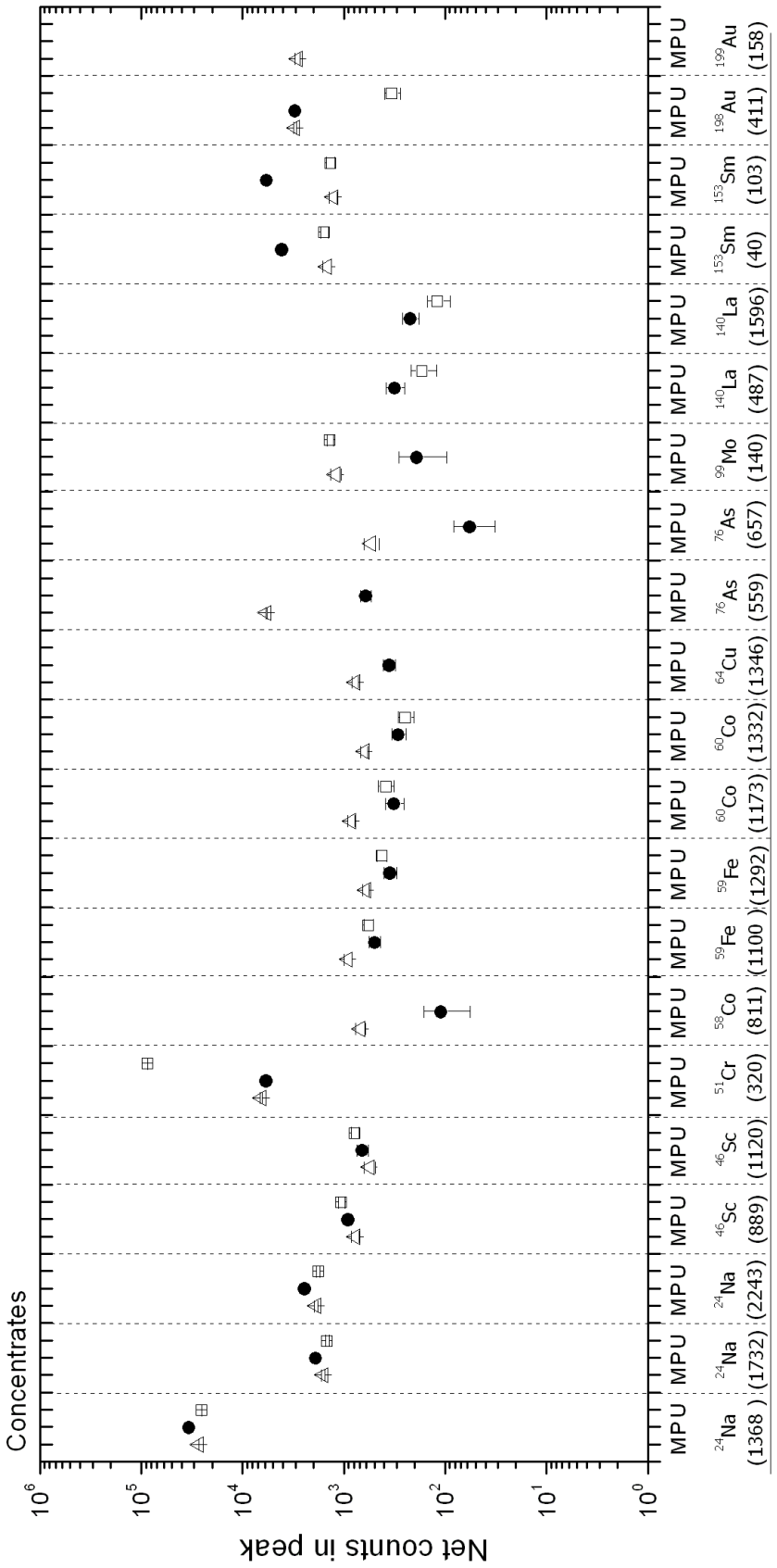

FIGURE 6.4: The net counts in the peaks of the radionuclides observed in the gamma-ray spectra of the concentrates after 3 days decay, for MRY (M; Δ), PPL (P; •), and UG2 (U; □).

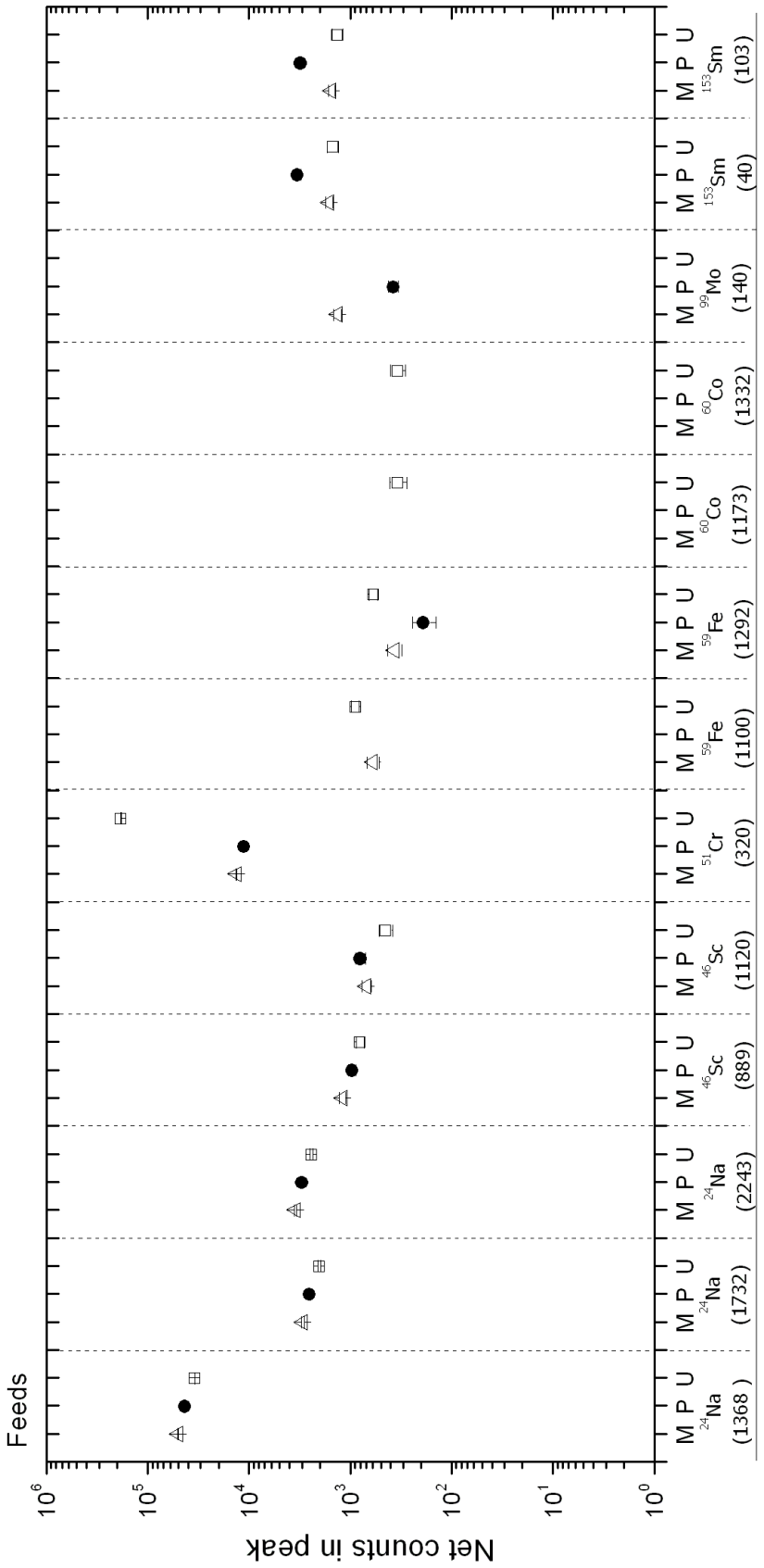

FIGURE 6.5: The net counts in the peaks of the radionuclides observed in the gamma-ray spectra of the feeds after 3 days decay, for MRY (M; Δ), PPL (P; •), and UG2 (U; □).

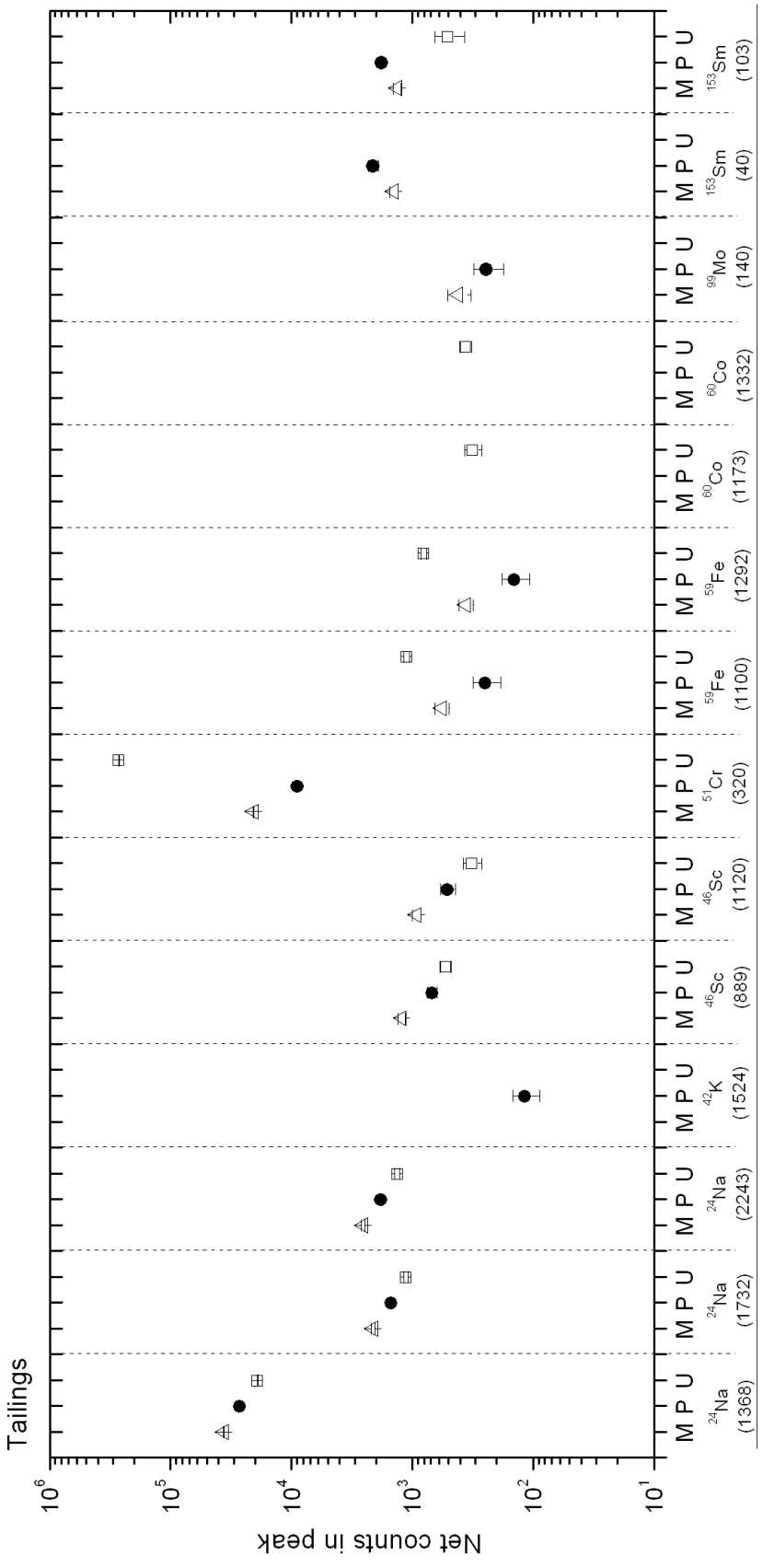

FIGURE 6.6: The net counts in the peaks of the radionuclides observed in the gamma-ray spectra of the tailings after 3 days decay, for MRY (M; Δ), PPL (P; •), and UG2 (U; □).

A comparative discussion of the observation of some of the main elements observed is as follows:

- **Sodium** was identified using ^{24}Na ($t_{1/2}$ = 14.9 hr), which emits gamma-rays of energy 1368 keV, in addition to single escape and double escape peaks at 1732 keV and 2243 keV, respectively. Sodium seems to be the element with the highest abundance in these MRY and PPL concentrate samples. Nonetheless, the amount of sodium in the concentrate samples is less compared to the feed samples.

  There was no overlap of the results of ^{24}Na in the concentrate samples over the 95% confidence level. The ratio of the net counts of the ^{24}Na peak in the PPL concentrate sample to the ratio in the MRY sample is greater than one (around 1.3 to 1), which is the same ratio between PPL to UG2 samples. Since this net counts is greater in the PPL sample compared to the other two, this may indicate that this PPL concentrate sample has a slightly higher content of sodium.

  In the feed samples, there was no overlap between the results of ^{24}Na in the three feed samples within the 95% confidence level. The ratio of net counts in MRY to UG2 is 1.5 to 1, MRY to PPL is around 1.2 to 1, and PPL and UG2 is around 1.3 to 1.

  In the tailings samples, there was no overlap between the results of ^{24}Na in the three feed samples within the 95% confidence level. The ratio of net counts in MRY to UG2 is 2 to 1, MRY to PPL is 1.4 to 1, and PPL and UG2 is also 1.4 to 1.

- **Potassium** was identified using the 1524 keV photopeak of ^{42}K ($t_{1/2}$ =12 hr). This was found only in PPL samples.

- **Scandium** was identified using ^{46}Sc ($t_{1/2}$ = 83 d) which is produced from the neutron capture reaction on ^{45}Sc. The 889 keV, 1120 keV peaks as well as the sum peak at 2010 keV of ^{46}Sc were observed in all the gamma-ray spectra of the samples analysed.

  The results of ^{46}Sc on the three concentrates overlapped within the 95% confidence level.

  In the feed samples, the results of ^{46}Sc overlapped between MRY and PPL, as well as UG2 and PPL. However, these results between MRY and UG2 do not overlap, and the ratio of the net counts of ^{46}Sc in MRY feed sample to UG2 feed sample is 1.5 to 1.

  In the tailings samples, the results of ^{46}Sc in PPL and UG2 overlapped, but no overlap is found between MRY and PPL (the ratio of MRY to PPL is 1.8 to 1), and MRY and UG2 (the ratio of MRY to UG2 is around 2.5 to 1).

- **Chromium** was identified using the 320 keV photopeak of ^{51}Cr ($t_{1/2}$ = 27 d). An important observation is that the amount of chromium in the concentrates, feeds and tailings is higher in UG2 samples. There is a significant difference in the amount of ^{51}Cr in the UG2 sample in comparison to the MRY and PPL samples. In the concentrate samples, the ratio between UG2 to MRY is 13 to 1, and the ratio of UG2 to PPL is around 15 to 1. However, the results in MRY and PPL do not overlap (ratio of MRY to PPL is 1.2 to 1).

  In the feed samples, the ratio of UG2 to MRY is around 14 to 1, and the ratio of UG2 to MRY is around 16 to 1. However, there is no overlap between MRY and PPL (the ratio of MRY to PPL is 1.2 to 1). A similar pattern is observed in the tailings samples, the ratio of UG2 to PPL is 30 to 1 and the ratio of UG2 to MRY is 13 to 1. The results of ^{51}Cr in MRY to PPL tailings samples do not overlap (the ratio of MRY to PPL is around 2.3 to 1).

  Chromium is of high abundance in the mafic ores, although the preparation of the concentrate samples via froth flotation process suppresses the chromium, which is a gangue mineral, and introduces it to the tailing phase. Considering the case of UG2 samples, it is observable that the amount of chromium reported to the concentrate samples in the flotation process is less than the amount of it originally in the feed sample, and much less than the amount in the tailing sample. Nevertheless, UG2 contains the highest amount of chromium in all the samples.

- **Nickel** was identified using the 811 keV gamma line of ^{58}Co ($t_{1/2}$ = 70 d), which is the indicator of nickel produced in the reaction ^{58}Ni(n,p)^{58}Co.

  In the concentrate samples, the results of ^{58}Co in the MRY and PPL do not overlap, the amount of ^{58}Co in the MRY is greater than that in the PPL with a ratio of 6 to 1, which may indicate that MRY concentrates contain higher amounts of nickel in comparison to PPL. The 811 keV photopeak was not observed in the UG2 concentrate sample, suggesting that this UG2 concentrate sample contains very low levels of nickel. This line was also not observed in the feeds or the tailings.

- **Iron** was identified in the samples with the photopeaks of 1100 keV and 1292 keV of ^{59}Fe ($t_{1/2}$ = 44 d). Mafic ores are both Mg-rich and Fe-rich.

  In the concentrate samples, the results of ^{59}Fe in the UG2 and PPL samples were found to be overlapped within the 95% confidence level. On the other hand, there was no overlap between the result of ^{59}Fe in the MRY concentrate sample and the UG2, or MRY and PPL samples. The MRY sample contains a greater amount of ^{59}Fe. The

ratio of net counts in the MRY to UG2 is 1.4 to 1 , and the ratio of MRY to PPL is around to 1.7 to 1.

In the feed samples, the results of ^{59}Fe in the MRY and UG2 feed samples do not overlap, and MRY and PPL also do not overlap. The ratio of UG2 to PPL is 3 to 1.

In the tailings samples, there was no overlap between MRY and PPL (the ratio of MRY to PPL is 2.5 to 1), MRY and UG2 (the ratio of UG2 to MRY is 2.2 to 1), and UG2 and PPL (the ratio of UG2 to PPL is around 5 to 1).

- **Cobalt** was identified using ^{60}Co ($t_{1/2}$ = 5.2 yrs), the product of the neutron capture reaction on ^{59}Co. In the concentrate samples, the results of cobalt in the UG2 and PPL are found to be overlapped within 95% confidence level. The result in the MRY concentrate sample does not overlap with any of the other two concentrates, where ^{60}Co is higher in the MRY concentrate. The ratio of MRY to UG2 is around 3 to 1, and ratio of MRY to PPL is around 2 to 1. This may indicate that MRY concentrate is richer in cobalt, in addition to nickel and iron.

  In the feeds and tailings, the 1332 keV and 1173 keV appear in the UG2 tailing samples and not in the other tailings samples.

- **Copper** was observed only in the gamma-ray spectrum of the MRY and PPL concentrate in the form of its indicator radionuclide ^{64}Cu ($t_{1/2}$ = 12 hr) using its photopeak at 1346 keV, which followed from the neutron capture reaction on ^{63}Cu. No lines of copper appeared in the feeds or tailings.

  Copper and nickel are base metal sulfides (BMS), and they usually report to the concentrate froth in the flotation process along with PGEs.

- **Arsenic** was identified using ^{76}As ($t_{1/2}$ = 1.07 d) peaks 559 keV and 657 keV and sum peak 1216 keV. The peaks 559 keV and 657 keV of ^{76}As ($t_{1/2}$ = 1.07 d) appear in MRY and PPL concentrates gamma-ray spectra, but do not appear in UG2 concentrate gamma-ray spectrum. This may indicate that UG2 concentrate contains no amounts of As or contains very little (ultra-trace) amounts of arsenic, that was not detected using this method.

  The results of ^{76}As in the MRY and PPL are found to differ with no overlap within the 95% confidence level. The amount of ^{76}As in the MRY sample is greater than PPL, with a ratio of around 10 to 1.

- **Molybdenum** was identified using the 140 keV peak of ^{99}Mo ($t_{1/2}$ = 65 hr). The results of ^{99}Mo in the MRY and UG2 are found to be overlapped over 95% confidence

level. The result of ^{99}Mo in the PPL concentrate sample does not overlap with MRY or UG2 concentrates. The amount of ^{99}Mo is less in the PPL sample, where the ratio of UG2 to PPL is 7 to 1 and the ratio of MRY to PPL is 6 to 1.

In the feed samples, the results of ^{99}Mo in the MRY and PPL do not overlap, the ratio of MRY to PPL is 3.6 to 1. The 140 keV peak was not observed in the UG2 feed sample. The same pattern is found in the tailings samples, and the ratio of MRY to PPL is 1.7 to 1.

- **Lanthanum**. The presence of ^{24}Na causes considerable background problems, so it is necessary to wait for around eight days after the end of irradiation in order to see a measurable ^{140}La signal. However, the weak lines of the 487 keV and 1596 keV photopeaks of ^{140}La appeared in the PPL concentrate and feed samples. The lines of ^{140}La were not found in the MRY concentrate sample spectrum. The results of ^{140}La in the UG2 and PPL concentrate samples were found to be overlapped within 95% confidence level.

- **Samarium** is a rare-earth element. The 40 keV and 102 keV peaks of ^{153}Sm ($t_{1/2}$ = 46 hr) begin to be seen, and can reliably be used, two to three days after the irradiation after the ^{24}Na activity had decayed sufficiently to reduce the background in the 100 keV region [14, 99].

  The result of ^{153}Sm overlapped in MRY and UG2 concentrate samples. The result of ^{153}Sm in the PPL sample does not overlap with the results in the MRY or UG2 samples, providing that there is a significant difference in the amount of ^{153}Sm in this PPL concentrate sample compared to the MRY and UG2 concentrate samples, where the amount of ^{153}Sm is greater in the PPL concentrate sample. The ratio of PPL to MRY is 5 to 1, and PPL to UG2 is 4 to 1. In the feed samples, the same pattern was observed, the ratio of PPL to MRY is 2 to 1, and the ratio of PPL to UG2 around 2.3 to 1. However, there was no overlap between any of the results of ^{153}Sm in the three tailings samples. The ratio of PPL to MRY is around 1.5, the ratio of MRY to UG2 is 2.6 to 1, and the ratio of PPL to UG2 is 3.5

- **Platinum** was identified using 158 keV gamma line of its indicator radionuclide ^{199}Au ($t_{1/2}$ = 3.1 d) from the reaction ^{198}Pt(n, γ) ^{199}Pt($t_{1/2}$ = 30 min) $\xrightarrow{\beta^-}$ ^{199}Au.

  In general, the observation of PGEs in the gamma-ray spectra using non destructive neutron activation analysis is not possible. To be able to observe clear lines of PGEs the samples need to undergo a special preparation process which involves chemical

treatment of the samples to eliminate the interfering radionuclides' peaks which mask the gamma-ray lines of PGEs.

In particular, spectral interferences on the 158 keV line may arise from other radionuclides formed during the neutron irradiation. The most important are ^{47}Sc (159 keV, $t_{1/2}$ = 3.4 days) daughter of ^{47}Ca from the reaction ^{46}Ca (n, γ) ^{47}Ca followed by β^- decay; as well as ^{123m}Te (158 keV, $t_{1/2}$ = 104 days) [37].

Since gold is present in geological samples, ^{199}Au will also be produced from the reactions ^{197}Au(n, γ)^{198}Au followed by ^{198}Au (n, γ) ^{199}Au. However, the production of ^{199}Au via this reaction may occur only after long irradiations at high neutron fluxes [108].

The 158 keV line of ^{199}Au was observed in MRY concentrate sample but not in PPL or in UG2 concentrate, which may indicate that MRY concentrate is richer in platinum. This line was not observed in the feeds and the tailings.

- **Gold** was identified using ^{198}Au ($t_{1/2}$ = 2.6 d), the daughter of ^{197}Au from the nuclear reaction ^{197}Au (n, γ) ^{198}Au.

  The 411 keV peak of gold is intense in both MRY and PPL concentrate samples. This peak is weaker in the UG2 sample. In the concentrate samples, the results of ^{198}Au in the MRY and PPL were found to be overlapped within 95% confidence level. However, there was no overlap found between MRY and the UG2 result or PPL and UG2. The ratio of the number of counts in MRY to UG2 is 9 to 1, this ratio is the same as in PPL to UG2.

These observations can be interpreted in a more useful means by finding certain isotopic ratios. For example, if four elements show the most observed variations within the samples, the ratio of these radionuclides may be determined and used to label the samples by means of isotopic ratios signatures. For the samples analysed, the only outstanding ratios found were between two major elements (^{51}Cr and ^{59}Fe) and two trace elements (^{153}Sm and ^{99}Mo). These ratios, in each sample, were calculated and plotted as in Fig 6.7, Fig 6.8, and Fig 6.9 for the concentrates, feeds and tailings respectively.

In the case of the concentrate samples (Fig 6.7), the UG2 sample has the highest ratio of chromium to iron (^{51}Cr/^{59}Fe), and a very low ratio of samarium to molybdenum (^{153}Sm/^{99}Mo). On the other hand, the PPL shows the opposite trend, while the MRY sample shows the lowest isotopic ratios. The same pattern as in the concentrate samples was observed in the case of the feeds and tailings samples.

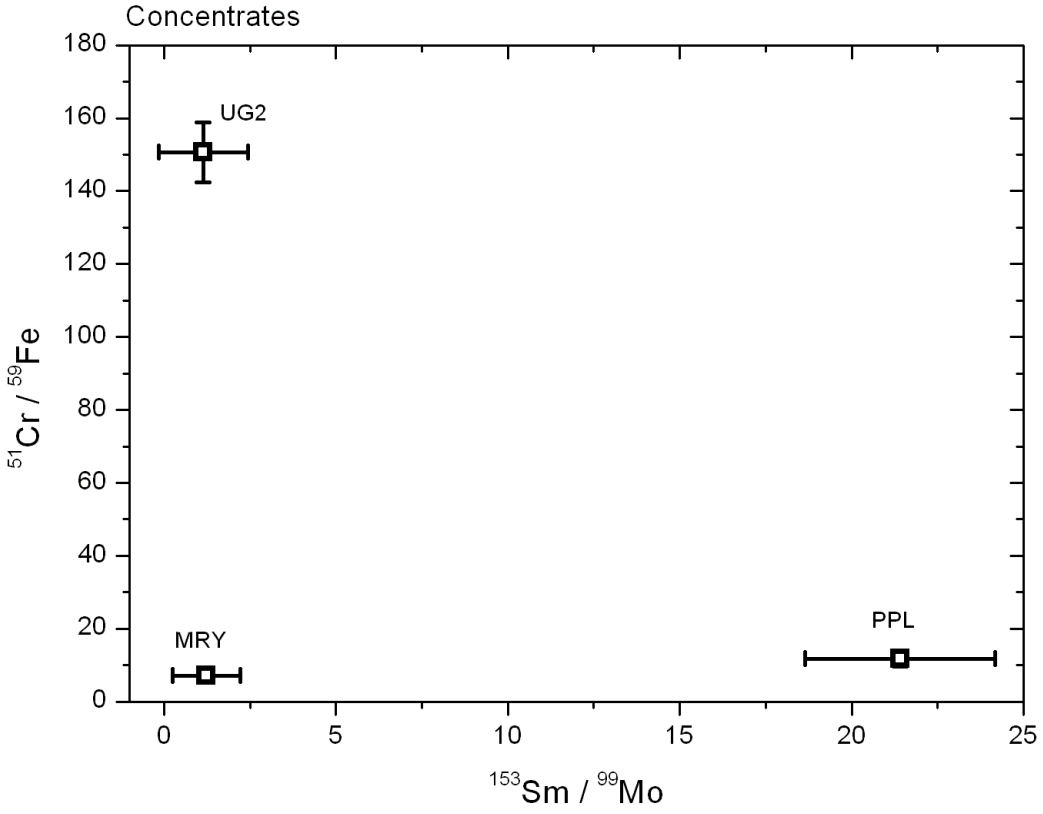

FIGURE 6.7: Ratio of ^{51}Cr to ^{59}Fe versus ^{153}Sm to ^{99}Mo for the concentrates MRY, PPL, and UG2.

From these observations, it is evident that this UG2 sample could be distinguished via the high ratio of (^{51}Cr/^{59}Fe) which is in the magnitude of a hundred, while the PPL samples could be identified with the high ratio of the trace elements (^{153}Sm/^{99}Mo) which varies from around 20 to 1 in the concentrate samples, to around 10 to 1 in the feeds as well as in the tailings.

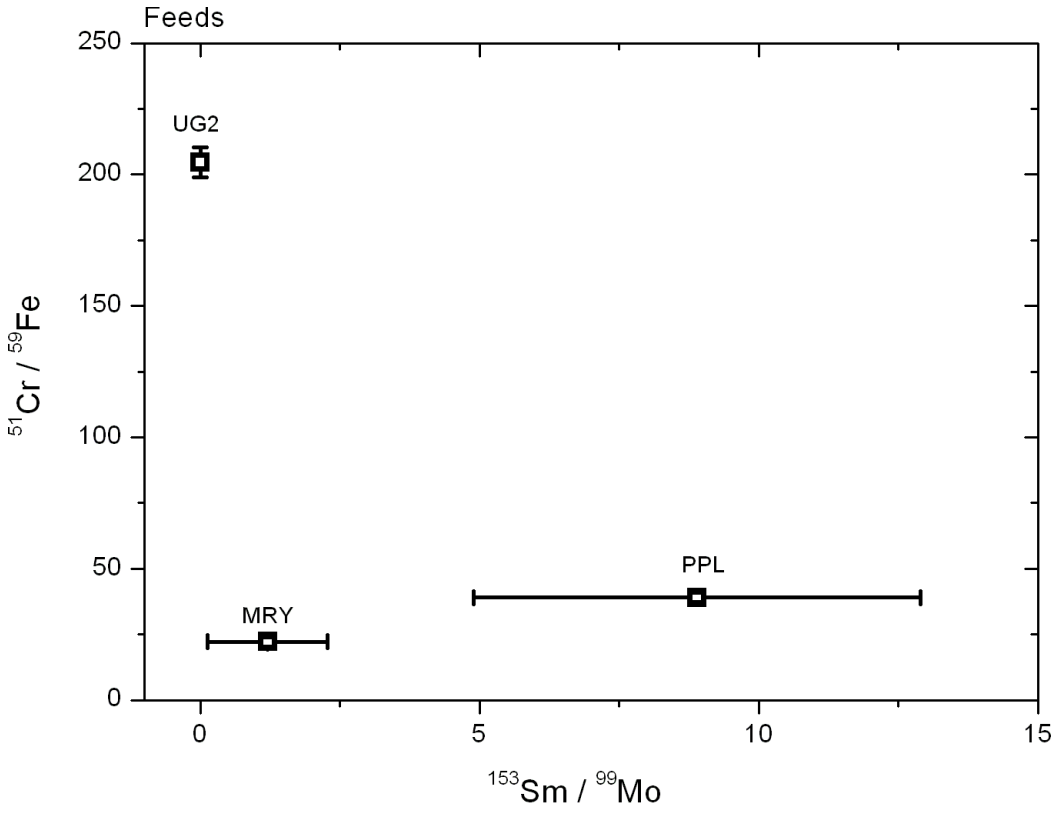

FIGURE 6.8: Ratio of ^{51}Cr to ^{59}Fe versus ^{153}Sm to ^{99}Mo for the feeds MRY, PPL, and UG2.

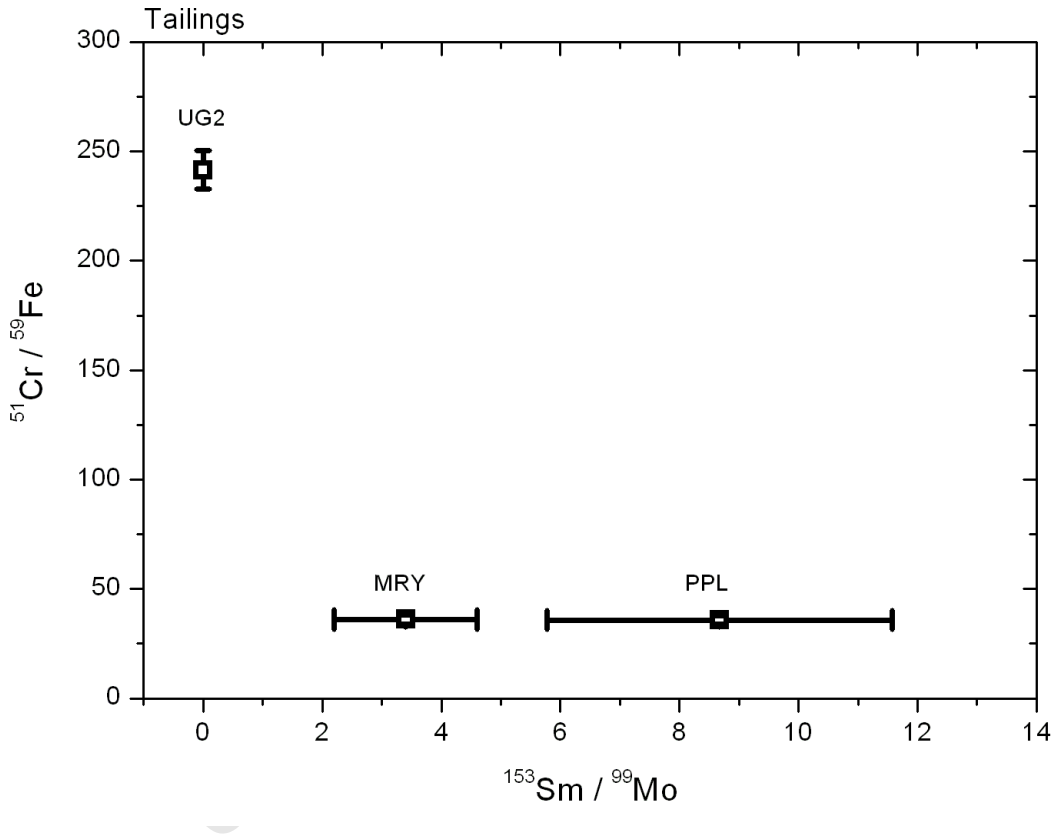

FIGURE 6.9: Ratio of ^{51}Cr to ^{59}Fe versus ^{153}Sm to ^{99}Mo for the tailings MRY, PPL, and UG2.

6.1.3 Spectra acquired after 16 days decay

After 16 days decay after irradiation the gamma-ray spectra of the samples were acquired again for another 30 minutes. The decay period of 16 days allowed short half-lives to decay, which allowed the determination of relatively longer lived radionuclides in the gamma-rays spectra with no serious interference problems.

The high activities produced from abundant, high cross section elements such as Mn, La, and Na often mask lower level activities from other short and medium half-life radionuclides, while activities from such elements as Sc and Co interfere with long half-life measurements. The gamma-ray spectra were acquired for the concentrates (Fig 6.10), feeds (Fig 6.11), and tailings (Fig 6.12). The results of the analyses of these gamma-ray spectra are tabulated in Tables 6.5 , 6.6, and 6.7. The radionuclides identified were ^{46}Sc, ^{51}Cr, ^{58}Co, ^{59}Fe, and ^{60}Co. These radionuclides were also observed in the gamma-ray spectra acquired after three days decay. These radionuclides are the indicators (daughters) of their parent elements (Table 6.1). Further discussion is given in Subsection 6.1.4.

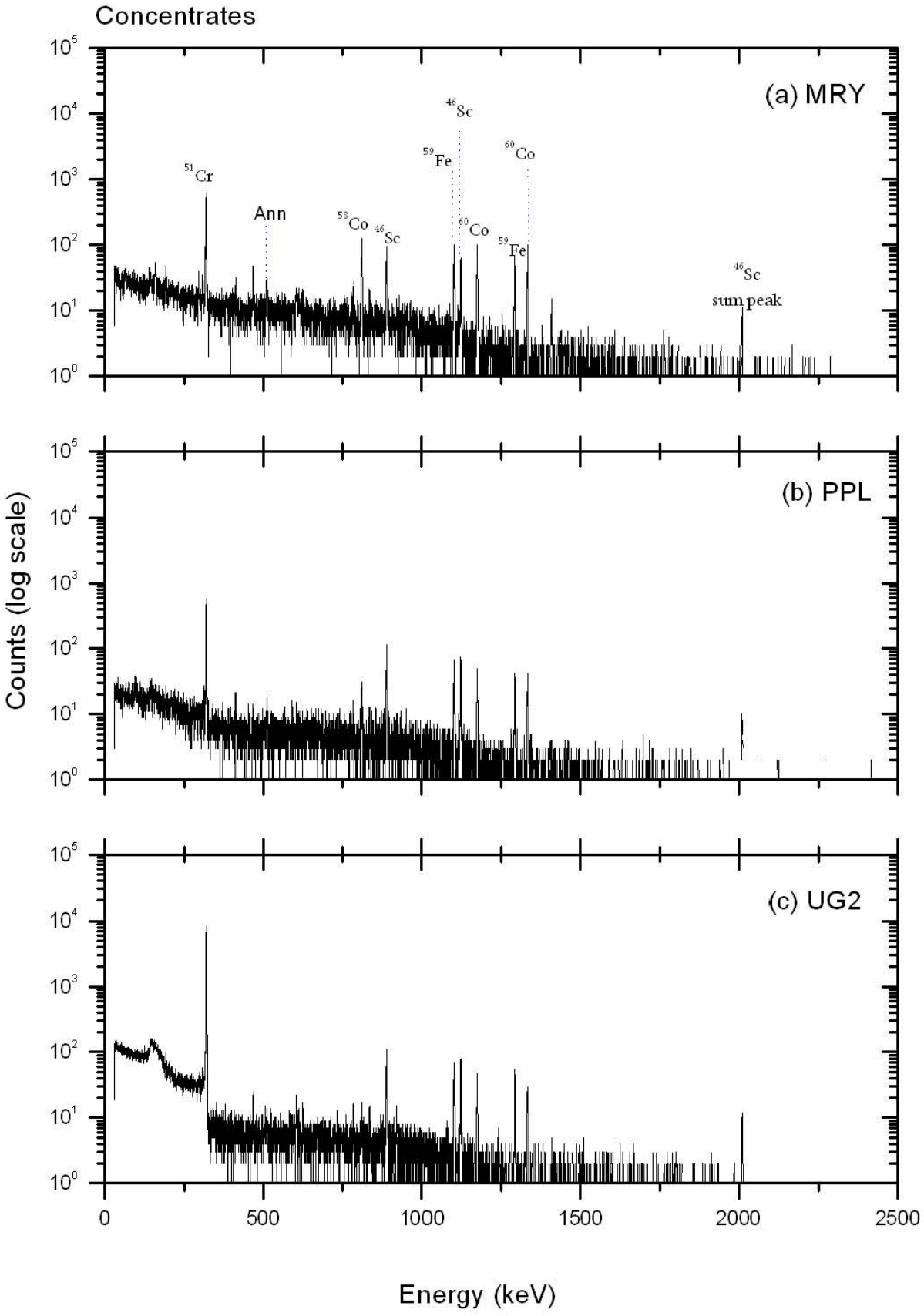

FIGURE 6.10: Gamma-ray spectra of the three concentrates: (a) Merensky, (b) Platreef, and (c) Upper group chromite (UG2), acquired after 16 days decay. In the top gamma-ray spectrum, the photopeaks are labeled with the identified radionuclides. The UG2 spectrum was counted for 60 minutes in the energy range 0-300 keV (in error).

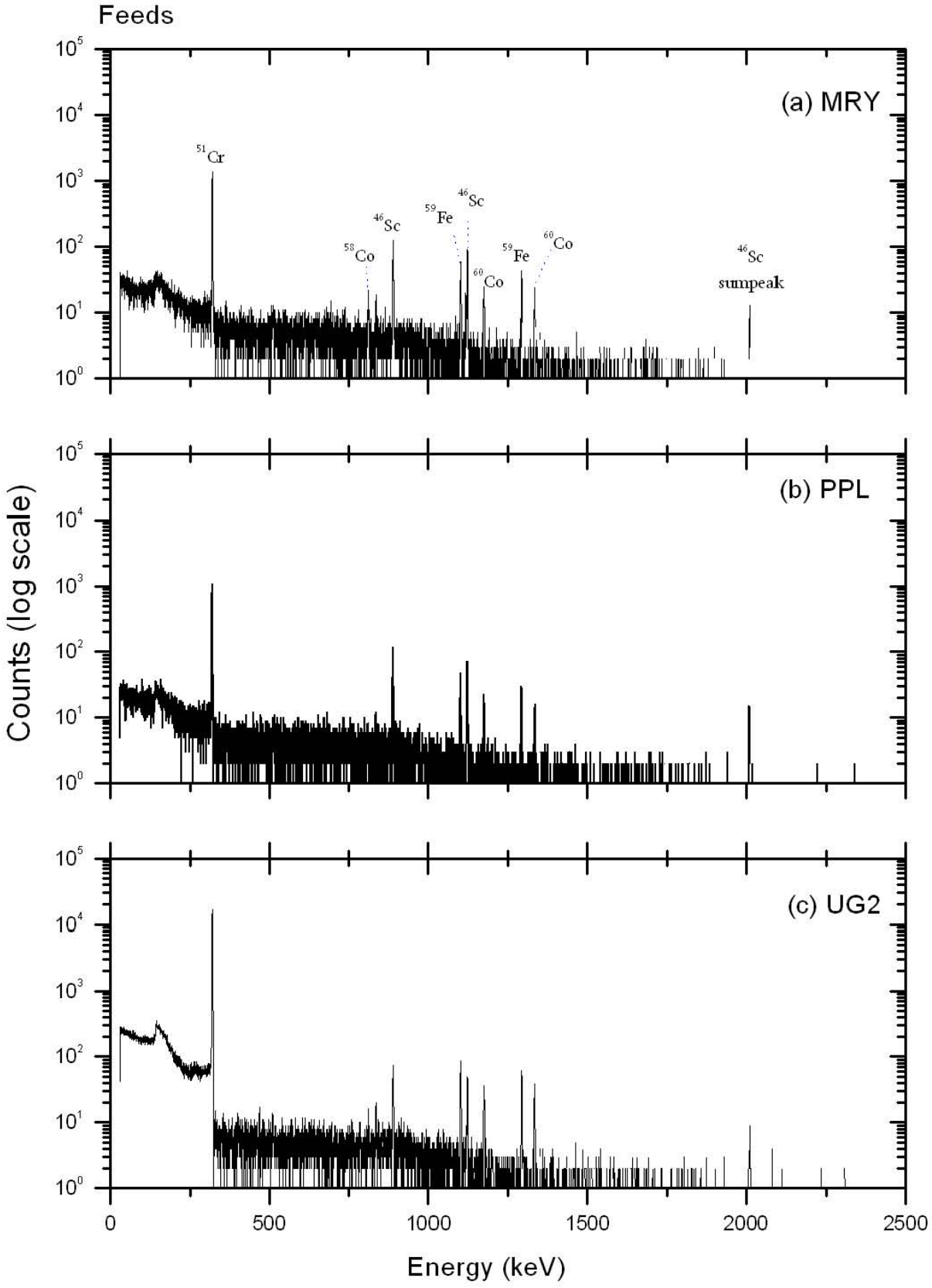

FIGURE 6.11: Gamma-ray spectra of the three feeds: (a) Merensky, (b) Platreef, and (c) Upper group chromite (UG2), acquired after 16 days decay. In the top gamma-ray spectrum, the photopeaks are labeled with the identified radionuclides. The UG2 spectrum was counted for 60 minutes in the energy range 0-300 keV (in error).

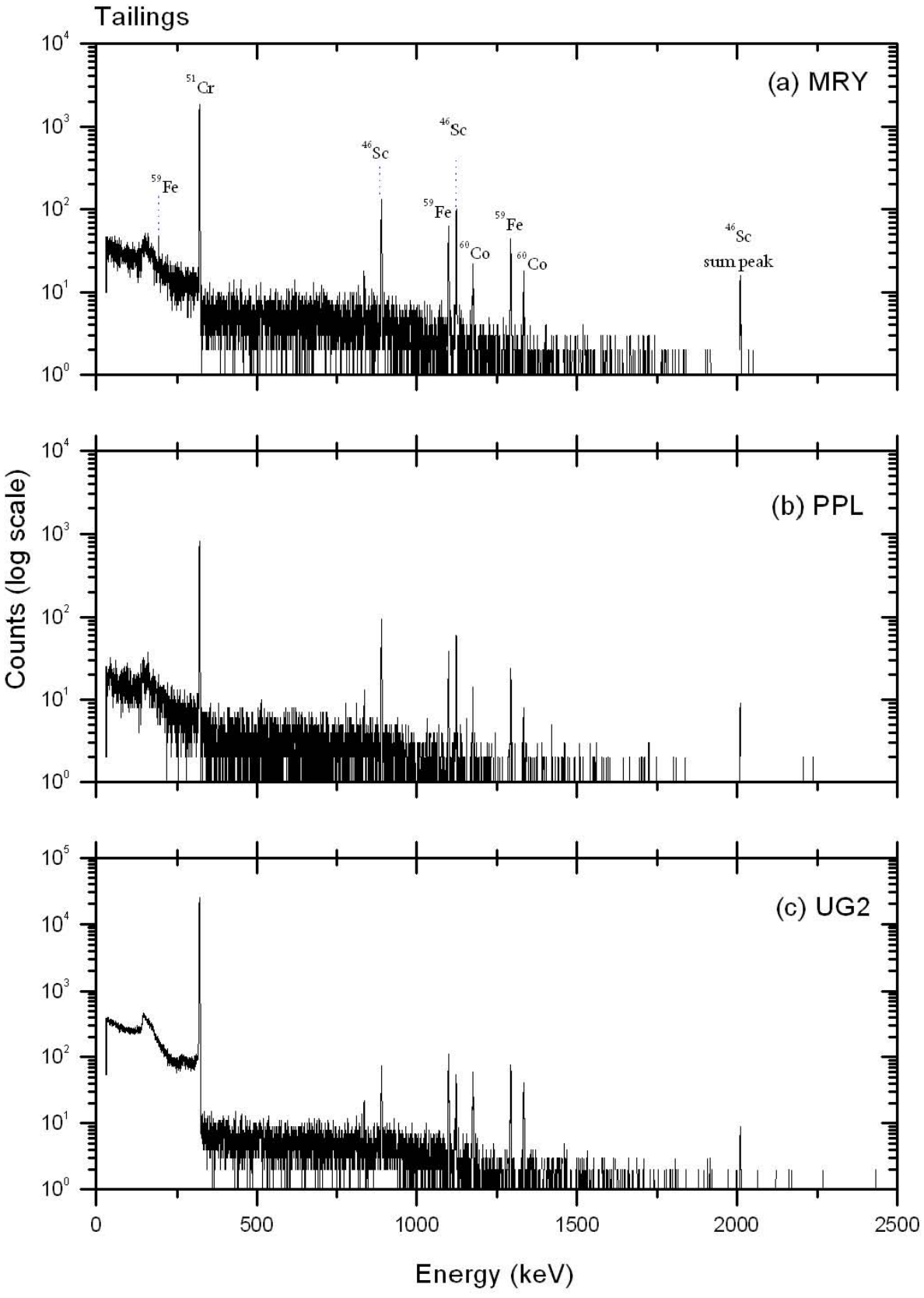

FIGURE 6.12: Gamma-ray spectra of the three tailings: (a) Merensky, (b) Platreef, and (c) Upper group chromite (UG2), acquired after 16 days decay. In the top gamma-ray spectrum, the photopeaks are labeled with the identified radionuclides. The UG2 spectrum was counted for 60 minutes in the energy range 0-300 keV (in error).

radionuclide	**Energy** (keV)	**MRY**	**PPL**	**UG2**
		$N_P \pm \sigma_p$	$N_P \pm \sigma_p$	$N_P \pm \sigma_p$
^{46}Sc	889	737 ± 36	888 ± 35	855 ± 35
	1120	500 ± 30	598 ± 29	567 ± 29
	2010	87 ± 10	86 ± 10	106 ± 11
^{51}Cr	320	4973 ± 83	4175 ± 119	62535 ± 254
^{58}Co	811	887 ± 38	224 ± 21	81 ± 15
^{59}Fe	192	137 ± 32	—	—
	1100	770 ± 34	472 ± 25	580 ± 27
	1292	544 ± 26	303 ± 20	376 ± 21
^{60}Co	1173	851 ± 33	376 ± 23	362 ± 21
	1332	747 ± 29	345 ± 21	284 ± 18
Ann+	511	216 ± 44	—	—

TABLE 6.5: Results of the gamma-ray spectra of the three concentrates acquired after 16 days decay.

radionuclide	**Energy** (keV)	**MRY**	**PPL**	**UG2**
		$N_P \pm \sigma_p$	$N_P \pm \sigma_p$	$N_P \pm \sigma_p$
^{46}Sc	889	962 ± 35	852 ± 33	560 ± 30
	1116	103 ± 12	—	—
	1120	715 ± 49	599 ± 27	414 ± 25
	2010	112 ± 11	109 ± 11	51 ± 8
^{51}Cr	320	9683 ± 103	8035 ± 93	132411 ± 369
^{58}Co	811	89 ± 18	—	59 ± 14
^{59}Fe	192	71 ± 26	—	—
	1100	455 ± 25	347 ± 21	777 ± 30
	1292	291 ± 20	205 ± 17	492 ± 23
^{60}Co	1173	204 ± 17	145 ± 14	315 ± 21
	1332	173 ± 16	98 ± 13	306 ± 20

TABLE 6.6: Results of the gamma-ray spectra of the three feeds acquired after 16 days decay.

radionuclide	**Energy** (keV)	**MRY**	**PPL**	**UG2**
		$N_P \pm \sigma_p$	$N_P \pm \sigma_p$	$N_P \pm \sigma_p$
^{46}Sc	889	1113 ± 38	601 ± 27	525 ± 28
	1120	845 ± 32	434 ± 23	379 ± 24
	2010	136 ± 12	70 ± 9	50 ± 8
^{51}Cr	320	14607 ± 124	6267 ± 82	191951 ± 444
^{59}Fe	192	77 ± 30	—	—
	1100	503 ± 25	231 ± 17	950 ± 33
	1292	315 ± 21	160 ± 15	635 ± 27
^{60}Co	1173	168 ± 17	79 ± 11	462 ± 25
	1332	126 ± 13	—	369 ± 21

TABLE 6.7: Results of the gamma-ray spectra of the three tailings acquired after 16 days decay.

6.1.4 Observations and comparative analysis of the gamma-ray spectra acquired after 16 days decay

Some of the radionuclides identified in the gamma-ray spectra after 3 days decay are also found in these spectra. These include ^{59}Fe, ^{51}Cr, ^{58}Co, ^{60}Co, ^{46}Sc, as well as ^{122}Sb and ^{124}Sb in some of the spectra. However, after 16 days, the background continuum below the photopeaks is much lower due to the decay and disappearance of the ^{24}Na photopeaks, which is one of the radioisotopes responsible for the large Compton continuum. High energy photopeaks, for example, due to ^{59}Fe and ^{60}Co, generate Compton plateaux at lower energies on which other photopeaks of interest set [71]. The ^{46}Sc photopeaks at 889 and 1120 keV are known to be among the largest in the gamma-ray spectrum for mafic ores [115], while iron is usually the element of highest abundance determined [115]. Sensitivity to long-lived radionuclides can be improved by an increased "cooling" time, which reduces the contribution of radionuclides with half-lives of a few days.

The analysis procedure in Subsection 6.1.2 was followed to analyse the gamma-ray spectra acquired after 16 days decay. The results of the analyses were plotted for the three concentrates (Fig 6.4), feeds (Fig 6.5), and tailings (Fig 6.6). The results were tested for possible agreement over 95% confidence level. Since these elements were extensively discussed in Subsection 6.1.2, only the statistical observations will be covered below.

- **Scandium** (^{46}Sc, $t_{1/2}$ = 83 d), the three concentrates contain approximately same amounts of Sc. All the results overlapped.

In the feeds samples, all the results overlapped except for MRY and UG2, the ratio of MRY to UG2 is around 2 to 1.

This amount is higher in MRY tailings samples, compared to the other two. The results in UG2 and PPL overlap. There was no overlap between MRY and PPL, and MRY and UG2. The ratio of MRY to PPL is 1.9 to 1, and the ratio of MRY to UG2 is 2.1 to 1.

- **Chromium** (^{51}Cr, $t_{1/2} = 27$ d), there was no overlap between any of the concentrate samples. The ratio of UG2 to MRY is 12.6 to 1, the ratio of UG2 to PPL is 15 to 1, and the ratio of MRY to PPL 1.2 to 1. This UG2 concentrate sample contains a higher amount of chromium by a factor of 10.

  In the feed samples, there was also no overlap between any of the samples. The ratio of UG2 to MRY is around 14 to 1, the ratio of UG2 to PPL is around (16.5 or) 17 to 1, and the ratio of MRY to PPL is 1.2 to 1

  The same was observed in the tailings samples, where there was no overlap between them. The ratio of UG2 to MRY is 13 to 1, the ratio of UG2 to PPL is 31 to 1, and the ratio of MRY to PPL is 2.3 to 1.

- **Nickel** (^{58}Co $t_{1/2} = 70$ d), in the concentrates, there was no overlap between any of the samples. The ratio of PPL to UG2 is 2.7 to 1, the ratio of MRY to UG2 is 10.9 to 1, and the ratio of MRY to PPL is 4 to 1.

  In the feed samples, thee results in MRY and UG2 overlap. The 320 keV line of ^{58}Co was not observed in the PPL gamma-ray spectrum.

- **Iron** (^{59}Fe, $t_{1/2} = 44$ d), in the concentrate samples, the results of ^{59}Fe in the three samples do not overlap over the 95 % confidence level. The ratio of MRY to PPL is 1.7 to 1, and the ratio of MRY to UG2 is around 1.4 to 1.

  In the feed samples, there was no overlap between any of the samples. The ratio of MRY to PPL is 1.3 to 1, the ratio of MRY to UG2 is 1.7 to 1, and the ratio of UG2 to PPL is 2.2 to 1.

  There was no overlap between the results for tailings samples. The ratio of MRY to PPL is 2 to 1, the ratio of UG2 to MRY is 2 to 1, and the ratio of UG2 to PPL is 4 to 1.

- **Cobalt** (^{60}Co, $t_{1/2} = 5.2$ yrs), in the concentrate samples, the results between UG2 and PPL overlapped over the 95 % confidence level. However, there was no overlap

between MRY and UG2, and MRY and PPL. The ratio of MRY to UG2 is 2.5 to 1, and the ratio of MRY to PPL is 2.3 to 1.

In the feed samples, the results overlap in the MRY and PPL. There was no overlap between MRY and UG2, and UG2 and PPL. The ratio of UG2 to MRY is around 1.6 to 1, and the ratio of UG2 to PPL is around 3 to 1.

In the tailings samples, there was no overlap between any of the samples at a 95 % confidence level. The ratio of UG2 to PPL is around 6 to 1, the ratio of UG2 to MRY is around 3 to 1, and the ratio of MRY to PPL is 2 to 1.

There were no useful differences, in terms of isotopic ratios, between the samples analysed after the 16 days decay.

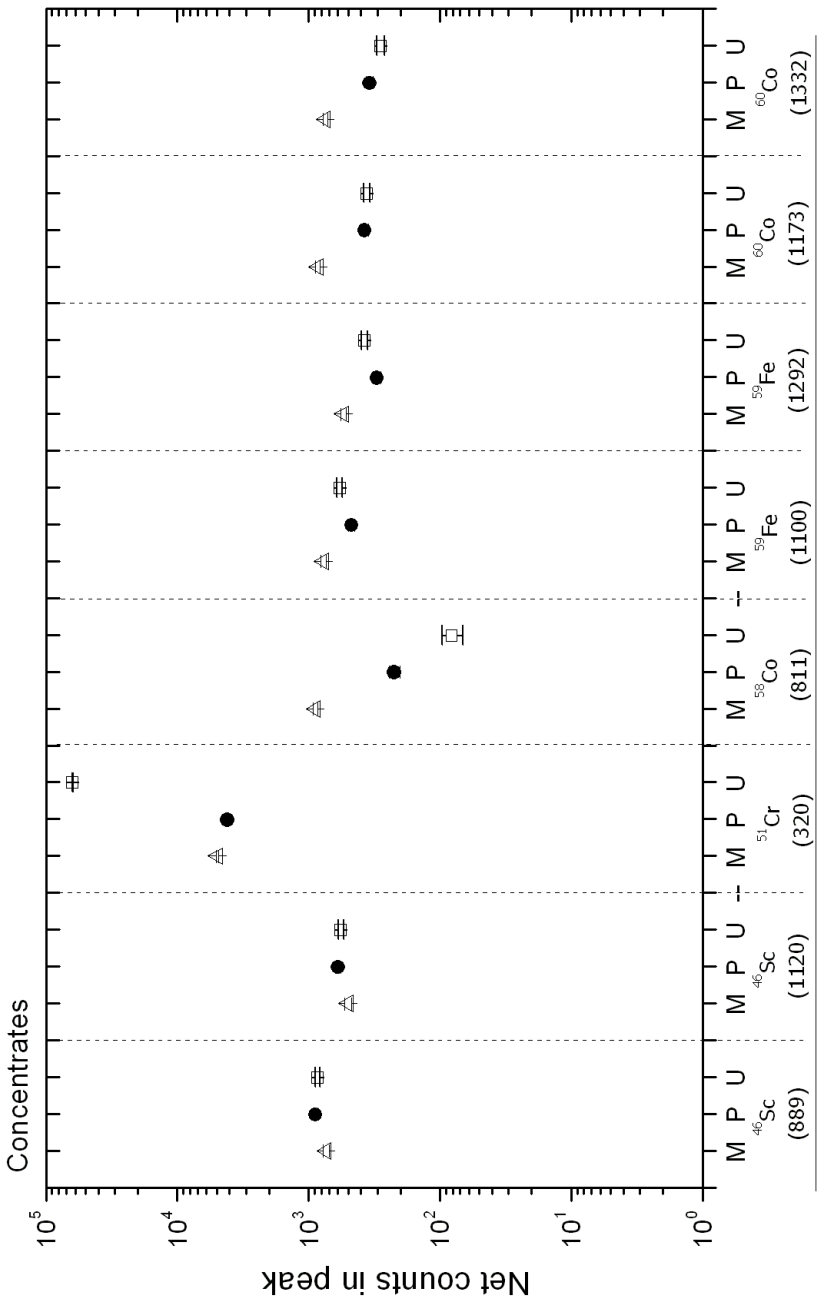

FIGURE 6.13: The net counts in the peaks of the radionuclides observed in the gamma-ray spectra of the concentrates after 16 days decay, for MRY (M; Δ), PPL (P; •), and UG2 (U; □).

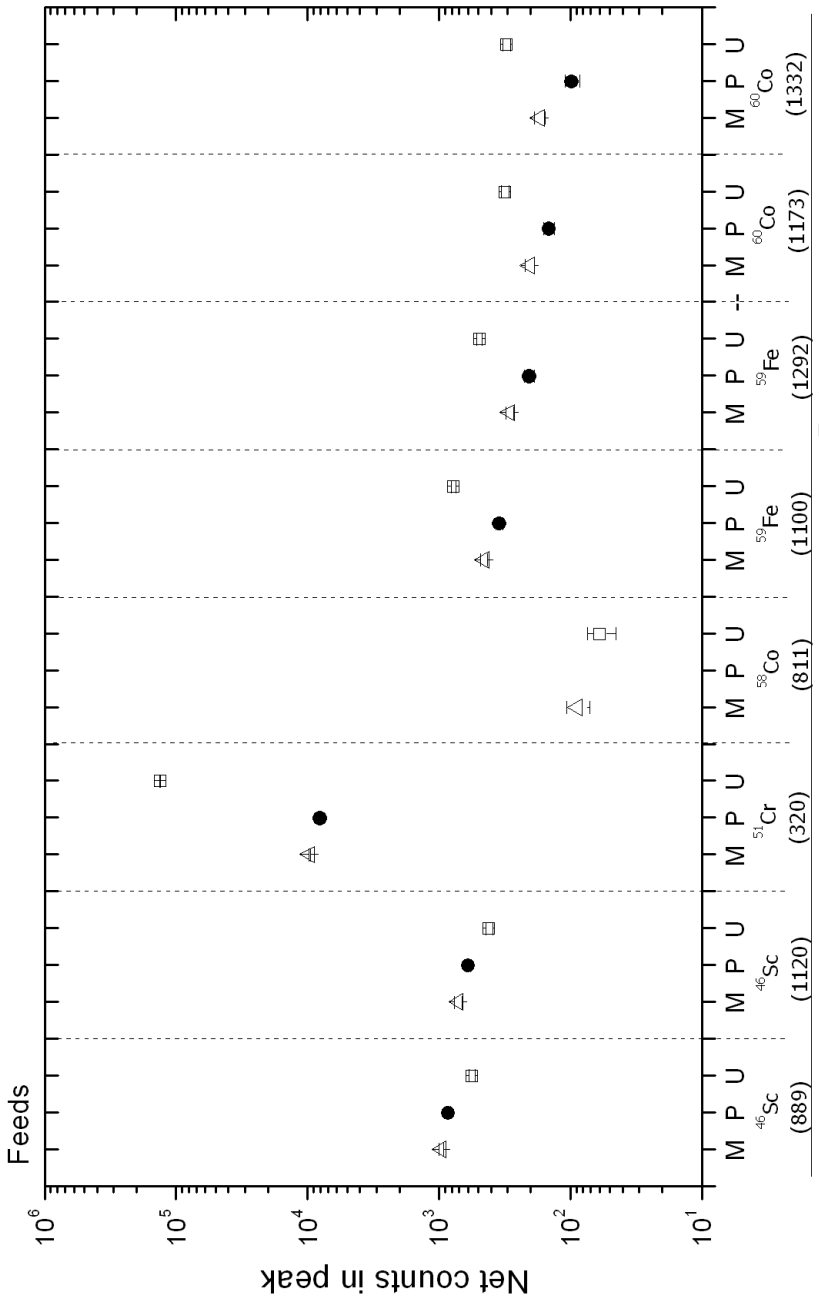

FIGURE 6.14: The net counts in the peaks of the radionuclides observed in the gamma-ray spectra of the feeds after 16 days decay, for MRY (M; Δ), PPL (P; •), and UG2 (U; □).

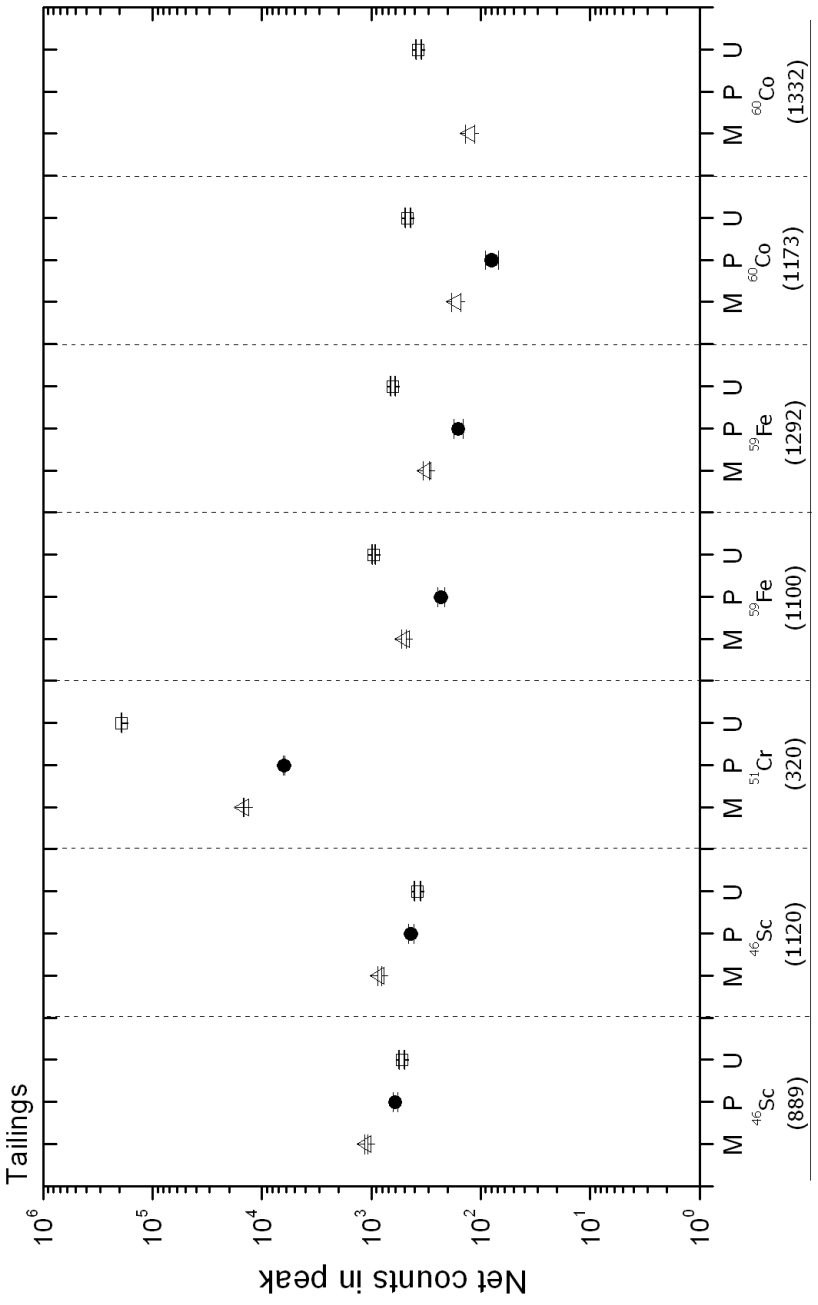

FIGURE 6.15: The net counts in the peaks of the radionuclides observed in the gamma-ray spectra of the tailings after 16 days decay, for MRY (M; Δ), PPL (P; •), and UG2 (U; □).

Chapter 7

Conclusion

This project relied on the Centre for Minerals Research at UCT to provide ore samples (MRY, UG2, and PPL) of known origin. The samples were analysed using the thermal neutron activation analysis technique, and the elements determined varied from being trace to minor and major elements. However, the irradiations and counting conditions used in this work have not allowed the determinations of all the platinum group elements in the samples. There are two possible reasons for this. Spectral interferences which masked the gamma lines of the platinum group elements, or the nuclear properties of PGEs such as neutron capture cross section and half-lives. Moreover, the complexities of the gamma-ray spectra from multielement samples, such as ores, often prevent the determination of many elements by strictly instrumental methods.

7.1 Summary of experiments at iThemba LABS

7.1.1 Fast neutron activation analysis

Three concentrate samples were irradiated for one hour using a ^{241}AmBe radioisotopic neutron source, and counted immediately for around 35 minutes. The gamma-ray spectra of the samples were analysed, and four radionuclides were chosen to perform the analysis: ^{24}Na , ^{27}Mg, ^{28}Al, and ^{56}Mn, which are radionuclides formed by the neutron capture reaction (n,γ). These elements are some of the major ones that could be found in igneous rocks. The only significant difference observed was in the amount of ^{56}Mn. The results of ^{56}Mn in the MRY and the UG2 concentrates were overlapped within the 95% confidence level. However,

the PPL concentrate gamma-ray spectrum contained a stronger line of ^{56}Mn at 846 keV, compared to MRY and UG2. The ratio of ^{56}Mn in PPL to UG2 is around 1.6 to 1, and PPL to MRY is around 1.9 to 1.

Activity concentrations have been calculated for these concentrate samples, for Run 1, Run 2 and Run 3. The activity concentrations for each radionuclide with more than one line, in the gamma-ray spectra, should be the same. However, the results obtained were slightly off. This is probably due to the procedure of peak fitting and calculation of the number of counts under the peak.

7.1.2 Radiometric measurements of the ore samples

Measurements of the naturally emitted radiation from the three ore samples for about 24 hours were dominated mainly by the uranium-series, thorium-series radionuclides, and the ^{40}K gamma-ray energy peak at 1460 keV. Uranium-series and thorium-series are highly important for the study of geochemical processes and frequently used in dating techniques. The PPL sample is found to have the highest concentration of uranium series radionuclides, while the UG2 sample is found to have the highest in terms of thorium series radionuclides.

The intensities of these gamma-ray energies were more enhanced in the PPL sample relative to the other two samples (MRY and UG2). This might be a clear evidence that the PPL ores are generally rich in term of uranium-series as well as thorium-series, and hence this could be a useful tool to discriminate between the three ore types (PPL, UG2, and MRY) in term of origin of extraction.

7.2 Summary of experiments at NECSA

The samples (feeds, tailings, and concentrates) were irradiated in the nuclear reactor for 10 seconds, and counted for 30 min after 3 days and 16 days decay periods. The gamma-rays spectra of the samples show variations in the intensities of the gamma-ray lines. Some radionuclides were found to be more abundant in the concentrates compared to the feeds. This significant difference is an indication that these elements have been recovered from the whole bulk, during the froth flotation process, and collected in the froth phase.

The data showed an appreciable variability for each constituent determined by NAA. For example, UG2 samples turned out to be high in ^{51}Cr, relative to the other two samples (MRY

and PPL). The possibility of labeling the samples according to specific elemental signatures was investigated by finding the ratios of selected radionuclides. The ratio between two major elements (^{51}Cr and ^{59}Fe) and two trace elements (^{153}Sm and ^{99}Mo) in each sample were compared. For all of the samples analysed (feeds, concentrates, and tailings), the UG2 sample was found to have the highest ratio of chromium to iron (^{51}Cr/^{59}Fe), and a very low ratio of samarium to molybdenum (^{153}Sm/^{99}Mo). On the other hand, the PPL shows the opposite trend, while the MRY sample shows the lowest isotopic ratios of the two.

7.3 Recommendations and future work

The results suggest that neutron activation analysis as a non-destructive analytical technique offers possibilities for the identification of PGM ore and concentrate based on trace element analysis. There are many naturally-occurring isotopes that can be used to provide unambiguous signatures for the concentrate materials, measured via NAA.

There are numerous ways in which this work may be advanced. It worth looking at the high-energy range (above 3 MeV) of gamma-rays because of the relative simplicity of the spectra compared with the more complicated spectra below this range. Consequently it is necessary in practice to choose the best compromises regarding irradiation and decay times in order to determine simultaneously as many of elements as possible with an acceptable precision, while limiting or minimizing the number of times of irradiation, of decay, and counting. The choice of radionuclides used as signatures will require adjusting the irradiation conditions accordingly. In this work, the analysed samples differ in mass and hence the peak contents should be "mass normalised" before a comparison between the samples from the three locations can be intercompared.

A careful calculations of the activity concentrations of the irradiated samples, and valid peak fitting procedures, would allows for more stringent differentiation between the samples. Moreover, by using the decay and growth equations and having the values of the unknowns, the activity concentration could be converted to elemental concentrations. This will provide a comprehensive picture of the element composition of the various samples and could focus on those elements which are hard to determine by chemical means, but are rather straight forward measured by neutron activation. In this work, the activity concentration have been calculated for the concentrate samples irradiated at iThemba LABS. However, the results were slightly off and the calculations were not taken further to calculate the elemental concentrations due to the absent values of some unknowns.

The natural radioactivity results for ores show statistically significant differences between the ores from Merensky/UG2 and Platreef - there is thus a potential to use natural radioactivity levels as a discriminator. Further work can include similar investigations for samples up to the concentrate level.

The present results are not definitive in the sense that the analyses were undertaken on one set of samples. Future work will focus on the reliability of the analyses (analyses need to be repeated to explore "sampling" issues), and should consider working with many samples from the same ore deposit, but from different localities.

In particular, the mineral industry is interested more in developing methods of identifying the platinum products at the smelting phase, i.e. after refining. Future work should focus on studying the variations between smelting samples from different mining companies. Moreover, adding a trace amount of a suitable element could provide a way of labeling the platinum product in terms of ownership or origin of extraction.

Bibliography

[1] B. Coetzee and R. Horn. *The Theft of Precious Metals from South African Mines and Refineries*. Institute of Security Studies (ISS), Pretoria, South Africa, 1st edition, 2006.

[2] T. B. Pierce. Recent developments in activation analysis. *Selected Annual Reviews of the Analytical Sciences*, 1:133–175, 1971.

[3] R. D. Reeves and R. R. Brooks. *Trace Element Analysis of Geological Materials*. John Wiley & Sons, Inc., 1978.

[4] D. A. Skoog and D. M. West. *Principles of Instrumental Activation Analysis*. Saunders college, 2nd edition, 1980.

[5] Z. B. Alfassi. *Activation Analysis*, volume I. CRC Press, Inc., 1990.

[6] J. Chadwick. The existence of a neutron. *Proceedings of the Royal Society of London. Series A, Containing Papers of a Mathematical and Physical Character*, 136:692–708, 1932.

[7] W. R. Corliss. *Neutron Activation Analysis*. U.S. Atomic Energy Commission Division of Technical Information, 1963.

[8] G. E. Boyd. Method of activation analysis. *Analytical Chemistry*, 21:335–347, 1949.

[9] B. E. Kogo, E. N. Gajere, J. K. Ogunmola, and J. O. Ogbole. Neutron activation analysis of soil samples from different parts of Abuja metropolis. *Middle-East Journal of Scientific Research*, 4:254–262, 2009.

[10] J. Hoste, R. Gijbels, and D. Soete. *Neutron Activation Analysis*. John Wiley & Sons, Inc., 1972.

[11] M. D. Glascock. An overview of neutron activation analysis. http://www.jeffreycreid.com/Analytical_Methods/NAA_theory.html, 1998.

[12] Elemental Analysis Inc. (EAI). Description of neutron activation analysis. http://elementalanalysis.com/services_naa.asp, 2010.

[13] W. D. Ehmann and D. E. Vance. Advances in neutron activation analysis. *CRC Critical Reviews in Analytical Chemistry*, 20:405–443, 1989.

[14] G. H. Morrison, J. T. Gerard, A. Travesi, R. L. Currie, S. F. Peterson, and N. M. Potter. Multielement neutron activation analysis of rock using chemical group separations and high resolution gamma spectrometry. *Analytical Chemistry*, 41:1633–1637, 1969.

[15] J. Perlman. Analysis of gamma-ray spectra. In Saadia Amiel, editor, *Studies in analytical chemistry 3: Nondestructive Activation Analysis*, chapter 3, pages 9–24. Elsevier, 1981.

[16] M. B. A. Vasconcellos, A. Figueriredo, L. Marques, and M. Armelin M. Saiki. Neutron activation analysis applied to the study of the composition of Brazilian geological samples. *Geochim. Brasil.*, 4:125–137, 1990.

[17] A. El-Taher. Rare-earth elements in Egyptian granite by instrumental neutron activation analysis. *Applied Radiation and Isotopes*, 65:458–464, 2007.

[18] C. Cristache, O. G. Duliu, C. Ricman, M. Toma, F. Dragolici, M. Bragea, and L. Done. Determination of elemental content in geological samples. *Romanian Journal of Physics*, 53:941–946, 2008.

[19] R. R. Greenberg. Pushing the limits of NAA: Accuracy, uncertainty and detection limits. *Journal of Radioanalytical and Nuclear Chemistry*, 278:231–240, 2008.

[20] I. I. Sadykov, V. G. Zinov'ev, and Z. O. Sadykova. Neutron activation analysis of manganese mercury telluride. *Journal of Analytical Chemistry*, 60:946–950, 2005.

[21] G. Rossi and A. F. Sedda. Bullets fragments identification by comparison of their chemical composition obtained using instrumental neutron activation analysis. *Forensic Science International*, article in press (doi: 10.1016/j.forsciint.2010.06.003), 2010.

[22] H. J. Im, H. Cho, B. C. Song, Y. J. Park, Y. Chung, and W. Kim. Analytical capability of an explosives detection by a prompt gamma-ray neutron activation analysis. *Nuclear instruments and methods in physics research*, section A 566:442–447, 2006.

[23] S. Park and N. H. Jang. Estimation and calibration of thermal neutron flux for neutron activation analysis. *Bulletin of the Korean Chemical Society*, 27:2061–2063, 2006.

[24] G. M. Kolesov. Neutron activation analysis of environmental materials. *Analyst*, 120:1457–1460, 1995.

[25] Z. B. Alfassi, T. U. Probst, and B. Rietz. Platinum determination by instrumental neutron activation analysis with special reference to the spectral interference of Sc-47 on the platinum indicator nuclide Au-199. *Analytica Chimica Acta*, 360:243–252, 1998.

[26] O. G. Duliu, C. Cristache, G. Oaie, and O. A. Culicov. ENAA studies of pollution in anoxic Black sea sediments. *Marine Pollution Bulletin*, 58:827–831, 2009.

[27] C. Cristache, K. Gmeling, O. Culicov, M. V. Frontasyeva, M. Toma, and O. G. Duliu. An ENAA and PGAA comparative study of anoxic Black sea sediments. *Journal of Radioanalytical and Nuclear Chemistry*, 79:7–12, 2009.

[28] B. Rietz, A. Krarup-Hansen, and M. Rorth. Determination of platinum by radiochemical neutron activation analysis in neural tissues from rats, monkeys and patients treated with cisplatin. *Analytica Chimica Acta*, 426:119–126, 2001.

[29] C. E. Huntington, S. M. Carleton, D. J. McBride, C. L. Phillips, and J. S. Morris. Multi-element analysis of bone from the osteogenesis imperfecta model (OIM) mouse using thermal and fast neutron activation analysis. *Journal of Radioanalytical and Nuclear Chemistry*, 276:65–69, 2008.

[30] M. D. Glascock and H. Neff. Neutron activation analysis and provenance research in archaeology. *Measurement Science and Technology*, 14:1516–1526, 2003.

[31] M. Ebihara, N. Saito, H. Akaiwa, and K. Tomura. Instrumental and radiochemical neutron activation analysis of trace iodine in geological samples. *Analytical Sciences*, 8:183–187, 1992.

[32] J. Op De Beeck and J. Hoste. Some modern applications of activation analysis. *Analyst*, 99:973–993, 1974.

[33] H. T. Millard, JR, and A. J. Bartel. A neutron activation analysis procedure determination of the noble metals in geological samples. In Brunfelt and Steinnes, editors, *Activation Analysis in Geochemistry and Cosmochemistry: proceeding of the NATO advanced study institute*, pages 353–358. Universitetsforlaget, 1971.

[34] V. I. Malyshev, M. B. Shiryaeva, Z. A. Sokolova, L. M. Lyubimova, Yu. P. Salmin, M. A. Tatarkin, K. N. Ryumina, and A. M. Shelyakina. Application of neutron activation analysis to determine the contents and isotopic ratios of elements in rocks and minerals. *Journal of Radioanalytical Chemistry*, 57:287–297, 1980.

[35] P. Makreski, R. Jacimovic, V. Stibilj, T. Stafilov, and G. Jovanovski. Determination of trace elements in iron minerals by instrumental and radiochemical neutron activation analysis. *Radiochimica Acta*, 96:855–861, 2008.

[36] N. Güngör, T. Tulun, and A. Alemdar. Determination of trace elements by instrumental neutron activation analysis in Anatolian bentonitic clays. *Nuclear Instruments and Methods in Physics Research B*, 142:555–560, 1998.

[37] G. Giaveri, E. Rizzio, and M. Gallorini. Preconcentration and preseparation procedure for platinum determination at trace levels by neutron activation analysis. *Analytical Chemistry*, 73:3488–3491, 2001.

[38] T. U. Probst, B. Rietz, and Z. B. Alfassi. Platinum concentrations in Danish air samples determined by instrumental neutron activation analysis. *J. Environ. Monit.*, 3:217–219, 2001.

[39] G. K. Muecke. *Short Course in Neutron Activation Analysis*. Mineralogical Association of Canada, Halifax, 1980.

[40] W. P. Griffith. The periodic table and the platinum group metals. *Platinum Metals Rev.*, 52:114–119, 2008.

[41] C. F. Vermaak. *The Platinum-group Metals: A Global Perspective*. Mintek, South Africa, 1st edition, 1995.

[42] Z. Xiao and A. R. Laplante. Characterizing and recovering the platinum group minerals–a review. *Minerals Engineering*, 17:961–979, 2004.

[43] A. Dubiella-Jackowska, Z. Polkowska, and J. Namiesnik. Platinum group elements: A challenge for environmental analytics. *Polish Journal of Environmental Studies*, 16:329–345, 2007.

[44] G. S. Reddi and C. R. M. Rao. Analytical techniques for the determination of precious metals in geological and related materials. *The Analyst, critical review*, 124:1531–1540, 1999.

[45] C. J. Penberthy, E. J. Oosthuyzen, and R. K. W. Merkle. The recovery of platinum-group elements from the UG2 chromitite, Bushveld Complex - a mineralogical perspective. *Mineralogy and Petrology*, 68:213–222, 2000.

[46] L. J. Cabri. *The Geology, Geochemistry, Mineralogy and Mineral Beneficiation of Platinum-group Elements*, volume 54 of CIM special volume. Canadian Institute of Mining and Metallurgy, 2002.

[47] R. G. Cawthorn. Platinum-group element mineralization in the Bushveld Complex– a critical assessment of geochemical models. *South African Journal of Geology*, 102:268–281, 1999.

[48] R. G. Cawthorn. The centenary of the discovery of platinum in the Bushveld complex. *Platinum Metals Review*, 50:130–133, 2006.

[49] R. P. Schouwstra and E. D. Kinloch. A short geological review of the Bushveld Complex. *Platinum Metals Rev.*, 44:33–39, 2000.

[50] R. G. Cawthorn. The platinum and palladium resources of the Bushveld Complex. *South African Journal of Science*, 95:481–489, 1999.

[51] C. Brough. An investigation into the process mineralogy of the Merensky Reef at Northam platinum limited. Master's thesis, University of Cape Town, 2008.

[52] A. Wilson and G. Chunnett. Trace element and platinum group element distributions and the genesis of the Merensky Reef, western Bushveld Complex, South Africa. *Journal of Petrology*, 47:2369–2403, 2006.

[53] I. McDonald, D. A. Holwell, and P. E. B. Armitage. Geochemistry and mineralogy of the Platreef and "critical zone" of the northern lobe of the Bushveld Complex, South Africa: implications for Bushveld stratigraphy and the development of PGE mineralisation. *Mineralium Deposita*, 40:526–549, 2005.

[54] J. G. Wiese, M. Becker, D. J. Bradshaw, and P. J. Harris. Interpreting the role of reagents in the flotation of platinum-bearing Merensky ores. *The Journal of South African Institute of Mining and Metallurgy*, 107:29–36, 2007.

[55] S. Barnes and W. D. Maier. Platinum-group elements and microstructures of normal Merensky Reef from Impala platinum mines, Bushveld Complex. *Journal of Petrology*, 43:103–128, 2002.

[56] R. C. Hochreiter, D. C. Kennedy, W. Muir, and A. L. Woods. Platinum in South Africa (metal review series no. 3). *Journal of South African Institute of Mining and Metallurgy*, 85:165–185, 1985.

[57] C. A. Lee. Trace and platinum-group element geochemistry and the development of the Merensky unit of the western Bushveld Complex. *Mineralium Deposita*, 18:173–190, 1983.

[58] S. K. Mondal and E. A. Mathez. Origin of UG2 chromitite layer. *Journal of petrology*, 48:495–510, 2007.

[59] T. D. Manyeruke and W. D. Maier. Major and trace element geochemistry of the Platreef on the farm Townlands, northern Bushveld Complex. *South African Journal of Geology*, 108:381–396, 2005.

[60] T. J. Napier-Munn. Mineral comminution circuits, their operation and optimization, JKMRC monograph series in mining and mineral processing 2. Julius Kruttschnitt Mineral Research Centre, University of Queensland, Australia, 1999.

[61] R. P. King. *Principles of Flotation*. South African Institute of Mining and Metallurgy, 1982.

[62] J. Turkstra, P. J. Pretorius, and W. J. De Wet. Nondestructive determination of platinum metals in ores, matte, and lead assay beads by reactor activation analysis and high resolution gamma spectrometry. *Analytical Chemistry*, 42:835–841, 1970.

[63] IAEA, International Atomic Energy Agency. *Nuclear Analytical Methods for Platinum-group Elements, IAEA-TECDOC-1443*. IAEA, Austria, 2005.

[64] Y. B. Qu. Recent developments in the determination of precious metals: A review. *The Analyst*, 121:139–161, 1996.

[65] M. E. A. Robertson and C. E. Feather. Determination of gold, platinum and uranium in South African ores by high-energy XRF spectrometry. *X-Ray spectrometry*, 33:164–173, 2004.

[66] W. Pretorius, D. Chipley, K. Kyser, and H. Helmstaedt. Direct determination of trace levels of Os, Ir, Ru, Pt and Re in kimberlite and other geological materials using HR-ICP-MS. *Journal of Analytical Atomic Spectrometry*, 18:302–309, 2003.

[67] D. N. Sutherland and P. Gottljeb. Application of automated quantitative mineralogy in mineral processing. *Minerals Engineering*, 4:753–762, 1991.

[68] W. R. Goodall, P. J. Scales, and A. R. Butcher. The use of QEMSCAN and diagnostic leaching in the characterization of visible gold in complex ores. *Minerals Engineering*, 18:877–886, 2005.

[69] P. W. de Lange, W. J. de Wet, J. Turksta, and J. H. Venter. Nondestructive neutron activation analysis of small samples of Witwatersrand ore for gold. *Analytical Chemistry*, 40:451–454, 1968.

[70] G. Friedlander, J. W. Kennedy, and J. M. Miller. *Nuclear and Radiochemistry*. John Wiley & Sons, Inc., 2nd edition, 1964.

[71] P. J. Potts. *A Handbook of Silicate Rock Analysis*. Blackie Chapman and Hall, Glasgow: New york, 1987.

[72] N. Tsoulfanidis. *Measurement and Detection of Radiation*. Hemisphere Publishing Corporation, 1983.

[73] M. F. L'Annunziata. *Handbook of Radioactivity Analysis*. Academic press, An imptint of Elsevier, 2nd edition, 2003.

[74] W. W. Meinke and R. E. Anderson. Activation analysis using low level neutron sources. *Analytical Chemistry*, 25:778–783, 1953.

[75] B. Keisch. *The Atomic Fingerprint: Neutron Activation Analysis*. University Press of the Pacific, 2003.

[76] G. Gilmore and J. D. Hemingway. *Practical Gamma-Ray Spectrometry*. John Wiley & Sons, Inc., 1995.

[77] J. A. Adams and P. Gasparini. *Gamma-Ray Spectrometry of Rocks: Methods in Geochemistry and Geophysics*, volume 10. Elsevier publishing company, 1970.

[78] K. S. Krane. *Introductory Nuclear Physics*. John Wiley & Sons, 2nd edition, 1988.

[79] G. F. Knoll. *Radiation Detection and Measurement*. John Wiley & Sons, New York, 3rd edition, 2000.

[80] D. Bodansky. *Nuclear Energy: Principles, Practices, and Prospects*. Springer, 2nd edition, 2004.

[81] CANada Deuterium Uranium (CANDU). CANDU fundamentals course manual. http://canteach.candu.org/library/20040700.pdf, 2004.

[82] E. Orvini and M. Speziali. Applicability and limits of instrumental neutron activation analysis: State of the art in the year 2000. *Microchemical Journal*, 59:160–172, 1998.

[83] Bekurt and Wiriz. *Nuclear Physics*. Springer-Verlag, Inc., 1964.

[84] International Atomic Energy Agency. Evaluated nuclear data file (ENDF). http://www-nds.iaea.org/exfor/endf.htm, Database Version of May 31, 2010.

[85] L. F. Curtiss. *Introduction to Neutron Physics*. D. Van Nostrand company, Inc., 1st edition, 1959.

[86] V. P. Guinn and C. d. Wagner. Instrumental neutron activation analysis. *Analytical chemistry*, 32:317–323, 1960.

[87] R. Gijbels and A. Govaerts. Practical aspects of neutron activation determination of the platinum metals. *Journal of Radioanalytical Chemistry*, 16:7–19, 1973.

[88] J. D. Brockman and J. D. Robertson. Analysis of k_o neutron activation analysis at the University of Missouri research reactor. *Applied Radiation and Isotopes*, 67:1084–1088, 2009.

[89] M. Oshima, Y. Toh, Y. Hatsukawa, T. Hayakawa, and N. Shinohara. A high-sensitivity and non-destructive trace element analysis based on multiple gamma-ray detection. *Journal of Nuclear Science and Technology*, 39:292–294, 2002.

[90] E. E. Rakovskii. Neutron activation method in the analysis of geological materials for noble metals. *Journal of Radioanalytical and Nuclear Chemistry*, 88:161–170, 1985.

[91] Th. Goldbrunner, G. Angloher, F. v. Feilitzsch, R. v. Hentig, and M. Neff. New records on low activity measurements with neutron activation analysis. *Nuclear Physics B (Proc. Suppl)*, 61:176–179, 1998.

[92] A. Perez-Andujar and L. Pibida. Performance of CdTe, HPGe and NaI(Tl) detectors for radioactivity measurements. *Applied Radiation and Isotopes*, 60:41–47, 2004.

[93] A. M. Hassan, E. Gantner, E. Mainka, H. Ruf, U. Kuhnes, and M. Mostafa. Analytical applications of neutron capture gamma-ray spectroscopy. *Journal of Physics D:Applied Physics*, 16:2061–2074, 1983.

[94] G. L. Molnár, Zs. Revay, T. Belgya, and R. B. Firestone. The new prompt gamma-ray catalogue for PGAA. *Applied Radiation and Isotopes*, 53:527–533, 2000.

[95] M. P. Falley, D. L. Anderson, W. H. Zoller, G. E. Gordon, and R. M. Lindstrom. Neutron-capture prompt γ-ray activation analysis for multielement determination in complex samples. *Analytical Chemistry*, 51:2209–2221, 1979.

[96] K. Sueki, K. Kobayashi, W. Sato, H. Nakahara, and T. Tomizawa. Nondestructive determination of major elements in a large sample by prompt gamma ray neutron activation analysis. *Analytical Chemistry*, 68:2203–2209, 1996.

[97] K. Heydorn. Radiochemical neutron activation analysis. In R.A. Meyers, editor, *Encyclopedia of Analytical Chemistry*, pages 12762–12782. John Wiley & Sons Ltd, Chichester, 2000.

[98] Nelson Eby, University of Massachusetts Lowell. Geochemical instrumentation and analysis: Instrumental neutron activation analysis (inaa). http://serc.carleton.edu/research_education/geochemsheets/techniques/INAA.html, 2007.

[99] J. C. Cobb. Determination of lanthanide distribution in rocks by neutron activation and direct gamma counting. *Analytical Chemistry*, 39:127–131, 1967.

[100] E. Vincent and A. Smales. The determination of palladium and gold in igneous rocks by radioactivation analysis. *Geochimica et Cosmochimica Acta*, 9:154–160, 1956.

[101] J. H. Crocket. Neutron activation analysis for noble metals in geochemistry. In Brunfelt and Steinnes, editors, *Activation Analysis in Geochemistry and Cosmochemistry: proceeding of the NATO advanced study institute*, pages 339–351. Universitetsforlaget, 1971.

[102] R. Gijbels. Neutron activation analysis for osmium, ruthenium, and iridium in some silicate rocks and rock-forming minerals. In Brunfelt and Steinnes, editors, *Activation Analysis in Geochemistry and Cosmochemistry: proceeding of the NATO advanced study institute*, pages 359–370. Universitetsforlaget, 1971.

[103] J. H. Crocket, R. R. Keays, and S. Hsieh. Determination of some precious metals by neutron activation analysis. *Journal of Radioanalytical Chemistry*, 1:487–507, 1968.

[104] S. Lahiri, S. Dey, T. K. Baidya, M. Nandy, D. Basu, and N. R. Das. Neutron activation analysis of noble and platinum group metals in the proterozoic dalma rocks of eastern india. *Applied Radiation and Isotopes*, 48:549–553, 1997.

[105] A. Diamantatos. Accurate determination of platinum, palladium, gold and silver in ores and concentrates by wet chemical analysis of the lead assay button. *Analyst*, 11:213–215, 1986.

[106] X. L. Li and M. Ebihara. Determination of all platinum-group elements in mantle derived Xenoliths by neutron activation analysis with NiS fire-assay preconcentration. *Journal of Radioanalytical and Nuclear Chemistry*, 255:131–135, 2003.

[107] A. O. Brunfelt and E. Steinnes. Determination of chromium in rocks by neutron activation and anion exchange. *Analytical Chemistry*, 39:833–834, 1967.

[108] R. A. Nadkarni and G. H. Morrison. Determination of the noble metals in geological materials by neutron activation analysis. *Analytical Chemistry*, 46:232–236, 1974.

[109] H. W. Stockman. Neutron activation determination of noble metals in rocks: A rapid radiochemical separation based on tellurium coprecipitation. *Journal of Radioanalytical Chemistry*, 78:307–317, 1983.

[110] L.A. McNelles and J.L. Campbell. Linear classes of Ge(li) detector efficiency functions. *Nuclear Instruments and Methods*, 109:241–251, 1973.

[111] R. L. Heath. *Scintillation Spectrometry, Gamma-Ray Spectrum Catalogue*, volume 1 (Rev.). Idaho National Engineering and Environmental Laboratory, 2nd edition edition, 1997.

[112] R. G. Helmer. *Gamma-Ray Spectrum Catalogue, Ge and Si detector spectra*. Idaho National Engineering and Environmental Laboratory, 4th edition, 1998.

[113] S. L. R. Ellison, M. Rosslein, and A. Williams. *EURACHEM/CITAC Guide: Quantifying Uncertainty in Analytical Measurement*. EURACHEM/CITAC, 2nd edition, 2000.

[114] W. Tian and W. D. Ehmann. Observations relative to epithermal and fast neutrons in INAA. *Journal of Radioanalytical and Nuclear Chemistry, Articles*, 84:89–102, 1984.

[115] J. W. Jacobs, R. L. Korotev, D. P. Blanchard, and L. A. Haskin. A well-tested procedure for instrumental neutron activation analysis of silicate rocks and minerals. *Journal of Radioanalytical Chemistry*, 40:93–114, 1977.